1973

Hydraulic performance of Pennsylvania highway drainage inlets installed in grassed channels

Erik Appel
Lehigh University

HYDRAULIC PERFORMANCE OF PENNSYLVANIA HIGHWAY DRAINAGE INLETS INSTALLED IN GRASSED CHANNELS

by

Erik Appel

A Thesis
Presented to the Graduate Committee
of Lehigh University
in Candidacy for the Degree of
Master of Science

in
Civil Engineering

Lehigh University
1972

CERTIFICATE OF APPROVAL

This thesis is accepted and approved in partial fulfillment of the requirements for the degree of Master of Science.

Date 27 November 1972

Arthur W Brune

Dr. Arthur W. Brune
Professor in Charge

Dr. David A. VanHorn,
Chairman
Department of Civil Engineering

ACKNOWLEDGMENTS

This study was sponsored by the Pennsylvania Department of Transportation in conjunction with the United States Federal Highway Administration. It was conducted in the Fritz Engineering Laboratory (Department of Civil Engineering) of Lehigh University at Bethlehem, Pennsylvania. Dr. Lynn S. Beedle is Director of the Fritz Engineering Laboratory, and Dr. David A. VanHorn is Chairman of the Department of Civil Engineering.

The author is indepted to Professors Arthur W. Brune and Walter H. Graf under whose direction this study was conducted. Further acknowledgments should be directed especially to Mr. Elias Dittbrenner who built the model and assisted in performing the tests, to Mr. John M. Gera who prepared the drawings, and to Mrs. Jane L. Lenner who typed the manuscript and assisted in proofreading.

TABLE OF CONTENTS

	Page
CERTIFICATE OF APPROVAL	II
ACKNOWLEDGMENTS	III
LIST OF TABLES	VI
LIST OF FIGURES	VII
ABSTRACT	1
1. INTRODUCTION	3
1.1 Background and Need for Investigation	3
1.2 Problem Statement	5
2. MODEL LAWS	7
2.1 General Remarks	7
2.2 Hydraulic Similitude	8
2.3 Dimensionless Numbers	10
2.4 Froude Model Law	12
2.5 Manning Model Law	13
2.6 Concluding Remarks	16
3. ESTABLISHING MODEL ROUGHNESS	17
3.1 General Remarks	17
3.2 "Astroturf"	17
4. EXPERIMENTAL INVESTIGATION	
4.1 Drainage Inlets	18
4.1.1 Type H Inlet	19
4.1.2 Type 4-Ft and Type 6-Ft Inlets	19
4.2 Laboratory Equipment	24
4.2.1 General Requirements	24
4.2.2 Apparatus	26
4.2.3 Model Construction	29
4.3 Establishment of Sump Effect	33
4.4 Installation of a Dike	33
4.5 Technique	34
4.5.1 Flow Measurements	34
4.5.2 Depth Measurements	36
4.5.3 Spread Measurements	36
4.6 Procedure	36

		Page
5.	RESULTS AND DISCUSSION	38
	5.1 Presentation of Experimental Results	38
	5.2 Discussion of Measurements	39
	5.2.1 Flow Measurements	39
	5.2.2 Depth Measurements	39
	5.2.3 Spread Measurements	40
	5.3 Efficiencies of Inlets	41
	5.3.1 Efficiencies of Type H Inlet	41
	5.3.1.1 General Remarks	41
	5.3.1.2 Efficiency Curves for Swale Slope 12:1	42
	5.3.1.3 Efficiency Curves for Swale Slope 6:1	43
	5.3.1.4 Concluding Remarks	44
	5.3.2 Efficiencies of Type 4-Ft Inlet and Type 6-Ft Inlet	61
	5.3.2.1 General Remarks	61
	5.3.2.2 Efficiencies of Type 4-Ft Inlet	62
	5.3.2.3 Efficiencies of Type 6-Ft Inlet	62
	5.4 Effect of Installation of a Dike	79
	5.5 Sump Effect for Type H Inlet	81
	5.5.1 General Remarks	81
	5.5.2 Results of Sump Effect	81
6.	CONCLUSION	87
	6.1 General Conclusions	87
	6.2 Type H Inlet Gratings	87
	6.3 Type 4-Ft and Type 6-Ft Inlet Gratings	88
7.	LIST OF RECURRING SYMBOLS	90
8.	BIBLIOGRAPHY	92
9.	APPENDIX-DETERMINATION OF MANNING'S ROUGHNESS COEFFICIENT OF LANDSCAPE SURFACE "ASTROTURF"	94
10.	VITA	100

LIST OF TABLES

Table	Title	Page
1.1	Summary of Channel Configurations	6
2.1	Model Scales for Froude Similitude and Manning Similitude	15
4.1	Standard Inlets	18
5.1	Comparison of Efficiencies of Type H Inlets	45
5.2	Efficiencies of the Type 4-Ft and the Type 6-Ft Inlet Gratings at 0.5% Longitudinal Slope	63
5.3	Efficiencies of the Type 4-Ft and the Type 6-Ft Inlet Gratings at 2% Longitudinal Slope	64
5.4	Efficiencies of the Type 4-Ft and the Type 6-Ft Inlet Gratings at 4% Longitudinal Slope	66
5.5	Efficiencies of the Type 4-Ft and the Type 6-Ft Inlet Gratings at 8% Longitudinal Slope	68
5.6	Discharge and Spread for Different Back and Swale Slopes for Type H Inlet Gratings Installed for Sump Condition	82

LIST OF FIGURES

Figure	Title	Page
2.1	Similitude of Highway Drainage Inlets	9
4.1	Grating for Model Type H Inlet	20
4.2	Gratings for Model Type H Inlet	21
4.3	Installation of Gratings for Type H Inlet	22
4.4	Gratings for Model Type 4-Ft and Model Type 6-Ft Inlets	23
4.5	Installation of Gratings for the Type 4-Ft Inlet and the Type 6-Ft Inlet	25
4.6	Schematic Diagram	27
4.7	Cutaway View of Testing Tank	30
4.8	Testing Tank with Channel and Inlet Grate	31
4.9	Installation of a Barrier	35
4.10	Installation of a Dike	35
5.1-5.4	Highest and Lowest Efficiencies for Type H Inlet Gratings (Long. Slope ½%-8%)	47-50
5.5-5.8	Efficiency Curves for Type H Inlet Gratings (Long. Slope ½%-8%, Swale Slope 12:1)	51-54
5.9-5.14	Efficiency Curves for Type H Inlet Gratings (Long. Slope ½%-8%, Swale Slope 6:1)	55-60
5.15	Highest and Lowest Efficiencies for Type 4-Ft Inlet Grating (Long. Slope ½%-8%)	69
5.16-5.19	Efficiency Curves for Type 4-Ft Inlet Grating (Long. Slope ½%-8%)	70-73
5.20	Highest and Lowest Efficiencies for Type 6-Ft Inlet Grating (Long. Slope ½%-8%)	74
5.21-5.24	Efficiency Curves for Type 6-Ft Inlet Grating (Long. Slope ½%-8%)	75-78
5.25	Vortex Developed in Test No. 268	80
5.26-5.31	Sump Effect for Type H Inlet Gratings	83-85

ABSTRACT

An experimental investigation is presented of the performance of some inlet gratings installed in grassed channels along highways in Pennsylvania. The purpose of this study was to provide information to aid in the design of spacing highway drainage inlets in grassed channels. The channel considered was triangular in cross section with one side (swale slope) having a slope of 12:1 or 6:1. The other side (back slope) had slopes ranging from 12:1 to ½:1.

The drainage inlet gratings studied were (1) the Type H Inlet Grating, (2) the Type 4-Ft Inlet Grating, and (3) the Type 6-Ft Inlet Grating. The gratings for the Type H Inlet consisted of a standard grating and two proposed gratings. All three types of inlet gratings are standard inlet gratings used by the Pennsylvania Department of Transportation.

Each model inlet grating was built to half the scale of the prototype, and each was tested under a variety of channel configurations and with a range of channel flow rates. The capacity of an inlet grating was determined by actual measurements, and thus the efficiency of the grating was obtained.

A series of curves, relating efficiency to capacity for a grating, are presented in the study. The curves, called efficiency curves, show that as more water flows in the channel toward an inlet grating the efficiency of the grating decreases. The knowledge obtained from this investigation provides information that is more

adequate to the designer in determining the spacing of highway drainage inlet gratings in grassed channels than the information presently available.

1. INTRODUCTION

1.1 Background and Need for Investigation

The problem of draining highways has been solved commonly by employing empirical or intuitional approaches, although the drainage system of a highway occupies a prominent place in the design of highways.

Runoff from precipitation must be removed from highways, that is, from both the paved surface and the adjacent areas, such as the embankment and the median, if any, between two pavements. The adjacent areas are usually covered by grass, and the water is removed by means of drainage inlets which lead the water into an underground drainage system. The drainage inlets are spaced along the roadside at intervals which are determined by the design runoff and by the expected capacity of the particular drainage inlets.

Inability of an inlet to intercept all the oncoming water will result in water overflowing and eventually bypassing the inlet. This flow will continue downstream in the channel to the next inlet which will be bypassed by more water; this condition will continue downstream to the lowest inlet, causing possible flooding of the roadway and adjacent areas at that station. This is undesirable for several reasons, such as (1) traffic safety, (2) maintenance of the pavement, which will deteriorate by the seepage water causing premature failure of the highway, (3) large amount of sediment and debris, which accumulate in low-lying areas. The bypassing water, or carryover, occurs apparently because the amount of water intercepted by the inlet is inadequate

owing to insufficient design and spacing or because the inlet openings are clogged by debris.

Estimation of the capacity of inlets has been based on past experience; furthermore, it is commonly assumed that a particular drainage inlet has a certain capacity regardless of channel configuration and the nature of channel surface. Thus, the actual capacities of some existing inlets are not known at present. Obviously, the hydraulic performance of any drainage inlet must be thoroughly understood in order to improve the design and spacing of inlets.

The characteristic curve of flow through a drainage inlet is almost impossible to obtain analytically because of the inherent complexity of the problem. Several variables are involved, such as the longitudinal slope, the two side slopes, the roughness of the channel, the different grates and sizes of inlets, and the significance of obstacles close to the inlets. The only alternative solution to the problem is actually testing the drainage inlets, using either prototype or model inlets. Models, smaller than the prototype, are used in this study; the justification for this is stated in Section 2.1.

A study of the available literature, made by YUCEL et al. (1969), showed that performance of drainage inlets has been investigated by numerous researchers. Most prominent of those are LARSON et al. (1949), investigators at the JOHNS HOPKINS UNIVERSITY (1956), and the U. S. ARMY CORPS OF ENGINEERS (1964). However, these studies involved only city street gutter inlets, using rather narrow channels, about three

feet in width at the maximum; thus no consideration was given to the adjacent areas.

1.2 Problem Statement

This study deals primarily with determining the capacity of drainage inlets by means of model experiments, using a prototype-model scale ratio of 2:1. Measurements from the model are transformed by use of model laws as discussed in Chapter 2. Also the encroachment of water onto the highway pavement and the depth of flow at three stations were measured. In addition, specific phenomena were investigated, such as the effect of a sump condition and the effect of a dike downstream from the inlet.

Six standard drainage inlets, as presently (1972) used by the Pennsylvania Department of Transportation (PennDOT), were tested in the model under a variety of conditions. The inlets that are customarily installed in paved channels had been previously tested (YEE (1972)). The remaining three inlets are installed in grass covered channels. The inlets are designated as the (1) Type H Inlet, (2) the Type 4-Ft Inlet, and (3) the Type 6-Ft Inlet; this study deals exclusively with those three inlets. The different channel configurations for which the three inlets were tested are indicated in Table 1.1.

All inlets were modeled according to PennDOT specifications, thus no attempt was made to alter the geometry of the inlet. However, on the basis of experimental data, such as those obtained in this study, the design and spacing of future drainage inlets can now be based on a considerably sounder background than previously.

Table 1.1: Summary of Channel Configurations

Inlet	Swale Slope	Back Slope	Longitudinal Slope
Type H	6:1,12:1	½:1, 1:1 2:1, 4:1	0.5%,2%,4%,8%
Type 4-Ft	6:1,12:1	4:1, 6:1 8:1,12:1	0.5%,2%,4%,8%
Type 6-Ft	6:1,12:1	4:1, 6:1 8:1,12:1	0.5%,2%,4%,8%

2. MODEL LAWS

2.1 General Remarks

Many problems in hydraulic engineering are too complicated to be solved analytically, owing to the present inadequate state of the art. Therefore, experiments have to be conducted to solve the problem. Commonly, the experiments are conducted on a model that is smaller than the prototype.

Inasmuch as a model simulates the prototype, one has to know the similitude between relevant properties in model and prototype, so that events in the model can be related to the prototype. This similitude is provided by means of model laws.

The justification for conducting experiments is, as argued, lack of an analytical solution, and the justification for using the results of model experiments is an economic one because models are usually smaller than the prototype and cheaper to fabricate. Another argument for the use of models is that model studies can be done more readily in or close to the laboratory, whereas to study the prototype requires a field installation.

In the present study of highway drainage inlets a scale ratio (length in prototype:length in model) of 2:1 is used. This ratio was determined after considering (1) the space available in the laboratory, (2) the available pumping facilities, (3) the cost of fabricating and operating the model, and (4) the effect of surface tension.

The literature has a vast amount of information on the theory of modeling. A comprehensive discussion is in STEVENS et al. (1942), GRAF (1971), and ENGELUND (1965). Illustrative examples and further references are available in MORRIS (1963) and HANSEN (1967).

2.2 Hydraulic Similitude

The correlation between physical quantities in the model and the prototype is called the similitude. In order to reproduce fully the real events in the model, three different similitudes have to be satisfied; they are, geometric similitude, kinematic similitude, and dynamic similitude.

Geometric Similitude. Two objects are said to be geometrical similar provided the ratios of corresponding dimensions are equal. In the model and prototype of Fig. 2.1 geometrical similitude exists if

$$L_R = \frac{D_p}{D_m}, \tag{1a}$$

$$L_R = \frac{L_p}{L_m}, \tag{1b}$$

$$L_R = \frac{\ell_p}{\ell_m}, \tag{1c}$$

where L and D denote length of the inlet and any depth of flow, respectively. L_R is the scale ratio and ℓ is a characteristic length. The subscripts p and m refer to prototype and model, respectively. The

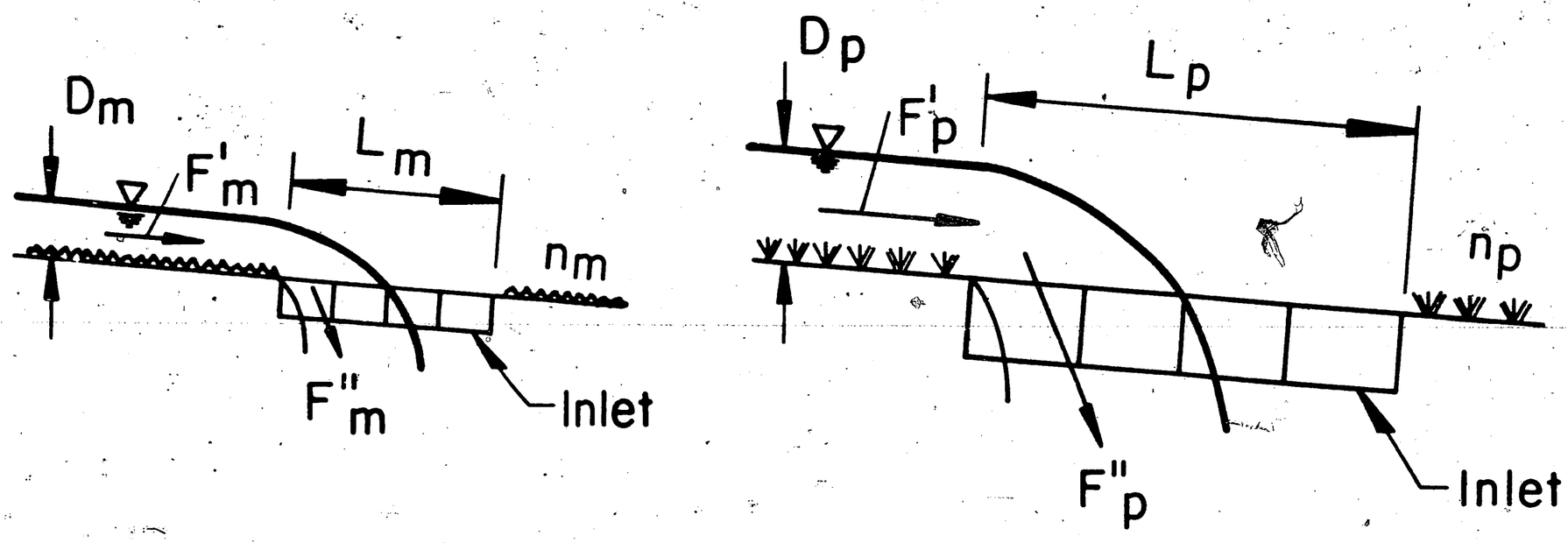

MODEL PROTOTYPE

Fig. 2.1: Similitude of Highway Drainage Inlets

similarity between areas and volumes can easily be derived from the scale ratio:

$$\frac{A_p}{A_m} = L_R^2, \text{ and} \tag{2a}$$

$$\frac{\forall_p}{\forall_m} = L_R^3, \tag{2b}$$

where A and $\forall$ denote area and volume, respectively. If the ratio of vertical distances does not equal the ratio of horizontal distances, the model is called a distorted model. However, no distortion in the scale ratio has been used in this study.

Kinematic Similitude. Two flow fields are said to be kinematically similar if the velocity vector-field of the model is similar to the velocity vector-field of the prototype.

Dynamic Similarity. Dynamic similarity exists between model and prototype if the corresponding forces are parallel and have the same force ratio at all points of the flow fields. From Fig. 2.1 the force ratio can be written as:

$$F_R = \frac{F'_p}{F'_m}, \text{ and} \tag{3a}$$

$$F_R = \frac{F''_p}{F''_m}, \tag{3b}$$

where F'_p and F''_p are two forces in the prototype, F'_m and F''_m are the corresponding forces in the model, and F_R is the force ratio. The types of forces which can affect a flow field are inertia F_I, gravity F_G, pressure F_P, viscosity F_V, elasticity F_E, and surface tension F_T. However, the latter two are considered negligible in this study because of the incompressible fluid and the size of the model. To secure complete dynamic similarity, the following equation must be satisfied:

$$\frac{(F_I)_p}{(F_I)_m} = \frac{F_{G_p}}{F_{G_m}} = \frac{F_{P_p}}{F_{P_m}} = \frac{F_{V_p}}{F_{V_m}} = F_R \tag{4}$$

2.3 Dimensionless Numbers

It is not so much the individual variables as certain dimensionless combinations of variables that are important in hydraulic modeling. The Euler number, the Froude number, and the Reynolds number represent such important dimensionless combinations, they will be discussed in the following.

The square root of the ratio of inertia force to pressure force expresses the Euler number, Eu:

$$Eu = \left(\frac{F_I}{F_p}\right)^{1/2} = \left(\frac{\rho\ V^2\ L^2}{\Delta p\ L^2}\right)^{1/2} = V\left(\frac{\rho}{\Delta p}\right)^{1/2} \qquad (5)$$

where ρ is density, V is a characteristic velocity, and Δp is a pressure difference. The square root of the ratio of inertia force to gravity force expresses the Froude number:

$$Fr = \left(\frac{F_I}{F_G}\right)^{1/2} = \left(\frac{\rho\ V^2\ L^2}{\rho\ L^3\ g}\right)^{1/2} = \frac{V}{(gL)^{1/2}} \qquad (6)$$

where g is gravitational acceleration. The ratio of inertia force to frictional force expresses the Reynolds number, Re:

$$Re = \frac{\rho\ V^2\ L^2}{\mu\ V\ L} = \frac{\rho\ V\ L}{\mu} \qquad (7)$$

where μ is dynamic viscosity. The dimensionless numbers, derived from the dynamic similarity, Eqs. (5) through (7), can in addition be derived by dimensional analysis.

Only two equations of Eqs. (5) through (7) are independent; that is, any third equation can be derived provided the other two are available. Consequently, dynamic similitude is ensured only if two of the three equations are simultaneously satisfied. However, this requirement for complete dynamic similarity is usually impossible to satisfy owing to certain limitations, such as inadequate fluids, and

limited space and facilities available in the laboratory. Fortunately, in most hydraulic engineering problems some forces are more significant than others. For example, if the force of gravity is one order of magnitude greater than the frictional force, Froude similarity alone is sufficient to ensure dynamic similitude between model and prototype.

2.4 Froude Model Law

The dimensionless combination of variables from Eq. (6) can be expressed for both the prototype and the model as follows:

$$Fr_p = Fr_m, \text{ or} \tag{8a}$$

$$\left(\frac{V^2}{g\ell}\right)_p = \left(\frac{V^2}{g\ell}\right)_m \tag{8b}$$

Solving for the velocity ratio and assuming constant acceleration of gravity, one obtains:

$$\frac{V_p}{V_m} = \left(\frac{\ell_p}{\ell_m}\right)^{1/2} = (L_R)^{1/2} \tag{9a}$$

Taking a scale ratio of 2.0, as used in the present study, the velocity ratio becomes:

$$\frac{V_p}{V_m} = 1.41 \tag{9b}$$

Knowing the velocity ratio, the flow-rate ratio is obtained from Eq. (2a) and (9a) as follows:

$$\frac{Q_p}{Q_m} = \frac{A_p}{A_m} \cdot \frac{V_p}{V_m} = (L_R)^2 \cdot (L_R)^{1/2} = (L_R)^{5/2} \qquad (10a)$$

With $L_R = 2.0$ in this study, Eq. (10a) becomes:

$$\frac{Q_p}{Q_m} = 5.66 \qquad (10b)$$

Knowing the model flow rate and the scale ratio, the prototype flow rate is calculated by means of Eq. (10b). Likewise the ratio of other flow parameters can be calculated; a complete list for Froude model similarity is in Table 2.1.

2.5 Manning Model Law

The effect of frictional forces was not incorporated in the Froude model law. Obviously, the channel roughness (grass) must have some influence on the flow pattern and consequently on the performance of the drainage inlets, hence a frictional criterion must be introduced. The Reynolds model law, which involves the frictional force, and the Froude model law cannot be fulfilled simultaneously if the same fluid has to be used. In such cases the Manning analogy is commonly introduced. This is an emperical frictional relationship derived from the Manning equation, which can be given for model and prototype as:

$$\left(\frac{R_h^{2/3} S^{1/2}}{V n}\right)_p = \left(\frac{R_h^{2/3} S^{1/2}}{V n}\right)_m \qquad (11)$$

where R_h is the hydraulic radius for the channel; S is the slope of the energy line; V, the mean velocity; and n, the Manning roughness

coefficient. For an undistorted model and with the hydraulic radius replaced by a suitable length, Eq. (11) becomes:

$$\left(\frac{\ell^{2/3}}{V\ n}\right)_p = \left(\frac{\ell^{2/3}}{V\ n}\right)_m \tag{12}$$

By introducing the Froude analogy from Eq. (9a), we obtain:

$$\frac{n_p}{n_m} = \left(\frac{L_p}{L_m}\right)^{1/6} \tag{13}$$

By rearranging Eq. (13) the flow-rate ratio evolves into

$$\frac{Q_p}{Q_m} = \left(\frac{L_p}{L_m}\right)^{8/3} \frac{n_p}{n_m} \tag{14}$$

Similarly, other flow characteristics can be found by simple manipulation; a list of prototype-model ratios for Manning model law is shown in Table 2.1.

The roughness of the prototype and the model, n_p and n_m, must be known in order to determine the flow-rate ratio in Eq. (14), which is of prime interest. The prototype roughness, which in this study is natural grass, has been stipulated to 0.035 according to CHOW (1959). An artificial grass known as "Astroturf" was used in the model to simulate natural grass; the Manning roughness coefficient of the model material was determined from flume tests to be 0.028 (see Chapter 3). The actual roughness ratio ($n_p/n_m = 1.125$) is found to be in very good agreement with the theoretical ratio (1.122), given by Eq. (13).

Table 2.1: Model Scales for Froude Similitude and Manning Similitude

		Froude Similitude	Lehigh Univ. Scale	Manning Similitude	Lehigh Univ. Scale*
Physical Properties	Length $\frac{\ell_p}{\ell_m}$	$\frac{\ell_p}{\ell_m}$	2.0	$\frac{\ell_p}{\ell_m}$	2.0
	Area $\frac{A_p}{A_m}$	$\left(\frac{\ell_p}{\ell_m}\right)^2$	4.0	$\left(\frac{\ell_p}{\ell_m}\right)^2$	4.0
	Volume $\frac{V_p}{V_m}$	$\left(\frac{\ell_p}{\ell_m}\right)^3$	8.0	$\left(\frac{\ell_p}{\ell_m}\right)^3$	8.0
Kinematic Properties	Time $\frac{t_p}{t_m}$	$\left(\frac{\ell_p}{\ell_m}\right)^{1/2}$	1.41	$\left(\frac{\ell_p}{\ell_m}\right)^{1/3} \frac{n_p}{n_m}$	1.38
	Velocity $\frac{v_p}{v_m}$	$\left(\frac{\ell_p}{\ell_m}\right)^{1/2}$	1,41	$\left(\frac{\ell_p}{\ell_m}\right)^{2/3} \frac{n_m}{n_p}$	1.27
	Discharge $\frac{Q_p}{Q_m}$	$\left(\frac{\ell_p}{\ell_m}\right)^{5/2}$	5.66	$\left(\frac{\ell_p}{\ell_m}\right)^{8/3} \frac{n_m}{n_p}$	5.10

*$n_m = 0.028$, $n_p = 0.035$

Introducing the actual roughness ratio and the scale ratio into Eq. (14), we obtain

$$\frac{Q_p}{Q_m} = 5.10 \qquad (15)$$

The application of the Manning equation requires that turbulent flow exist in both the prototype and the model. Inasmuch as practically all open-channel flow in nature is turbulent, the prototype flow is assumed turbulent. Considering the relatively low scale ratio (2.0) and the fact that the model roughness is the same as the roughness of the prototype, the flow in the model can also be assumed turbulent.

2.6 Concluding Remarks

Table 2.1 shows that Froude similitude, involving gravitational effects, does not differ significantly from Manning similitude involving frictional effects; which one to be selected is a matter of choice. Because the gravitational forces are of obvious importance, Froude similitude was selected to convert the results in this model investigation into prototype values.

3. ESTABLISHING MODEL ROUGHNESS

3.1 General Remarks

The roughness of the prototype surface, the highway embankments, is due to grass. Inasmuch as natural grass is inconvenient to use in the model, some kind of artificial roughness elements must be used instead. A desirable roughness coefficient can be determined from Manning model law. If both Froude similitude and Manning similitude are to be fulfilled, the ratio of prototype roughness to model roughness is given by Eq. (13). Assuming $n_p = 0.035$ and a scale ratio of 2.0, the model Manning roughness coefficient becomes 0.031. The problem is to find a material which has a Manning roughness coefficient of about 0.031.

3.2 "Astroturf"

Landscape Surface "Astroturf", which is a product of Mansanto Chemical Company, was selected to provide the necessary roughness of the model. The Manning roughness coefficient of "Astroturf" was determined as 0.028 from flume tests (see Appendix). This coefficient was considered satisfactorily close to the theoretical one of 0.031; thus "Astroturf" was used to simulate natural grass.

The advantages of using "Astroturf" is (1) it is reasonable in cost, (2) it is easy to handle, and (3) it has a favorable psychological effect on the observer.

4. EXPERIMENTAL INVESTIGATION

4.1 Drainage Inlets

Six different inlets are currently (1972) being used on the state highways of Pennsylvania. They are (1) the Type 4-Ft Special, (2) the Type 6-Ft Special, (3) the Type J, (4) the Type H, (5) the Type 4-Ft, and (6) the Type 6-Ft. Specifications of these inlets, designated as standards of the PennDOT, are summarized in Table 4.1. Note that the

Table 4.1: Standard Inlets

Inlet	Swale Slope	Back Slope	Origin*
Type 4-Ft Special	Paved Area	Paved Area	(a)
Type 6-Ft Special	Paved Area	Paved Area	(a)
Type J	Paved Area	Paved Area	(b)
Type H	Grassed Area	Grassed Area	(c)
Type 4-Ft	Grassed Area	Grassed Area	(a)
Type 6-Ft	Grassed Area	Grassed Area	(a)

*Standard Drawings, Pennsylvania Department of Transportation.

(a) Standard Drawing: S.I. 4&6, Rev. Nov. 1, 1961.

(b) Standard Drawing: Misc. Inlets, Type H and Type J Inlets, Approved May 8, 1968.
SD-13, Type B Divisor, Approved May 13, 1966.

(c) Standard Drawing: Misc. Inlets, Type H and Type J Inlets, Approved May 8, 1968.
Grating: (1) Standard Drawing: Misc. Inlets-Supplemental Sheet A.
(2) Longitudinal Bars, at 3-inch centers, suggested design.
(3) Diagonal Bars, at 3-inch centers, suggested design.

Type H inlet consists of three variants, a standard inlet and two with configurations different from the standard.

Only the inlets that are installed on grassed areas, that is, inlets (4) to (6), were investigated in this study. The channel configurations under which the inlets were tested are summarized in Table 1.1. The first three types of inlets were investigated by YEE (1972).

All inlets used in this study were made of wood. Each inlet differs from the other in either size or geometry of grate openings. All inlets were tested for the same set of longitudinal slopes and swale slopes, only the back slopes differ for the three types of inlets.

4.1.1 Type H Inlet

Figure 4.1 shows the geometry of the grating for the Type H Standard Inlet. Figures 4.2 (a) and (b) show the Type H Inlet with longitudinal and diagonal bars, respectively. Figure 4.3 shows the installation of the Type H Inlets for an arbitrary set of side slopes. The surface of the grating was flush with the underside of the artificial turf which covered all the different slopes except the steepest back slope ($\frac{1}{2}$:1). The surface of this slope was made of painted plywood which simulates concrete (YEE (1972)).

4.1.2 Type 4-Ft and Type 6-Ft Inlets

Figures 4.4 (a) and (b) show the geometry of the gratings for the Type 4-Ft Inlet and for the Type 6-Ft Inlet, respectively. For purposes of rigidity the wooden frames of these inlet gratings were $2\frac{1}{2}$ inches deep on the model rather than $1\frac{1}{2}$ inches as required from the

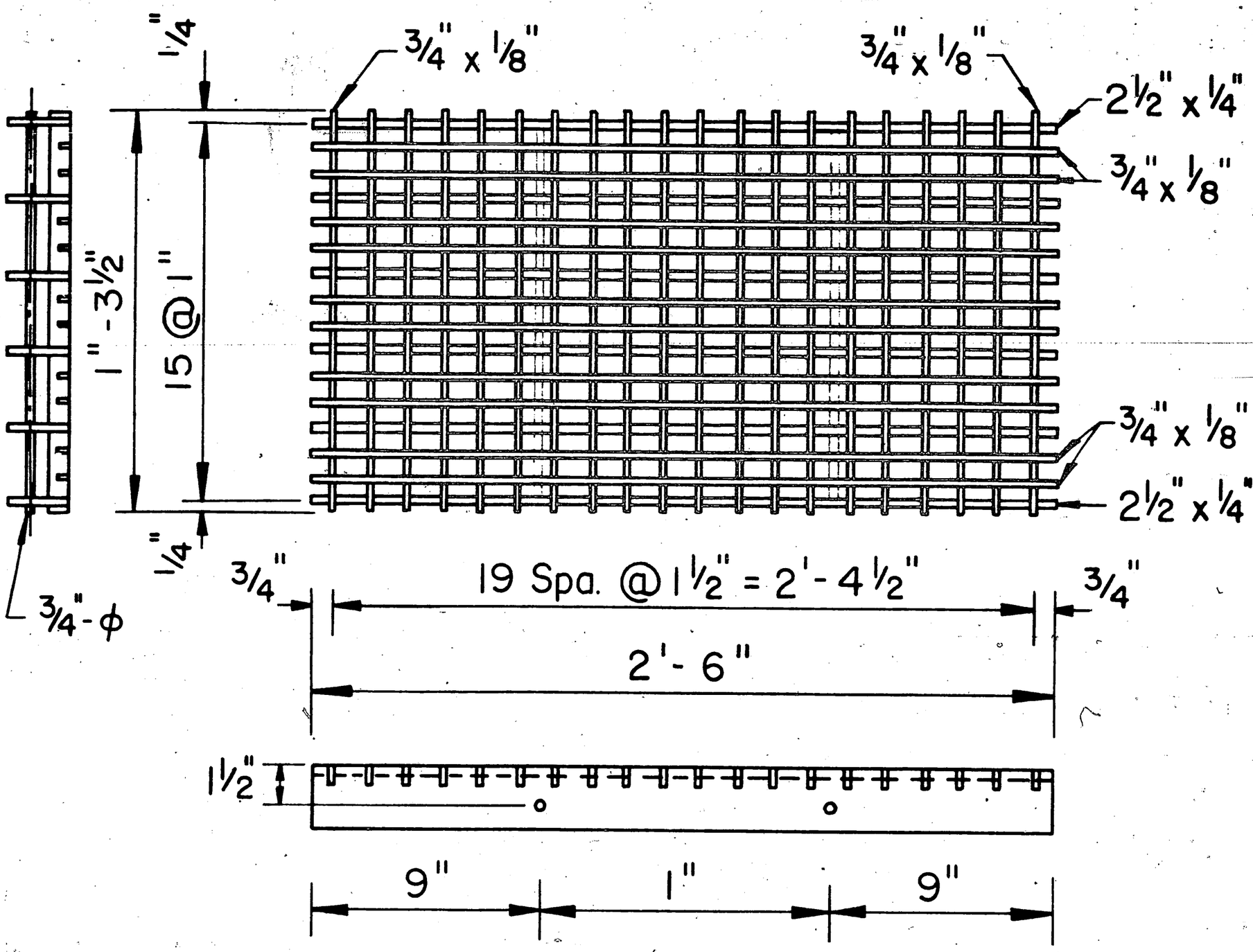

Fig. 4.1: Grating for Model Type H Standard Inlet

specifications. This change in depth of frames was considered to have no significance for the flow of water through the gratings. The installation of these two inlets differed from the installation of the Type H Inlets in two ways: First, they were placed symmetrically about the invert and in such a way that the inlets had the same longitudinal slope as the remainder of the model, whereas the inlets had a horizontal slope perpendicular to the invert of the channel. Second, the inlets could be lowered in two steps: to either ½-inch or 1-inch depression below grade, which in the prototype corresponds to 1-inch and 2-inch depression below grade, respectively. A rubber skirt was installed to prevent leakage around the inlets. Both side slopes were

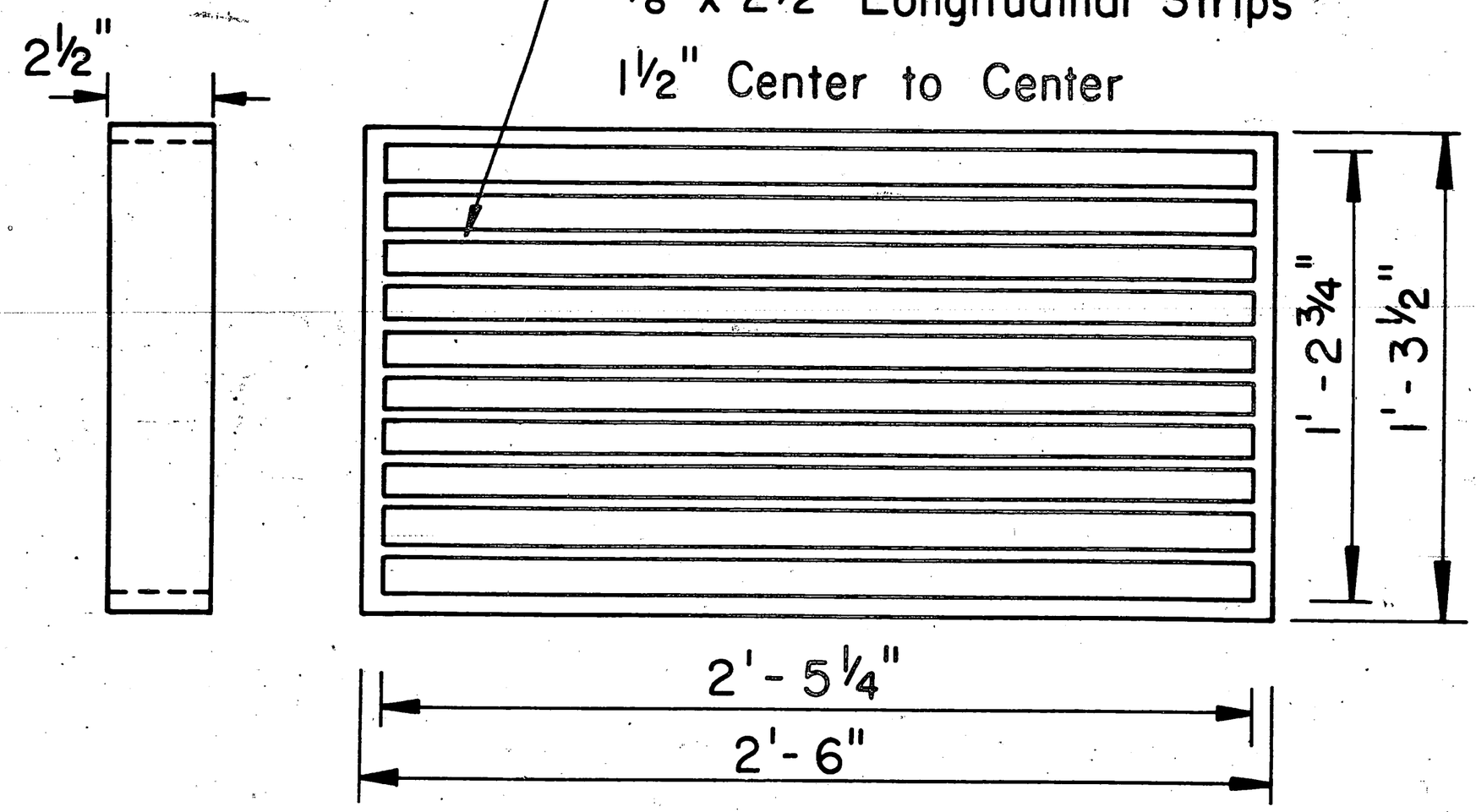

(a) Type H Longitudinal Bars

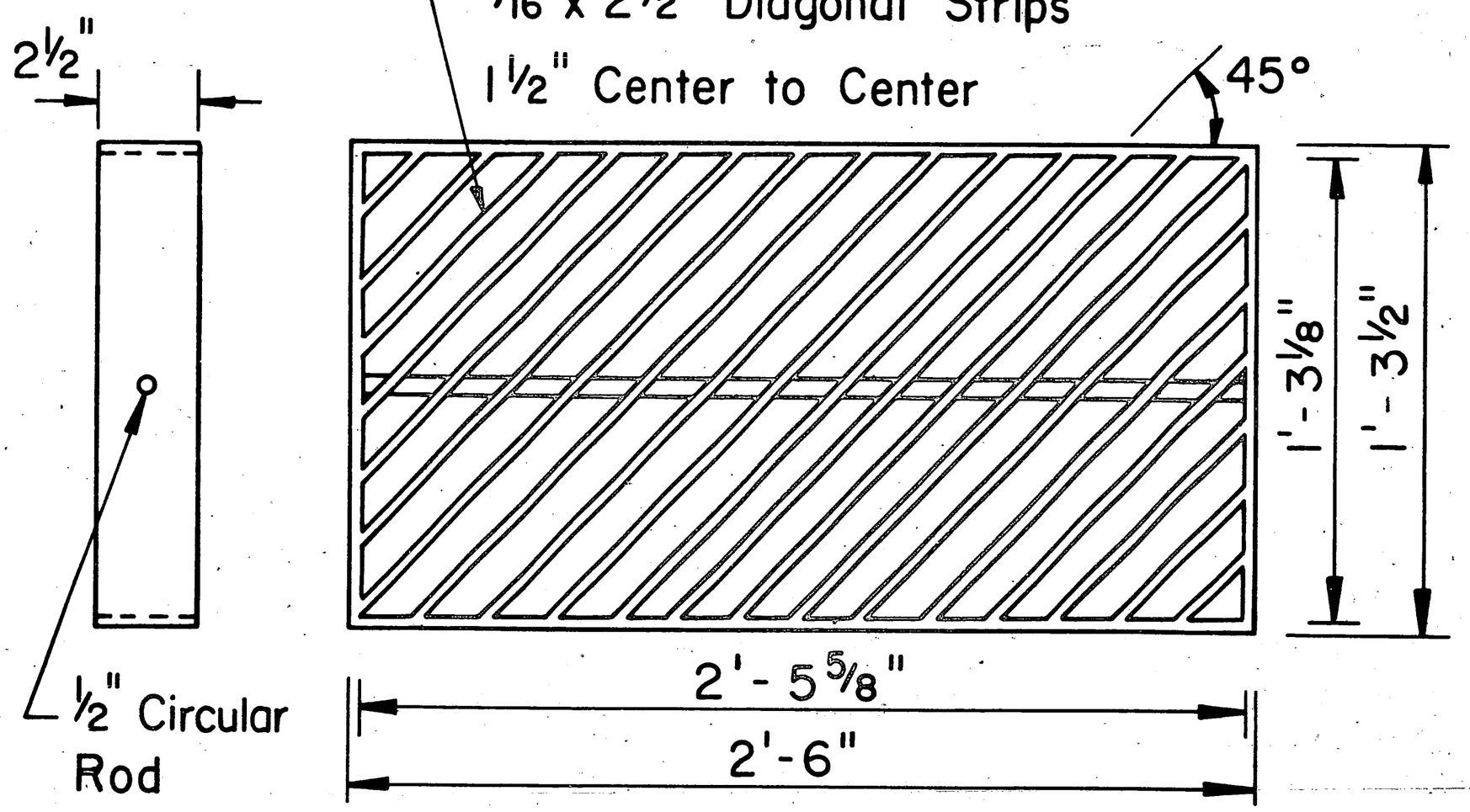

(b) Type H Diagonal Bars

Fig 4.2: Gratings for Model Type H Inlet

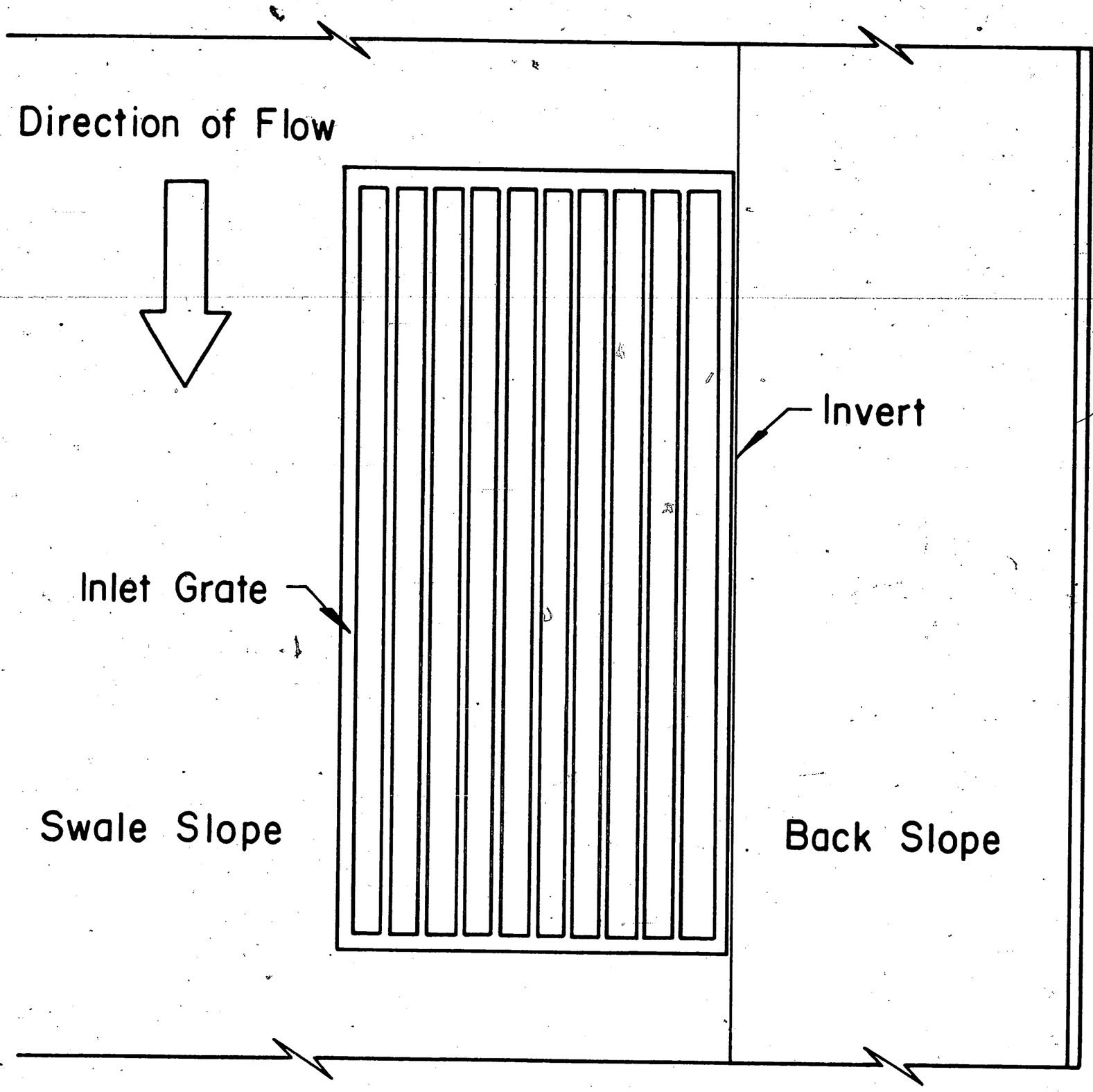

(a) Plan View

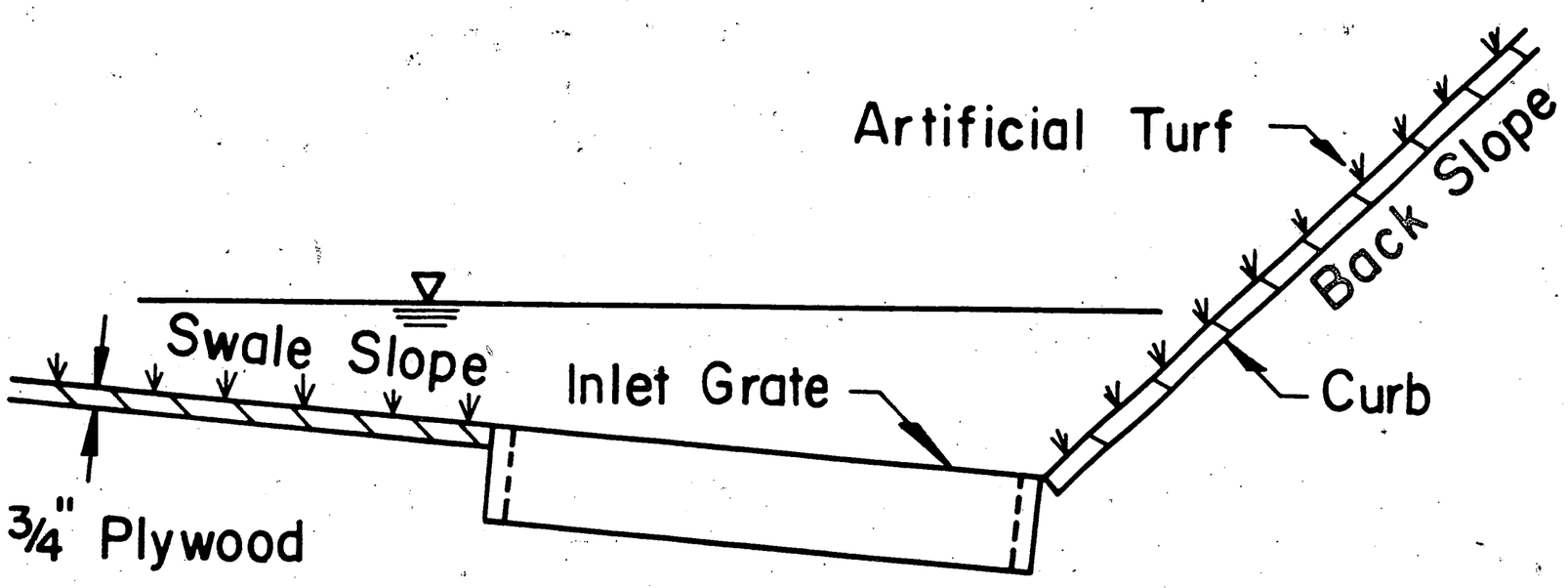

(b) Elevation View

Fig. 4.3: Installation of Gratings for Type H Inlet

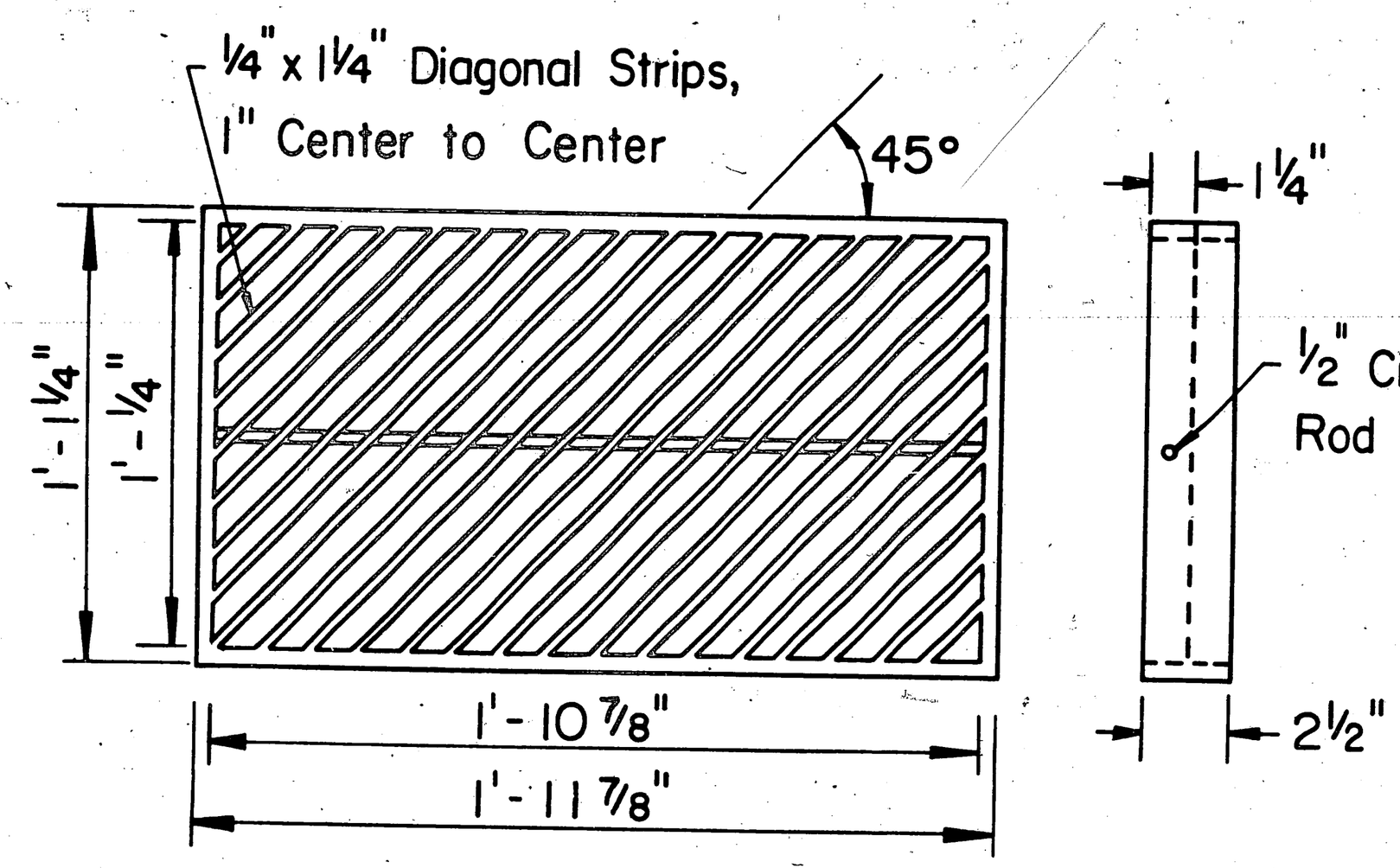

(a) Type 4-ft. Inlet

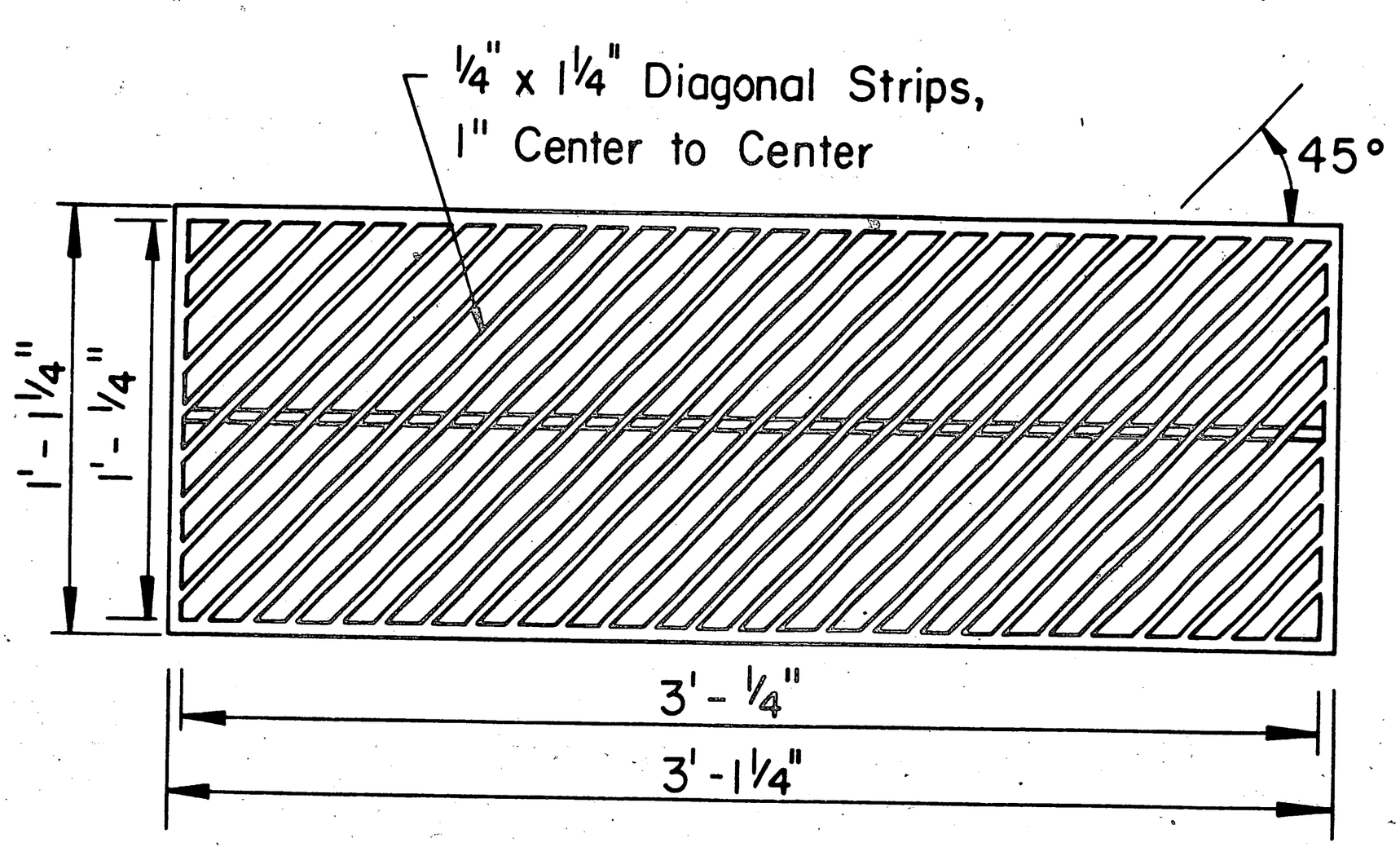

(b) Type 6-ft. Inlet

Fig. 4.4: Gratings for Model Type 4-Ft Inlet and Model Type 6-Ft Inlet

covered by artificial turf during all tests of Type 4-Ft and Type 6-Ft Inlets. Figure 4.5 shows the installation of the Type 4-Ft Inlet and the Type 6-Ft Inlet for a 1-inch depression.

4.2 Laboratory Equipment

4.2.1 General Requirements

A full-size model would be ideal in performing the experiments. However, owing to limited laboratory facilities, such as space and pump capacity, model experiments have to be carried out at a reduced scale. A prototype:model ratio of 2:1 was selected as a reasonable compromise as mentioned in Chapter 2.

The channel should be long enough to establish uniform flow upstream from an inlet. Water must be introduced onto the channel causing a minimal amount of flow distortion. In order to achieve this, baffles or vanes could be installed.

The frame supporting a model should be rigid. On the other hand, the model itself must be versatile, because the experiments to be performed involve longitudinal slopes that range from 0.2% to 8.0%, swale slopes from 8% to 16%, and back slopes from 8% to 200%. The mechanism used to change these slopes should be simple and rugged. The installation of the inlet gratings should be arranged so that the replacement of gratings requires a minimum of modification.

The surface roughness of the channel should bear a close resemblance to that of natural grass, that is, the Manning roughness

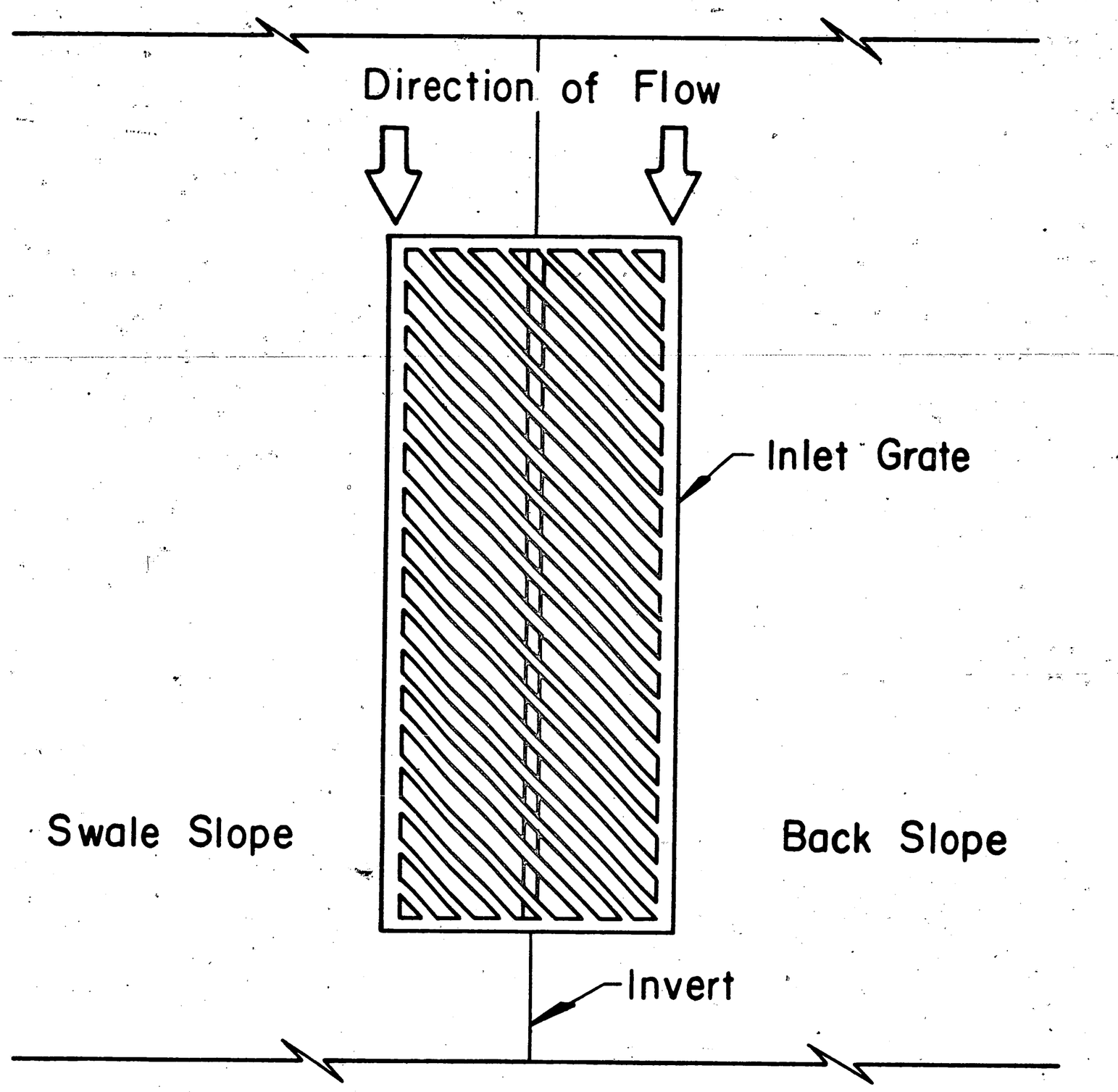

(a) Plan View

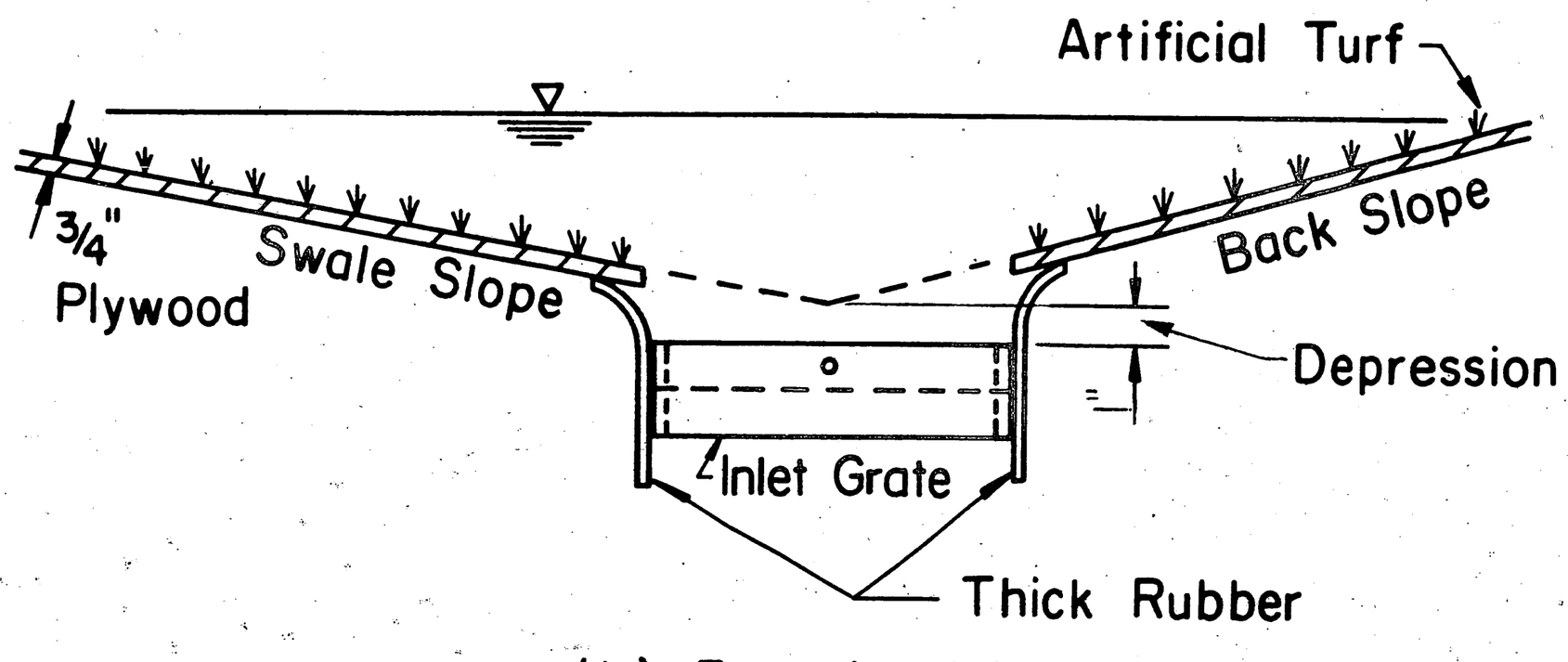

(b) Elevation View

Fig. 4.5: Installation of Gratings for the Type 4-Ft Inlet and the Type 6-Ft Inlet

coefficient for the prototype and the model should be as similar as possible. The Manning roughness coefficient of the material used in the model would have to be determined in the laboratory to ensure it has the proper roughness (see Appendix).

Inasmuch as the paramount objective of this study was to determine the efficiencies of different inlets under a variety of conditions, efforts should be made to ensure that measurements of the flow rate be made as accurate as possible. Obviously, leakage of water should be prevented in the entire system.

4.2.2 Apparatus

A schematic diagram of the testing arrangement is shown in Fig. 4.6. Two pumps (B) raise water from the main sump (A) into the pressure tank (D). The two pumps can be operated either in parallel or in series by adjusting the three valves (C).

Each pump is driven by a Westinghouse 9B Type HF Induction Motor equipped with a rheostatic control. One motor had a rating of 40 hp with a maximal speed of 1740 rpm; the other motor had a rating of 35 hp with a maximal speed of 1720 rpm. The system operates on 220 volts AC. During a test both motors were adjusted to a rate of discharge that was fairly constant over a period of time.

Each pump is a single-stage, double-suction, centrifugal pump, Type I of DeLaval manufacture. One pump had a 10-inch suction line and an 8-inch discharge line, whereas the other pump had an 8-inch suction line and a 6-inch discharge line.

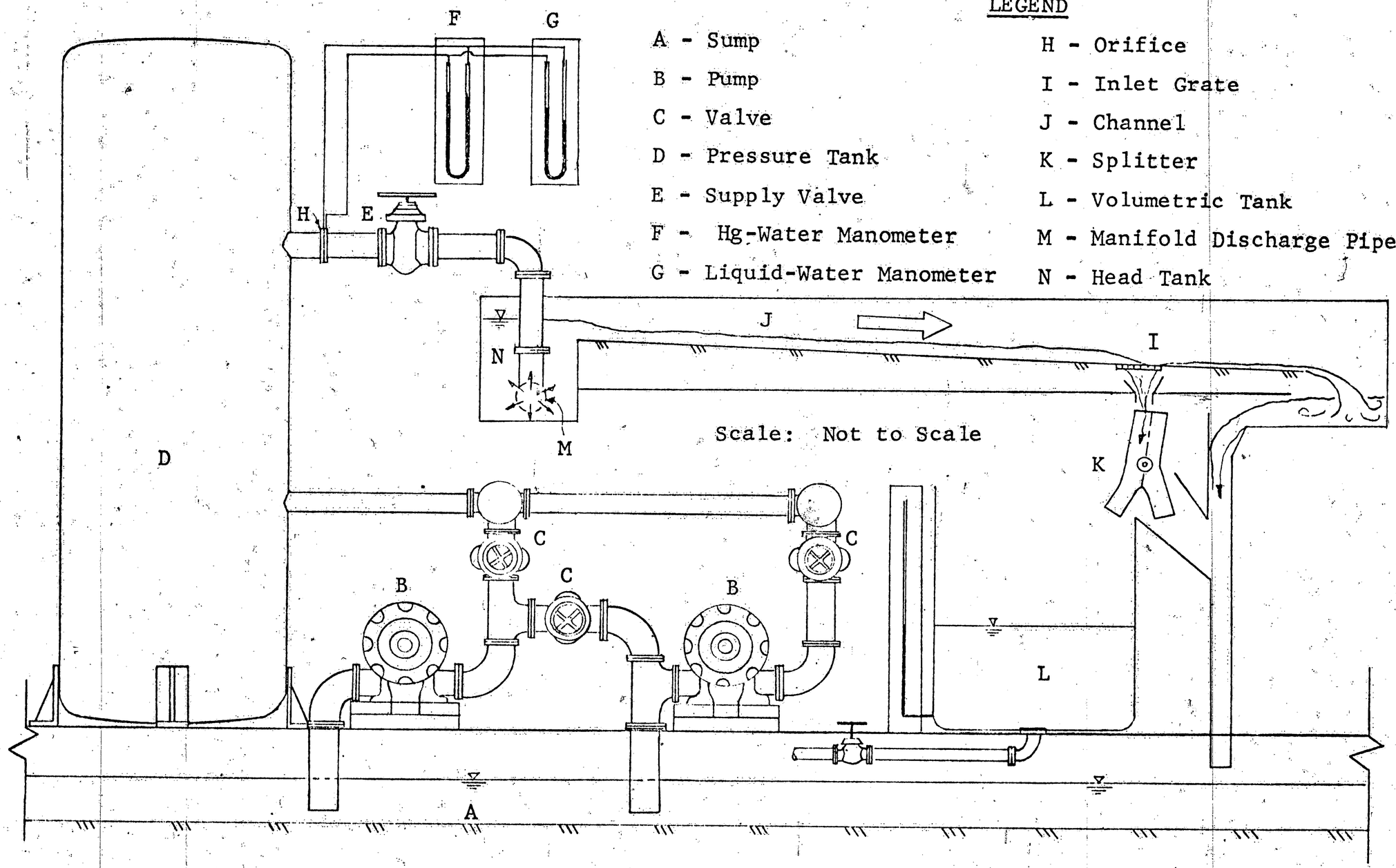

LEGEND

A - Sump
B - Pump
C - Valve
D - Pressure Tank
E - Supply Valve
F - Hg-Water Manometer
G - Liquid-Water Manometer
H - Orifice
I - Inlet Grate
J - Channel
K - Splitter
L - Volumetric Tank
M - Manifold Discharge Pipe
N - Head Tank

Scale: Not to Scale

Fig. 4.6: Schematic Diagram

The circular pressure tank (D) is 5½ feet in diameter and 34 feet high. The rate of discharge delivered to the manifold discharge pipe (M) in the head tank (N) was obtained by opening the supply valve (E). The rate of inflow was measured by means of a 4-inch orifice (H) placed upstream from the supply valve in a 12-inch pipe, using either a liquid-water manometer (G) for a discharge less than 1.5 cfs or by a mercury-water manometer (F) for a discharge greater than 1.5 cfs. The manometer liquid had a specific gravity of 2.95. The 4-inch orifice had been calibrated at the start of the testing and again after half of the tests had been made; each time with the same result, given as:

$$Q = 0.42\ H^{1/2}, \tag{16}$$

where Q is the discharge in cubic feet per second and H is the pressure drop across the orifice in feet of water.

From the head tank (N) the water flowed through the channel (J) toward the inlet (I). The amount of water intercepted by the inlet was directed by the splitter (K) into the volumetric tank (L), if a measurement of the interception was to be taken, or the water was returned directly to the main sump (A). The volumetric tank has a capacity of about 450 cubic feet. The amount of carryover was returned to the main sump (A).

The testing tank is rectangular in shape and made of ¼-inch steel plate framed by 3-inch angle iron (see Fig. 4.7). The bottom of the tank rests on beams placed transversely on 4-foot centers along the entire length of the testing tank. These beams are 2-inch by 7-inch

channels. The testing tank has an overall length of 33 feet, a width of 16 feet, and a depth of 3 feet. The head tank containing the manifold discharge pipe is 2½ feet long, 16 feet wide, and 4 feet deep.

Figure 4.7 is a cutaway view of the testing tank, and Fig. 4.8 shows the model placed in the testing tank. A conveyance channel (R), 1-foot deep with an average width of 2 feet, carries the water intercepted by the drainage inlet to an opening (T) connected to a volumetric tank. Another opening (U) near the downstream end of the testing tank is connected to the main sump.

During the process of calibrating the orifice, gates 1 and 3 were closed so that all water drained into the volumetric tank through opening (T) for measurement. During normal tests, gates 1 and 4 were closed in order to guide either the intercepted water to the volumetric tank or the carryover to the main sump.

4.2.3 Model Construction

Two steel frames were constructed to support the swale (O) (see Fig. 4.8) and back slope (P) which form a triangular channel. One frame was 28 feet long and 12 feet wide, and the other was 28 feet by 3½ feet. Both frames were made of S4 x 9.5 I-beams welded together. The welded joints were reinforced by clip angles in order to prevent any failure and to minimize deflection. The outer edges of the frames were made of S7 x 15.3 I-beams.

Both frames were covered with ¾-inch outdoor plywood; each piece, measuring 4 by 8 feet, was treated with one coat of preservative

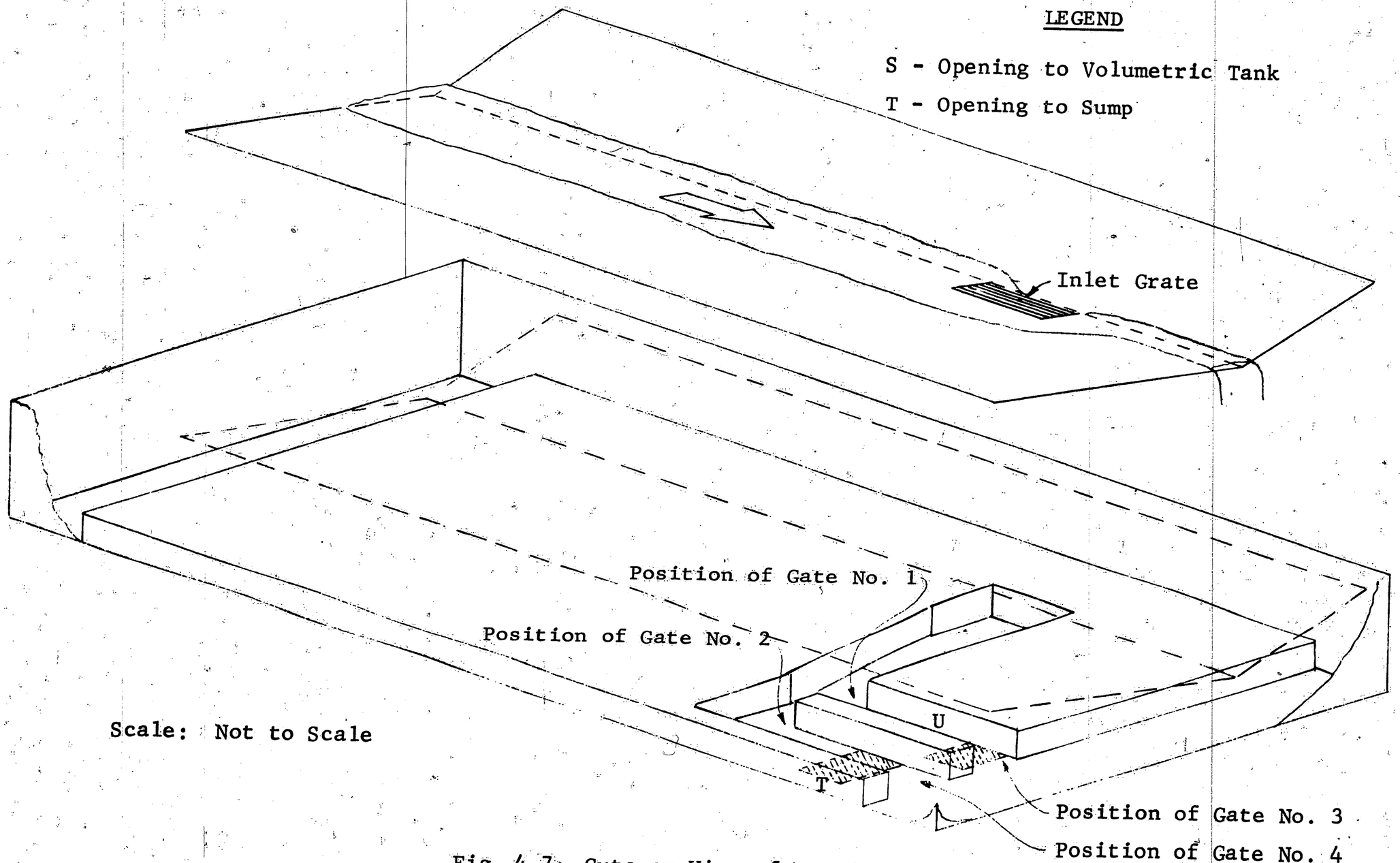

Scale: Not to Scale

Fig. 4.7: Cutaway View of Testing Tank

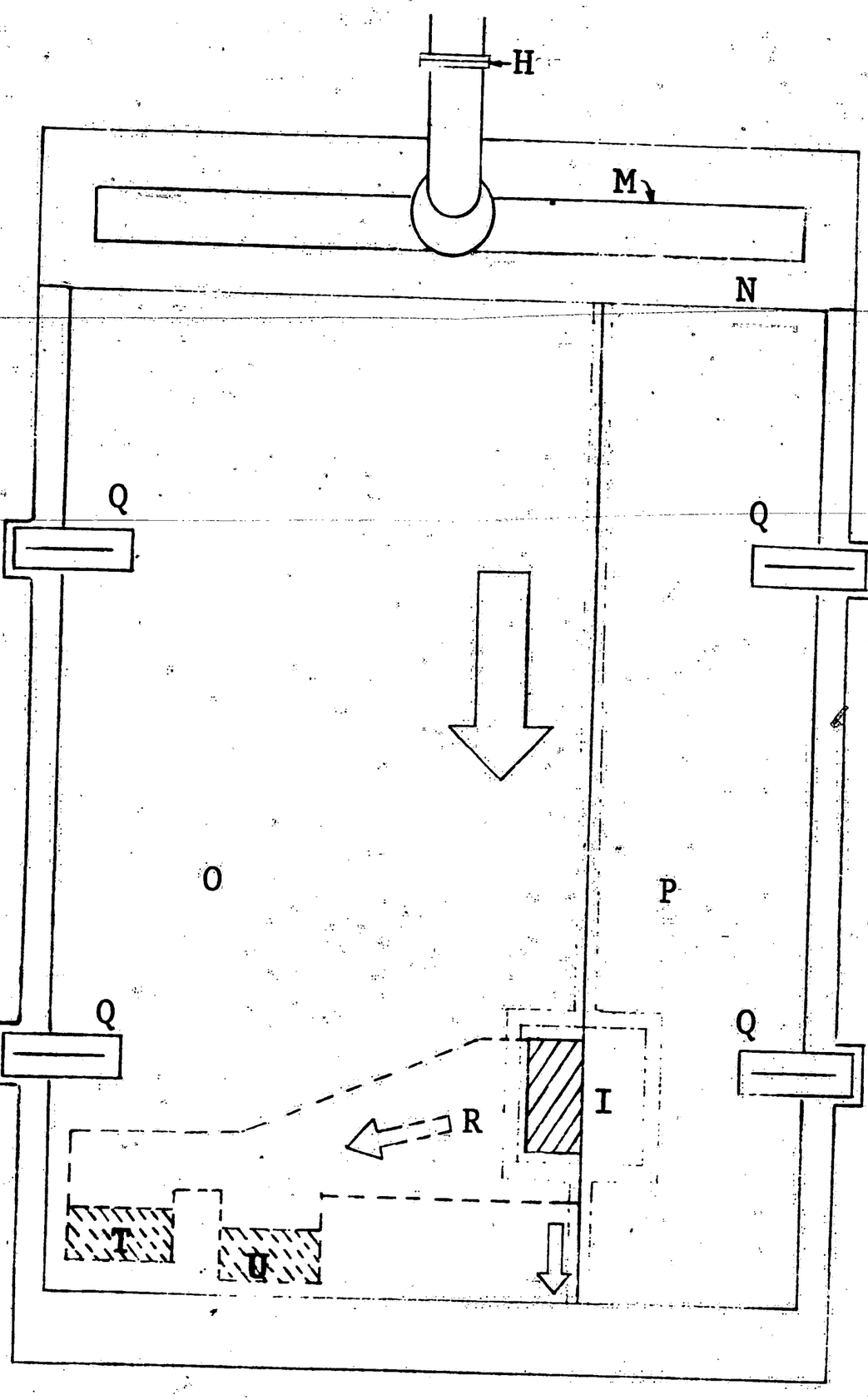

(a) Plan View

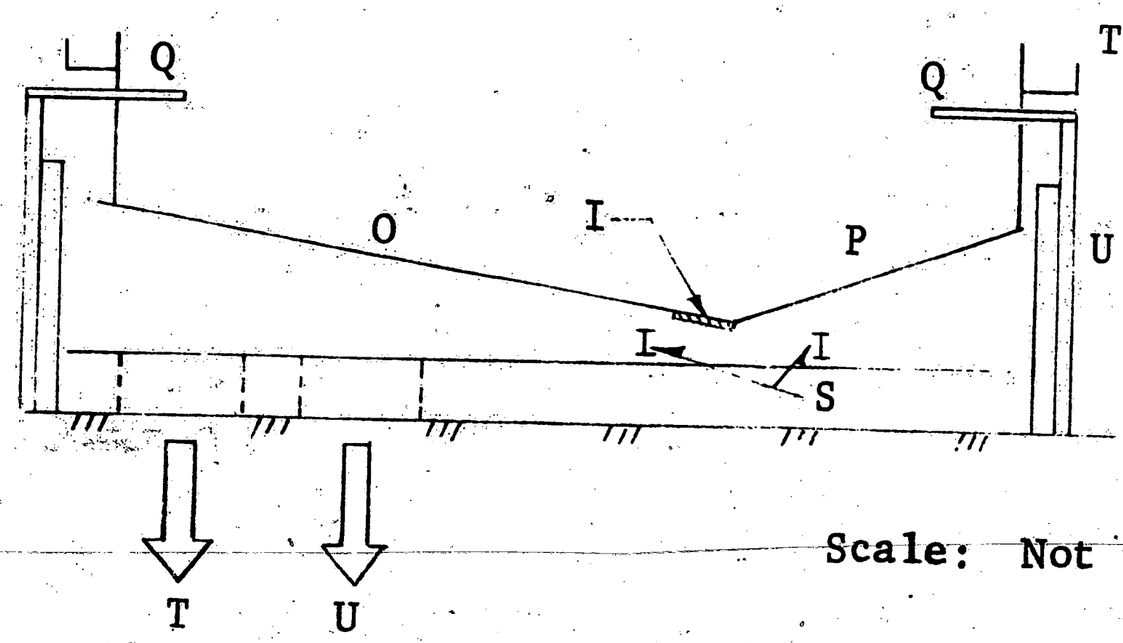

(b) Elevation View

LEGEND

H - Orifice

M - Manifold Discharge Pipe

N - Head Tank

O - Swale Slope

P - Back Slope

Q - Side-Slope Adjustment Rods

R - Conveyance Channel

S - Main Supporting I-Beam

I - Inlet Grates

T - Opening to Volumetric Tank

U - Opening to Sump

Scale: Not to Scale

Fig. 4.8: Testing Tank with Channel and Inlet Grate

and with two coats of enamel paint. The joints of the plywood were covered with a 2-inch self-adhesive transparent tape. The tape was later covered with an enamel paint. Hinges were welded to the invert of the channel in order to prevent the two steel frames from separating and to provide freedom for the frames to rotate about the invert whenever different side slopes were desired.

The entire length of the invert rests on a W8 x 40 I-beam (S). This main supporting I-beam is 28 feet in length and is hinged at its downstream end. By providing the proper height of support at the upstream end of the I-beam, any amount of longitudinal slope of the channel could be obtained to a maximal desired slope of 8.0%. Midpoint deflection of the I-beam was virtually eliminated by providing support at mid-span.

The main supporting beam was cut just upstream and downstream from the inlet (see Fig. 4.8) and a box section, made of the same material as the main beam, was installed to replace the cut piece of the main beam. This modification was done so that the water intercepted by the inlet could drop directly downward without splashing over any obstacle and so that each inlet could be lowered from its initial position.

The outer edge of the two frames was supported by four $^3/_4$-inch threaded tension rods (Q). Hence, each side slope could be raised or lowered independently of the other. Baffles were installed at the upstream end of the channel so as to aid in developing uniform flow as water approached the inlet.

4.3 Establishment of a Sump Effect

Highway drainage inlets located at the lowest point of a highway stretch are of special interest because water is approaching these inlets from both directions. Depending on the capacity of the particular inlet, a possible flooding or ponding condition will occur for sufficient high rate of flow. The effect of ponding, called the sump effect, has to be determined in the model. In order to do so one should introduce water into the channel from both ends with the inlet located at the lowest point of the model. However, due to limited space available in the laboratory this situation cannot be established. An approximate method was employed by installing a barrier perpendicular to the longitudinal direction of the model and placed on the centerline of the inlet, thus only permitting water to go through half of the inlet grate. Figure 4.9 shows how the barrier was installed. The barrier was made of $\frac{3}{4}$-inch plywood.

Because some inlet gratings do not have a symmetrical pattern, the flow situation of the water that should have been introduced from the opposite end of the model is not strictly the same as the one we are actually measuring. However, this inaccuracy was considered negligible, thus the full model capacity of an inlet placed at the bottom of a vertical curve is twice as much as that measured in the model.

4.4 Installation of a Dike

For some tests of the Type 4-Ft Inlet and of the Type 6-Ft Inlet, a dike was installed just downstream from the inlets perpendicular to the longitudinal direction. The dike was 6 inches high and both

slopes had an inclination of approximately 16%. This geometry of the dike was maintained for different longitudinal slopes. Figure 4.10 shows the installation of the dike. The slopes of the dike were covered with artificial turf.

4.5 Technique

4.5.1 Flow Measurements

As mentioned in Section 4.2.2, the flow rate into the head tank (N) was determined by means of the 4-inch orifice installed in the supply line. The orifice had previously been calibrated by a standard volumetric measuring method. The liquid manometer was used at discharge rates less than 1.5 cfs because it yielded more accurate results than the mercury manometer when the pressure drop across the orifice was small. The maximal obtainable discharge for the 4-inch orifice was 3.5 cfs, corresponding to a prototype discharge of 19.8 cfs. A higher discharge would necessitate a larger orifice.

The water intercepted by the inlet is directed into the volumetric tank after properly positioning the four gates in the conveyance channel. The amount of intercepted water was obtained by recording the change in water level in the volumetric tank. The flow rate (Q_2) is the amount of water measured in the volumetric tank divided by the time interval involved. The carryover flow (Q_3) is the difference between the channel or supply flow rate (Q_1) and the intercepted flow rate (Q_2).

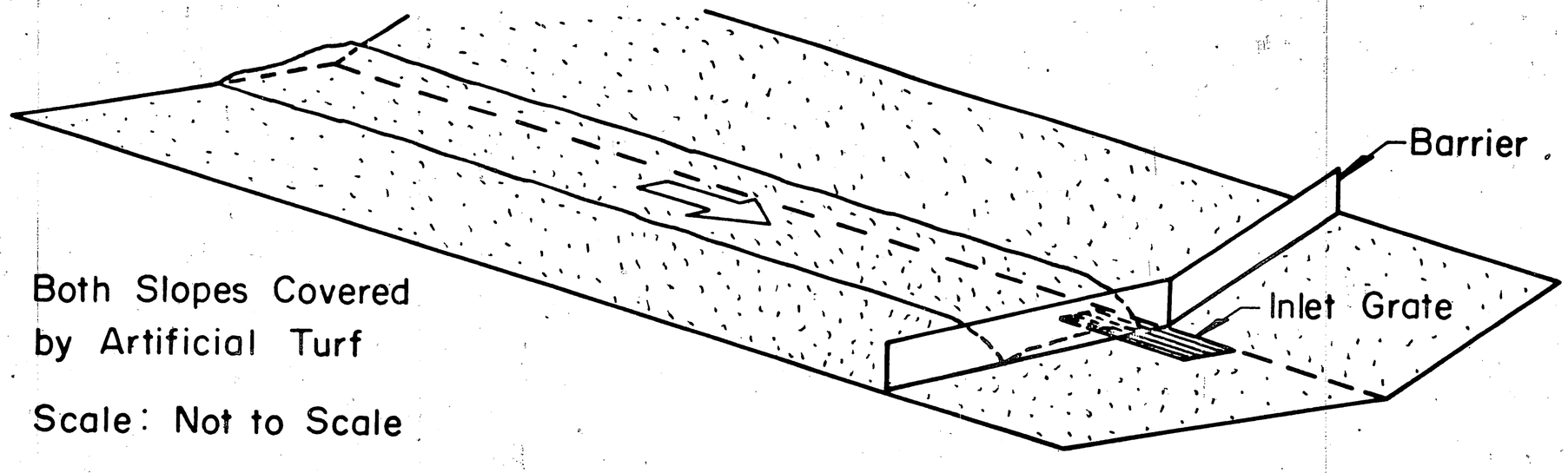

Fig. 4.9: Installation of a Barrier

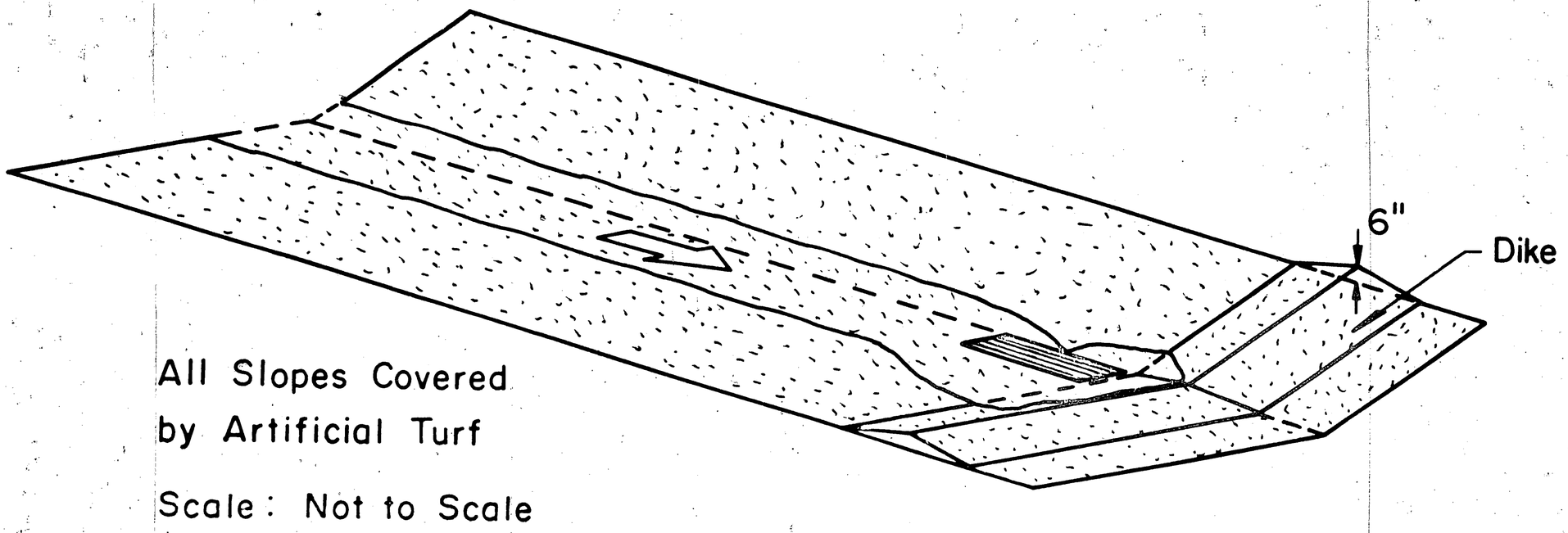

Fig. 4.10: Installation of a Dike

4.5.2 Depth Measurements

A point gage graduated to 0.001 ft was used for all depth measurements. The gage was mounted on a small carriage that rolls along a 3-inch by 5-inch aluminium rectangular channel 17 feet long. The aluminum channel was placed 2 feet above and at right angles to the invert of the channel. Both ends of the aluminum channel are supported by a monorail system which permits the beam to travel freely above the invert of the channel. Such an arrangement permits a depth measurement to be made at any point in the channel. During a test, measurements of depth were taken at stations that were 1 foot, 2 feet, and 3 feet upstream from the inlet gratings.

4.5.3 Spread Measurements

The spread of water on both side slopes was measured using the aluminum beam as range finder and a plumb bob to drop the perpendicular from the beam to the edges of the water. During a test, measurements of spread were taken at sections that were 1 foot, 2 feet, and 3 feet upstream from the inlet gratings.

4.6 Procedure

Prior to a test, the particular inlet grating was installed according to PennDOT specifications. The longitudinal slope was then adjusted and checked with the use of a surveyor's level. The appropriate side slopes were then established and checked by using triangular shaped templets and a level.

Subsequently, the supply valve was opened to a certain flow rate (Q_1) which was obtained by reading the pressure drop across the

orifice from the appropriate manometer; Eq. (16) was used to calculate Q_1.

A suitable time-interval (1 to 2 minutes) elapsed until a steady-state flow was obtained in the channel. Subsequently, depth and spread measurements were made. The amount of water intercepted by the inlet during half of a minute was guided by the splitter into the volumetric tank for determination of the interception, Q_2. By subtracting the intercepted flow rate (Q_2) from the supply flow rate (Q_1), the carryover flow rate (Q_3) was obtained.

After all measurements corresponding to one flow rate were recorded, the supply flow rate was slightly changed and the entire procedure was repeated. Usually 3 or 4 flow rates were considered sufficient to define an efficiency curve. The experimental data are in part summarized in Chapter 5.

5. RESULTS AND DISCUSSION

5.1 Presentation of Experiment Results

The entire testing program for this study is summarized in Tables 5.1 to 5.6. Significant trends of the results from all the tests* are displayed in Figs. 5.1 to 5.31.

The schedule for a test was arranged in such a way that a minimum of alteration and least amount of time were required in order either to change inlet gratings or to alter any of the three slopes of the channel. A few tests were repeated owing either to inadequate data points or to unsatisfactory results.

The efficiency of an inlet, indicated as η, is defined as $(Q_2/Q_1) \times 100\%$, where Q_1 is the channel flow (supply discharge) in cfs and Q_2 is the rate of flow, in cfs, intercepted by the inlet gratings. The efficiency, thus defined, is a significant variable which is used to illustrate the hydraulic performance of different inlets. Efficiency curves for certain gratings are presented in Figs. 5.1 to 5.4. The model channel flow rate, Q_1, is plotted on the lower horizontal axis against the efficiency in percent on the vertical axis. The upper horizontal axis represents the prototype channel flow rate; this quantity is related to the model channel flow rate by Eq. (10b).

In order to compare the efficiency of different inlets or the effect of various channel configurations, a family of efficiency curves is shown in each figure. The three dashes on a curve show the flow rate at which a water spread of more than 8 feet is exceeded on the swale

*Raw data are on file in Fritz Engineering Laboratory of Lehigh University.

in the prototype channel, corresponding to a spread of 4 feet in the model. The absence of the three dashes on a curve indicates that the spread of 4 feet on the swale of the model channel was not obtainable.

5.2 Discussion of Measurements

5.2.1 Flow Measurements

An orifice placed in the pipe that supplied the channel flow was to measure the flow rate. The range of channel flow rates was from 0.42 cfs to 3.40 cfs. Equation (16) was used to calculate the flow rate after obtaining the pressure drop across the orifice. The equation was corroborated by recalibration of the orifice.

The point of 100% efficiency is characterized by zero carryover ($Q_3 = 0$). This condition was obtained by actual observation of the carryover at the downstream side of the channel as the flow was decreased in small steps.

The intercepted flow rate was obtained by means of a volumetric measurement over a period of time, usually 30 seconds. It was found that such a time interval was both adequate and convenient.

5.2.2 Depth Measurements

As mentioned in Section 4.2.2, all depth measurements were obtained by means of a point gage. Depths were measured at the invert of the channel. Three depth readings for each flow rate were taken at stations that were 1-foot, 2 feet, and 3 feet horizontally upstream from the upper end of the inlet grating. If either the slope of the channel

was steep or the channel flow rate high, it was difficult to take depth measurements accurately owing to fluctuations of the water surface about some mean point. Another inaccuracy of the depth measurements was introduced by the poor definition of the channel bottom, because of the uneven texture of the mattresses of the artificial turf, which constituted the bottom of the channel (see Appendix). Consequently, the depth measurements are not considered accurate in the third decimal; thus, depth measurements are given to an accuracy of 0.01 foot.

Baffles were used at the upstream end of the channel in order to aid in developing uniform flow. The baffles were made of ¼-inch galvanized hardware cloth that was deformed and then placed in layers which were being successively soldered together.

5.2.3 Spread Measurements

The spread is defined as the encroachment of water onto either side slope. As mentioned in Section 4.2.3, each spread was measured as the horizontal normal distance from the invert of the channel to the edge of water on either side slope.

For slopes flatter than 4:1 the accuracy of the spread measurements was assumed no better than 0.1 foot, owing to fluctuations in the spread and to poor definition of the water edge on the artificial turf. For slopes steeper or equal to 4:1 the accuracy of the spread measurements was assumed to be 0.01 foot. Three spread readings on either slope were taken for each flow rate at stations that were 1-foot, 2 feet, and 3 feet horizontally upstream from the upper end of the inlet grating.

5.3 Efficiencies of Inlets

The main purpose of this study was to determine experimentally the efficiencies of three different types of inlet gratings used by the PennDOT under the channel configurations as indicated in Table 1.1. Inasmuch as the three types of inlet gratings are not identical in construction and installation, the efficiencies will differ from type to type when tested under the same conditions. Hence, it is only reasonable to compare the efficiencies of any particular type of inlet grating under certain different channel configurations. If a type of inlet grating consists of different variants, as is the case of the Type H Inlet, a comparison of the performance of these inlets will be sensible only if the gratings are similarly installed and have approximately the same grate openings but different grate patterns.

The efficiency curves of the three types of inlet gratings are shown in Figs. 5.1 to 5.24. By observation of these curves some general trends can be observed: (1) for a particular grating placed in a channel with fixed side slopes the efficiency decreases with increasing longitudinal slope, (2) the efficiency increases with increasing swale slope and is maximal if the back slope is equal to the swale slope, and (3) the efficiency of gratings with longitudinal bars is higher than the efficiency of gratings with diagonal and rectangular bars for any set of channel slopes.

5.3.1 Efficiencies of Type H Inlet

5.3.1.1 General Remarks

Figures 5.1 through 5.14 show efficiency curves for the three different gratings of the Type H Inlet. Table 5.1 summarizes

the testing program for the Type H Inlet and the capacity of the gratings for an efficiency of 100%.

Figures 5.1 through 5.4 show, each for a different longitudinal slope, curves for the channel configurations that gave the highest inlet efficiencies together with curves for the channel configurations that gave the lowest efficiencies for all three gratings. The curves indicate that the swale slope of the channel has a significant effect on the efficiency of the inlet gratings. An increase of the swale slope from 12:1 to 6:1 increases the efficiency approximately 12%.

The longitudinal slope of the channel also has effect on the efficiency of the inlet grating although not as significant as the swale slope. Generally, the efficiency of an inlet grating decreases as the longitudinal slope increases. If the longitudinal slope of the channel is steeper than 2%, some water, owing to its high inertia, flows or splashes along the top surface of the grating; thus, it bypasses the inlet. This phenomenon is assumed to be responsible for the relatively great scattering of the efficiency curves for the 8% longitudinal slope of the channel (Fig. 5.4). The inlet grating with longitudinal bars has much higher efficiency than the standard inlet grating for steep swale and longitudinal slopes owing to the different amount of water splashing over the surfaces of the two inlet gratings.

5.3.1.2 Efficiency Curves for Swale Slope 12:1

The differencies in the efficiencies of the three Type H Inlet gratings for a swale slope of 12:1 and different back and longitudinal

slopes are not very significant as indicated on Figs. 5.1 through 5.4. An example is the efficiency difference for the standard grating at a longitudinal slope of 0.5% and 8%, which only varies about 7%. Figures 5.5 through 5.8 present the efficiency curves for the three gratings for a fixed swale slope (12:1) but different back slopes. The longitudinal slope varies from one plot to another. Each grating was investigated for four different back slopes; thus, there are 12 efficiency curves from each longitudinal slope. The solid curve on each of Figs. 5.5 to 5.8 was drawn by eye to represent the 12 efficiency curves. A sample of the technique is shown on Fig. 5.5, which includes both the 12 efficiency curves and the representative curve. Those curves for the four different longitudinal slopes represent the efficiency curves with an accuracy of the efficiency of less than 5%, except for the 8% longitudinal slope where the accuracy is approximately 10%.

5.3.1.3 Efficiency Curves for Swale Slope 6:1

As previously mentioned, the scatter of the efficiency curves of the inlet gratings is larger for steep swale slopes than for flat swale slopes. This indicates that the efficiency curves for the inlet gratings in a channel with steep swale slopes cannot be represented by a single curve with a reasonable accuracy.

Figures 5.9 through 5.14 show the efficiency curves for the three different inlet gratings for a swale slope of 6:1 and different back slopes. The longitudinal slope varies from one plot to another. Figures 5.9 through 5.14 show that the grade of the back slope and the

particular type of grating become more and more important for the efficiency of an inlet grating as the longitudinal slope increases. For a longitudinal slope of ½%, the 12 efficiency curves can be represented by two curves with an accuracy of the efficiency of approximately 5%; whereas the efficiencies of gratings installed on an 8% longitudinal slope have such a scatter that they cannot be represented by a single line, as indicated on Figs. 5.13 and 5.14, where each line represents the efficiency curve for a particular channel configuration.

5.3.1.4 Concluding Remarks

The effect of the different inlet gratings on the efficiency of an inlet depends on the channel configuration, especially the longitudinal slope and the swale slope.

For a flat swale slope (12:1), the efficiency of an inlet grating installed at a particular longitudinal slope is practically the same for all of the three inlet gratings that were tested. The efficiency decreases only slightly with increasing longitudinal slope.

For a steep swale slope (6:1) both the type of inlet gratings, the back slope, and the longitudinal slope are found to be significant concerning the efficiency of an inlet. Generally, the standard inlet grating has a lower efficiency (approximately 5% at 0.5% longitudinal slope) than the inlet gratings with diagonal and longitudinal bars. The grating with longitudinal bars is more efficient (3% to 8% at 8% longitudinal slope) than the grating with diagonal bars on steep longitudinal slopes, whereas the opposite is true on flat longitudinal slopes.

Table 5.1: Comparison of Efficiencies of Type H Inlets

Run No.	Type H Inlet	Longl. Slope	Swale Slope	Back Slope	Q_2^{100} (cfs)
64	Stand.	0.5%	12:1	4:1	1.36
65	Long.	"	"	"	1.12
66	Diagl.	"	"	"	1.17
67	Stand.	"	6:1	"	1.79
68	Long.	"	"	"	1.58
69	Diagl.	"	"	"	1.57
70	Stand.	"	"	2:1	2.00
71	Long.	"	"	"	2.70
72	Diagl.	"	"	"	2.90
73	Stand.	"	12:1	"	1.18
74	Long.	"	"	"	1.20
75	Diagl.	"	"	"	1.29
76	Stand.	"	"	1:1	1.28
77	Long.	"	"	"	1.31
78	Diagl.	"	"	"	1.30
79	Stand.	"	6:1	"	2.43
80	Long.	"	"	"	2.65
81	Diagl.	"	"	"	2.69
82	Stand.	"	"	½:1	2.33
83	Long.	"	"	"	2.56
84	Diagl.	"	"	"	2.40
85	Stand.	"	12:1	"	1.35
86	Long.	"	"	"	1.35
87	Diagl.	"	"	"	1.43
88	Stand.	2%	12:1	½:1	1.12
89	Long.	"	"	"	1.25
90	Diagl.	"	"	"	1.43
91	Stand.	"	6:1	"	1.69
92	Long.	"	"	"	2.80
93	Diagl.	"	"	"	1.65
94	Stand.	"	"	1:1	2.17
95	Long.	"	"	"	2.67
96	Diagl.	"	"	"	2.40
97	Stand.	"	12:1	"	1.23
98	Long.	"	"	"	1.10
99	Diagl.	"	"	"	1.08
100	Stand.	"	"	2:1	1.27
101	Long.	"	"	"	1.25
102	Diagl.	"	"	"	1.31
103	Stand.	"	6:1	"	1.64
104	Long.	"	"	"	2.91
105	Diagl.	"	"	"	1.80
106	Stand.	"	"	4:1	1.54
107	Long.	"	"	"	1.62
108	Diagl.	"	"	"	1.42
109	Stand.	"	12:1	"	1.32
110	Long.	"	"	"	1.27
111	Diagl.	"	"	"	1.41

Note: (1) Longl.: Longitudinal
(2) Stand.: Standard
(3) Long.: Longitudinal bars
(4) Diagl.: Diagonal bars
(5) Q_2^{100} : Channel flow rate, Q_2, at an inlet efficiency of 100%

Table 5.1: Contd.

Run No.	Type H Inlet	Longl. Slope	Swale Slope	Back Slope	Q_2^{100} (cfs)	Run No.	Type H Inlet	Longl. Slope	Swale Slope	Back Slope	Q_2^{100} (cfs)
112	Stand.	4%	12:1	4:1	1.26	136	Stand.	8%	12:1	½:1	0.71
113	Long.	"	"	"	1.35	137	Long.	"	"	"	0.92
114	Diagl.	"	"	"	1.26	138	Diagl.	"	"	"	0.90
115	Stand.	"	6:1	"	1.25	139	Stand.	"	6:1	"	0.82
116	Long.	"	"	"	1.28	140	Long.	"	"	"	2.77
117	Diagl.	"	"	"	1.35	141	Diagl.	"	"	"	0.93
118	Stand.	"	"	2:1	1.36	142	Stand.	"	"	1:1	1.10
119	Long.	"	"	"	2.70	143	Long.	"	"	"	2.63
120	Diagl.	"	"	"	1.59	144	Diagl.	"	"	"	1.40
121	Stand.	"	12:1	"	1.07	145	Stand.	"	12:1	"	0.71
122	Long.	"	"	"	1.05	146	Long.	"	"	"	0.81
123	Diagl.	"	"	"	1.05	147	Diagl.	"	"	"	0.74
124	Stand.	"	"	1:1	0.89	148	Stand.	"	"	2:1	0.81
125	Long.	"	"	"	0.90	149	Long.	"	"	"	0.79
126	Diagl.	"	"	"	0.92	150	Diagl.	"	"	"	0.79
127	Stand.	"	6:1	"	1.65	151	Stand.	"	6:1	"	0.83
128	Long.	"	"	"	2.45	152	Long.	"	"	"	2.20
129	Diagl.	"	"	"	2.12	153	Diagl.	"	"	"	1.12
130	Stand.	"	"	½:1	1.40	154	Stand.	"	"	4:1	0.93
131	Long.	"	"	"	2.83	155	Long.	"	"	"	0.99
132	Diagl.	"	"	"	1.61	156	Diagl.	"	"	"	0.94
133	Stand.	"	12:1	"	0.92	157	Stand.	"	12:1	"	1.03
134	Long.	"	"	"	1.13	158	Long.	"	"	"	1.03
135	Diagl.	"	"	"	1.13	159	Diagl.	"	"	"	0.98

Note: (1) Longl.: Longitudinal
(2) Stand.: Standard
(3) Long.: Longitudinal bars
(4) Diagl.: Diagonal bars
(5) Q_2^{100} : Channel flow rate, Q_2, at an inlet efficiency of 100%

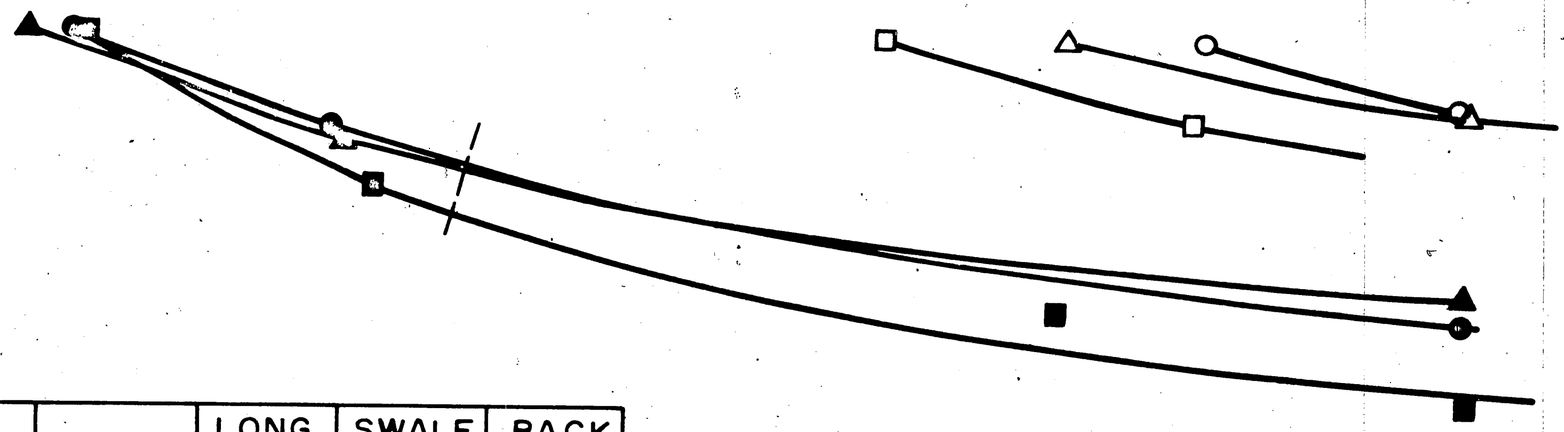

RUN	GRATE	LONG. SLOPE	SWALE SLOPE	BACK SLOPE	
79	Stand.	½%	6:1	1:1	□
71	Long.	½%	6:1	2:1	△
72	Diagl.	½%	6:1	2:1	○
73	Stand.	½%	12:1	2:1	■
65	Long.	½%	12:1	4:1	▲
66	Diagl.	½%	12:1	4:1	●

— — — Prototype Swale Spread 8 ft.

Fig. 5.1: Highest and Lowest Efficiencies for Type H Inlet Gratings (Long. Slope ½%)

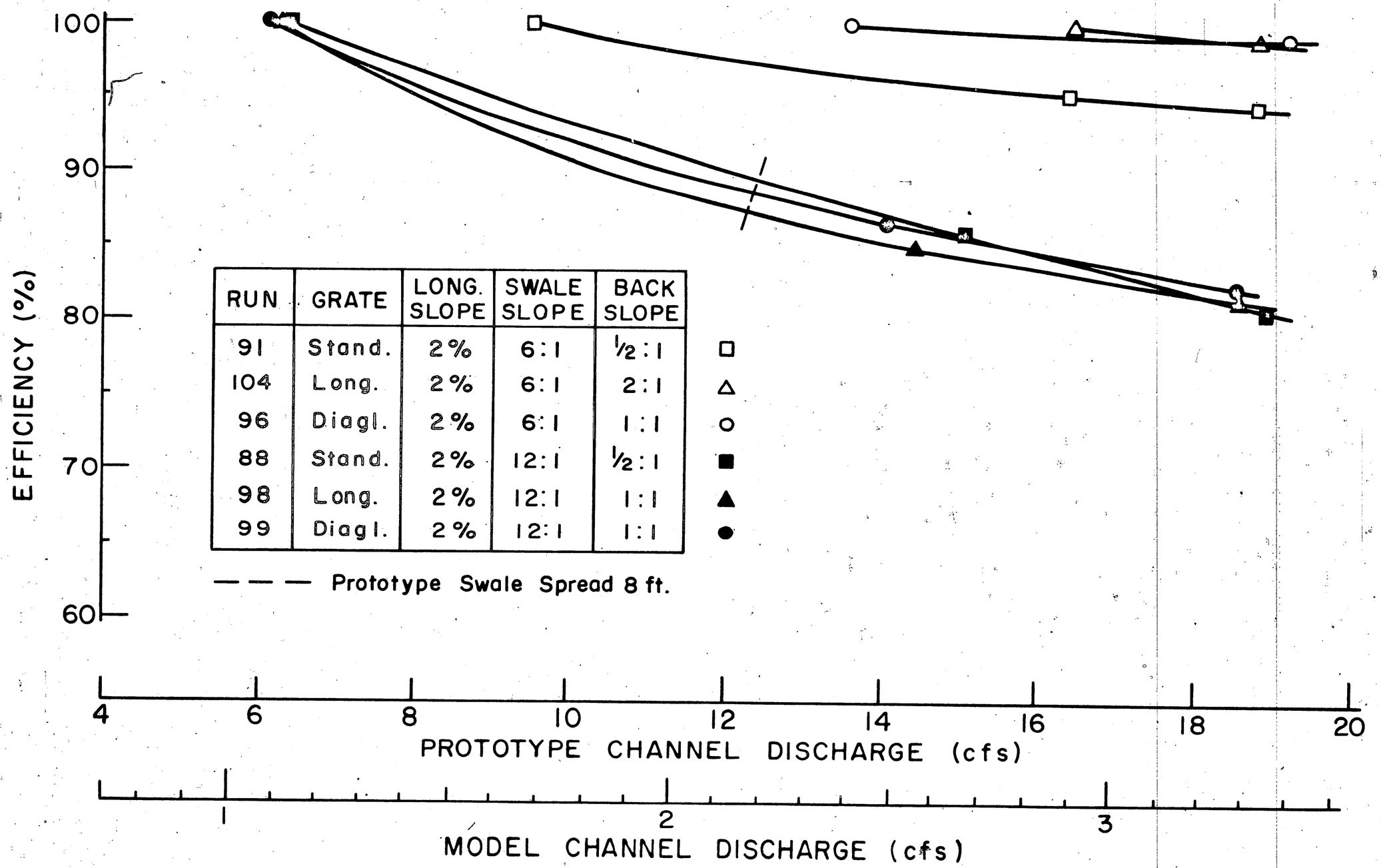

RUN	GRATE	LONG. SLOPE	SWALE SLOPE	BACK SLOPE	
91	Stand.	2%	6:1	½:1	□
104	Long.	2%	6:1	2:1	△
96	Diagl.	2%	6:1	1:1	○
88	Stand.	2%	12:1	½:1	■
98	Long.	2%	12:1	1:1	▲
99	Diagl.	2%	12:1	1:1	●

Fig. 5.2: Highest and Lowest Efficiencies for Type H Inlet Gratings (Long. Slope 2%)

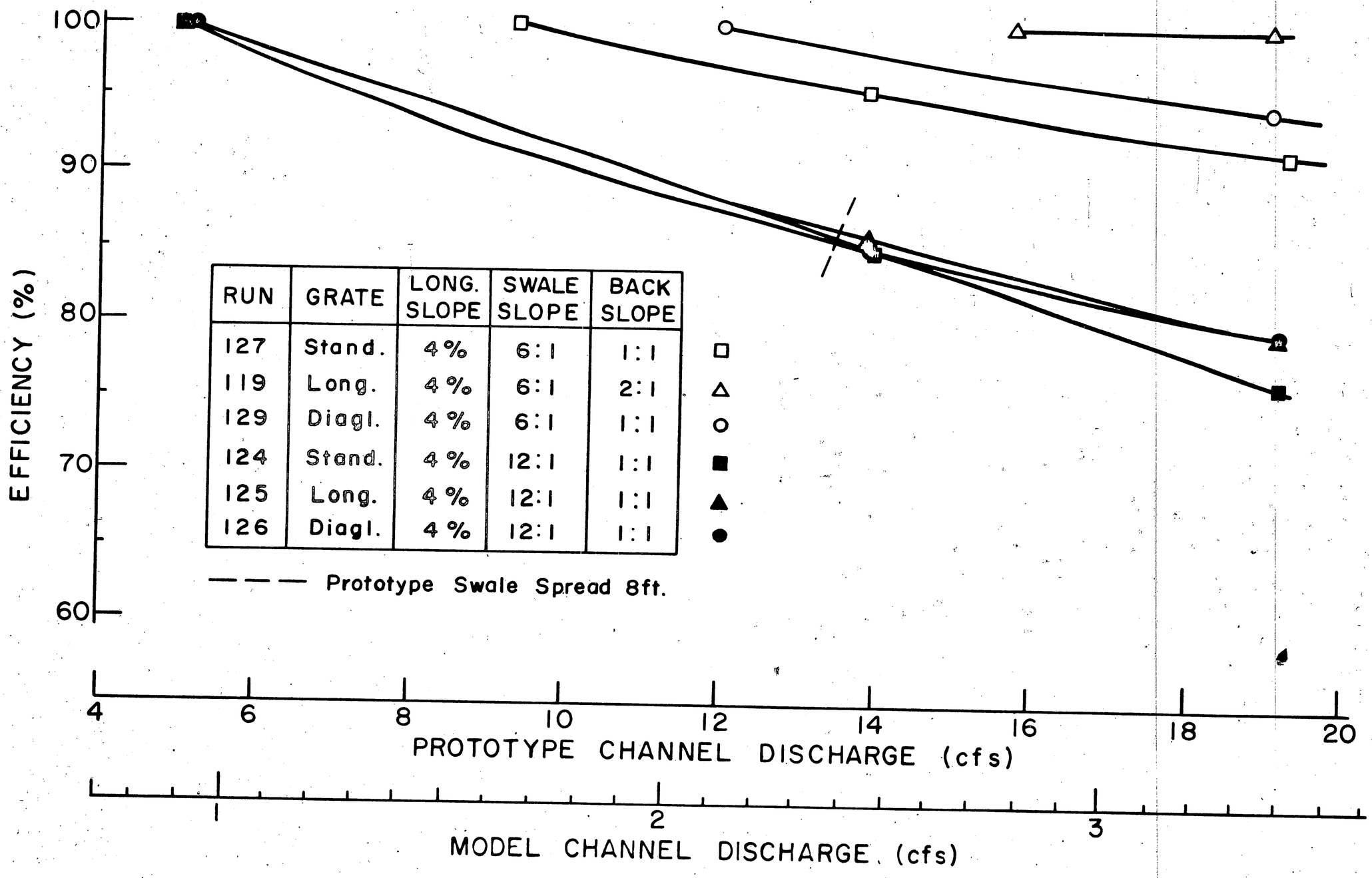

RUN	GRATE	LONG. SLOPE	SWALE SLOPE	BACK SLOPE	
127	Stand.	4%	6:1	1:1	□
119	Long.	4%	6:1	2:1	△
129	Diagl.	4%	6:1	1:1	○
124	Stand.	4%	12:1	1:1	■
125	Long.	4%	12:1	1:1	▲
126	Diagl.	4%	12:1	1:1	●

Fig. 5.3 Highest and Lowest Efficiencies for Type H Inlet Gratings (Long. Slope 4%)

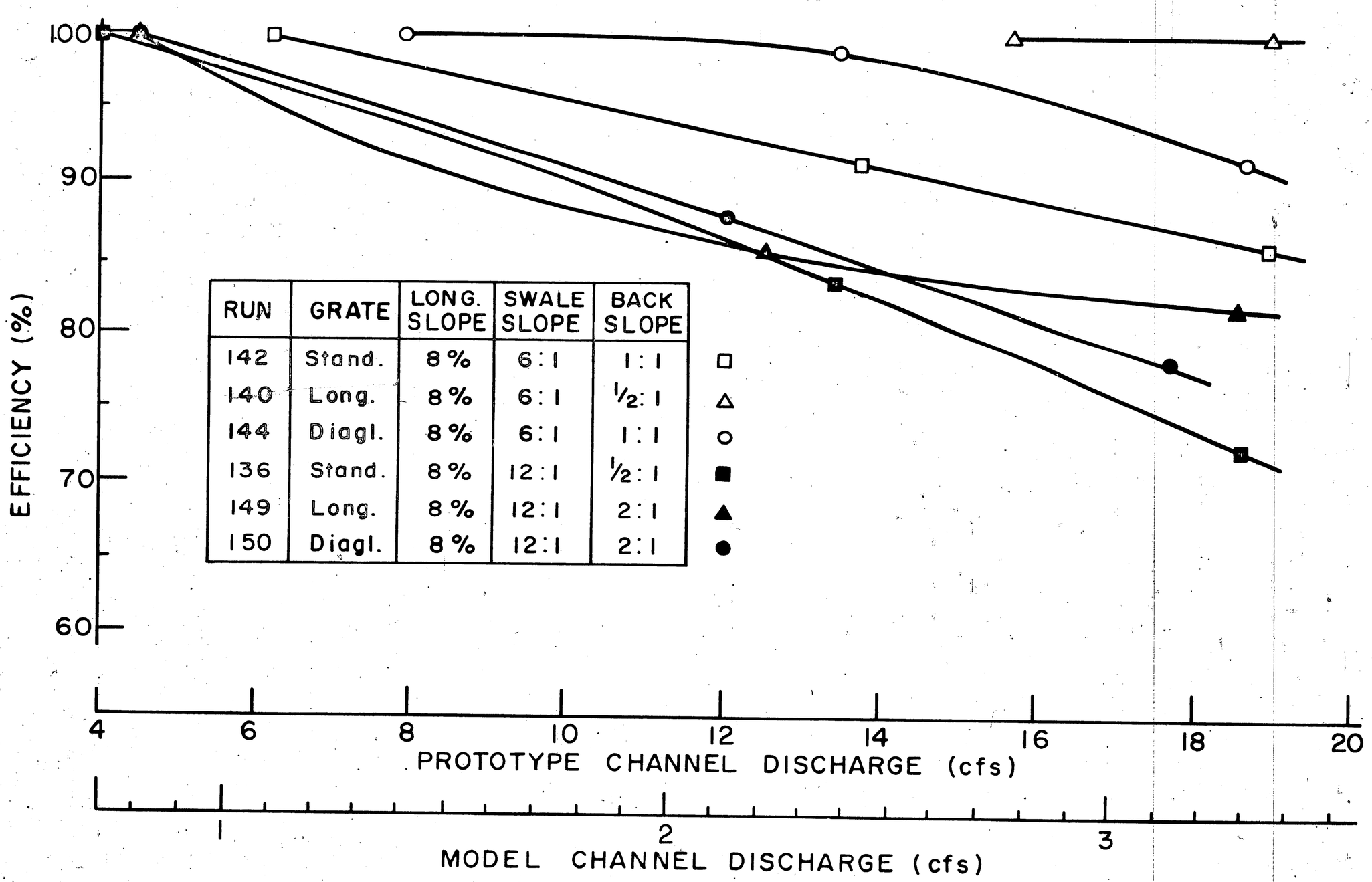

RUN	GRATE	LONG. SLOPE	SWALE SLOPE	BACK SLOPE	
142	Stand.	8%	6:1	1:1	□
140	Long.	8%	6:1	½:1	△
144	Diagl.	8%	6:1	1:1	○
136	Stand.	8%	12:1	½:1	■
149	Long.	8%	12:1	2:1	▲
150	Diagl.	8%	12:1	2:1	●

Fig. 5.4: Highest and Lowest Efficiencies for Type H Inlet Gratings (Long. Slope 8%)

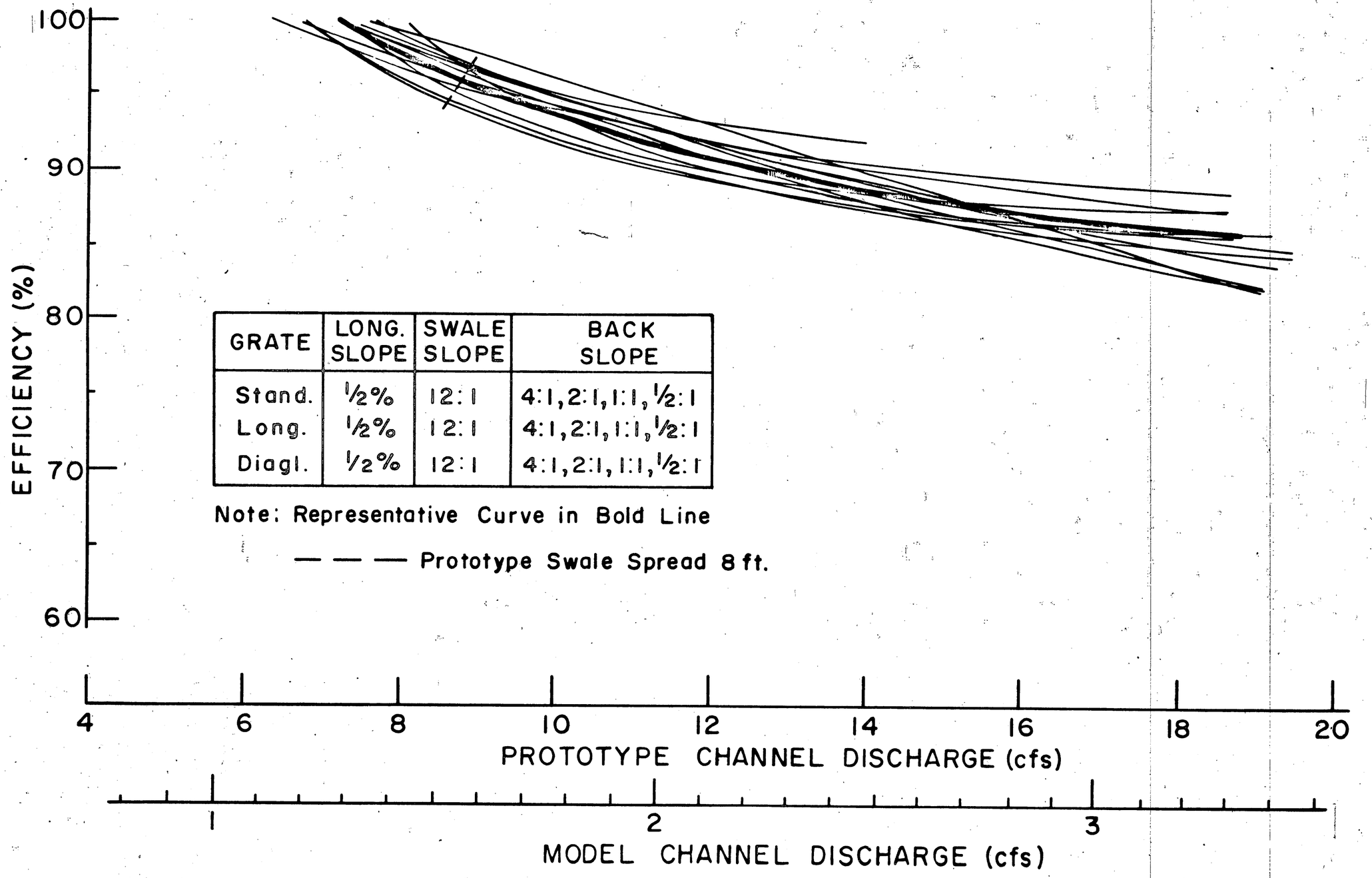

GRATE	LONG. SLOPE	SWALE SLOPE	BACK SLOPE
Stand.	½%	12:1	4:1, 2:1, 1:1, ½:1
Long.	½%	12:1	4:1, 2:1, 1:1, ½:1
Diagl.	½%	12:1	4:1, 2:1, 1:1, ½:1

Note: Representative Curve in Bold Line

— — — Prototype Swale Spread 8 ft.

Fig. 5.5 Efficiency Curves for Type H Inlet Gratings (Long. Slope ½%, Swale Slope 12:1)

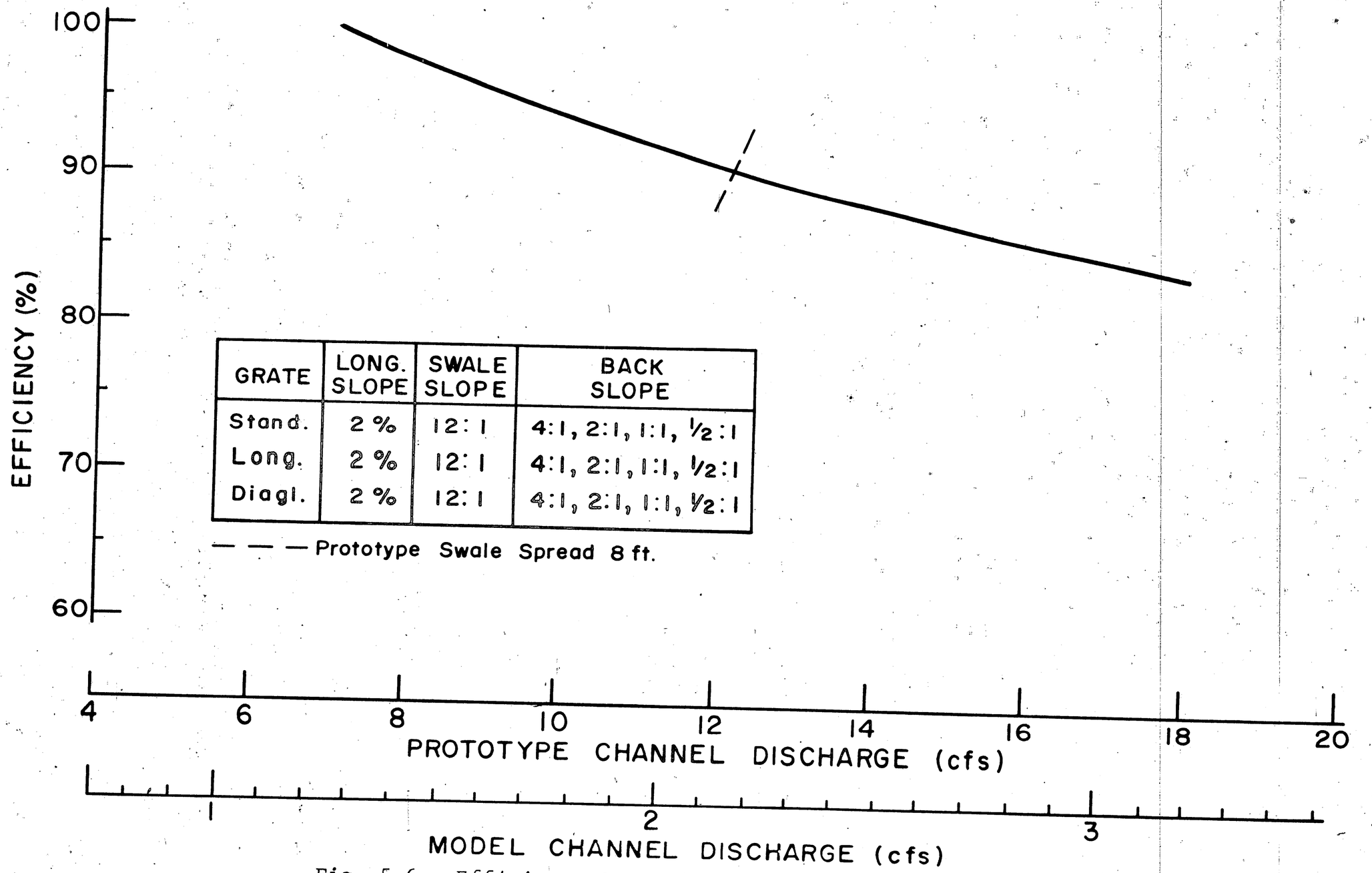

GRATE	LONG. SLOPE	SWALE SLOPE	BACK SLOPE
Stand.	2 %	12:1	4:1, 2:1, 1:1, ½:1
Long.	2 %	12:1	4:1, 2:1, 1:1, ½:1
Diagl.	2 %	12:1	4:1, 2:1, 1:1, ½:1

— — — Prototype Swale Spread 8 ft.

Fig. 5.6: Efficiency Curve for Type H Inlet Gratings (Long. Slope 2%, Swale Slope 12:1)

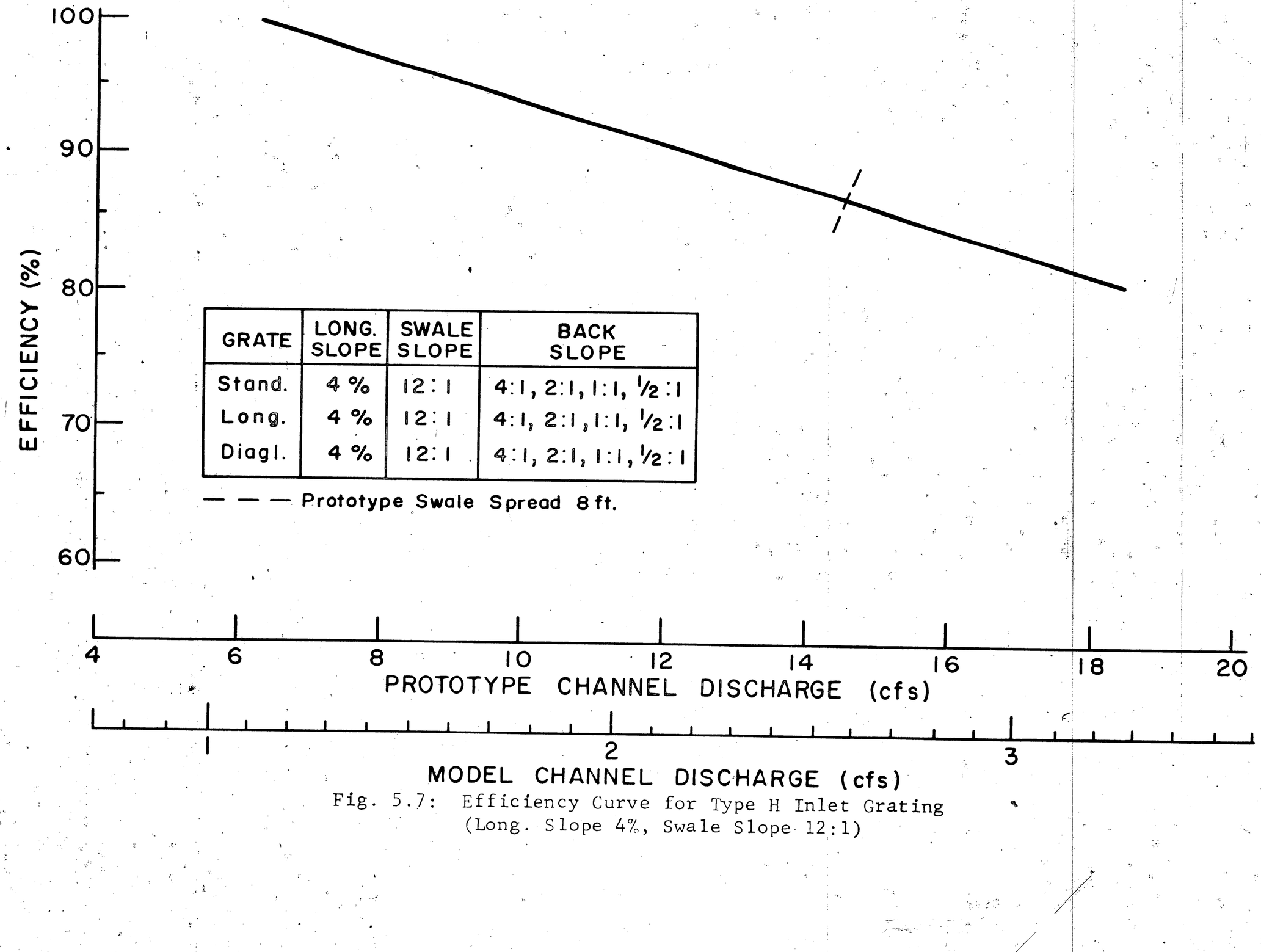

GRATE	LONG. SLOPE	SWALE SLOPE	BACK SLOPE
Stand.	4 %	12 : 1	4:1, 2:1, 1:1, ½:1
Long.	4 %	12 : 1	4:1, 2:1, 1:1, ½:1
Diagl.	4 %	12 : 1	4:1, 2:1, 1:1, ½:1

— — — Prototype Swale Spread 8 ft.

Fig. 5.7: Efficiency Curve for Type H Inlet Grating (Long. Slope 4%, Swale Slope 12:1)

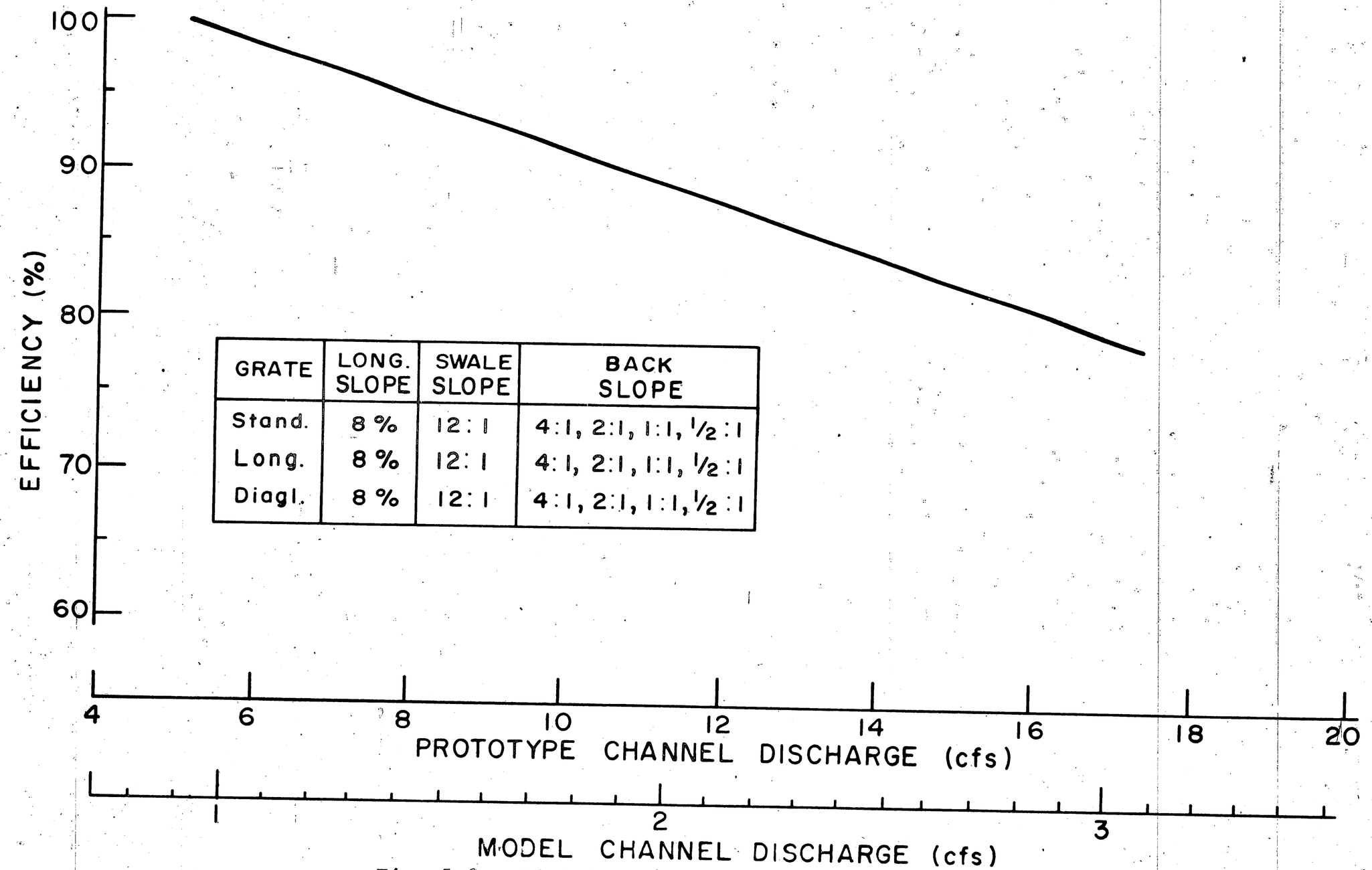

GRATE	LONG. SLOPE	SWALE SLOPE	BACK SLOPE
Stand.	8 %	12 : 1	4:1, 2:1, 1:1, ½ : 1
Long.	8 %	12 : 1	4:1, 2:1, 1:1, ½ : 1
Diagl.	8 %	12 : 1	4:1, 2:1, 1:1, ½ : 1

Fig. 5.8: Efficiency Curve for Type H Inlet Gratings (Long. Slope 8%, Swale Slope 12:1)

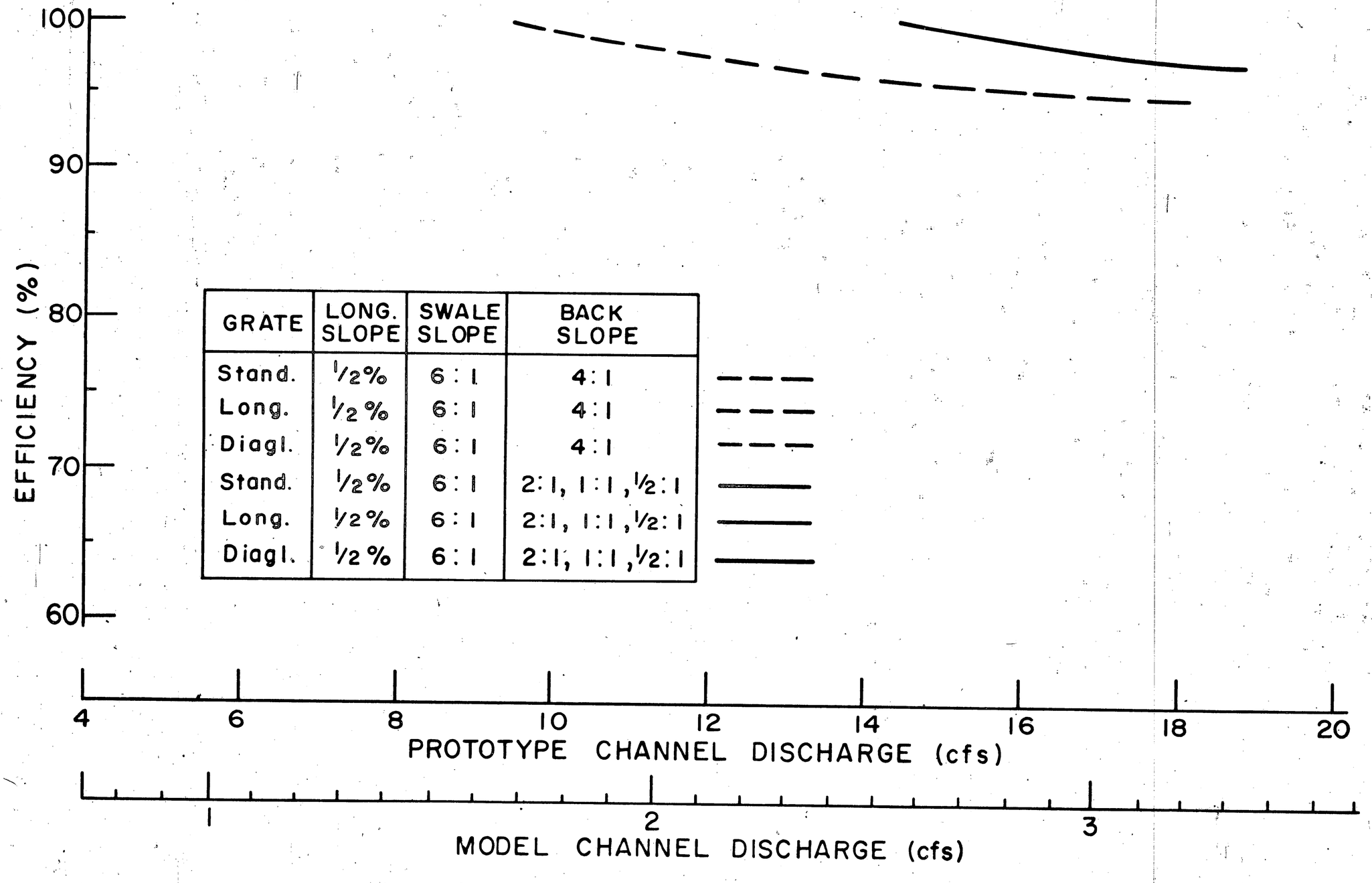

GRATE	LONG. SLOPE	SWALE SLOPE	BACK SLOPE
Stand.	½%	6 : 1	4 : 1
Long.	½%	6 : 1	4 : 1
Diagl.	½%	6 : 1	4 : 1
Stand.	½%	6 : 1	2:1, 1:1, ½:1
Long.	½%	6 : 1	2:1, 1:1, ½:1
Diagl.	½%	6 : 1	2:1, 1:1, ½:1

Fig. 5.9: Efficiency Curves for Type H Inlet Gratings (Long. Slope ½%, Swale Slope 6:1)

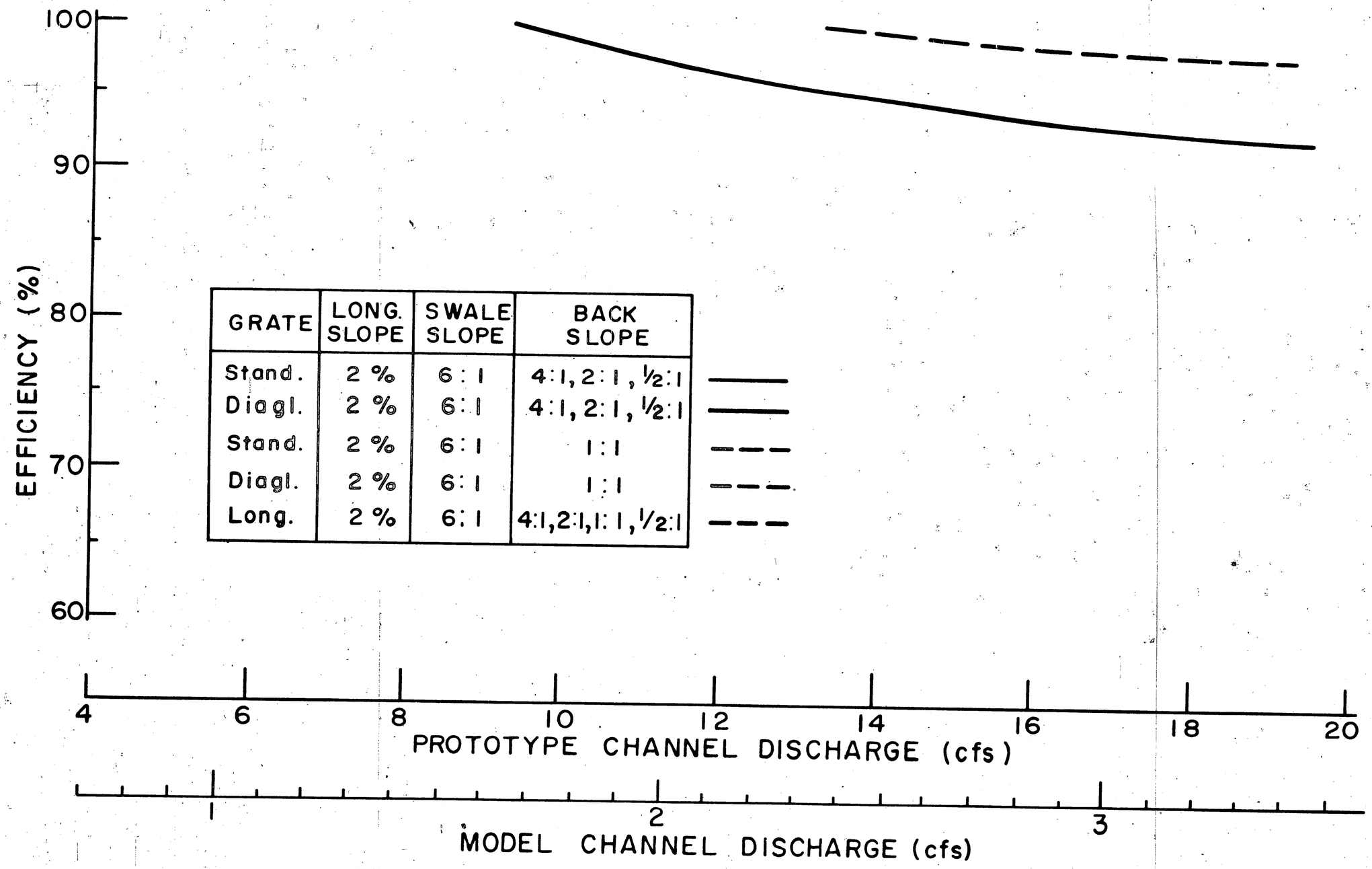

GRATE	LONG. SLOPE	SWALE SLOPE	BACK SLOPE
Stand.	2 %	6 : 1	4:1, 2:1, ½:1
Diagl.	2 %	6 : 1	4:1, 2:1, ½:1
Stand.	2 %	6 : 1	1:1
Diagl.	2 %	6 : 1	1:1
Long.	2 %	6 : 1	4:1, 2:1, 1:1, ½:1

Fig. 5.10: Efficiency Curves for Type H Inlet Gratings (Long. Slope 2%, Swale Slope 6:1)

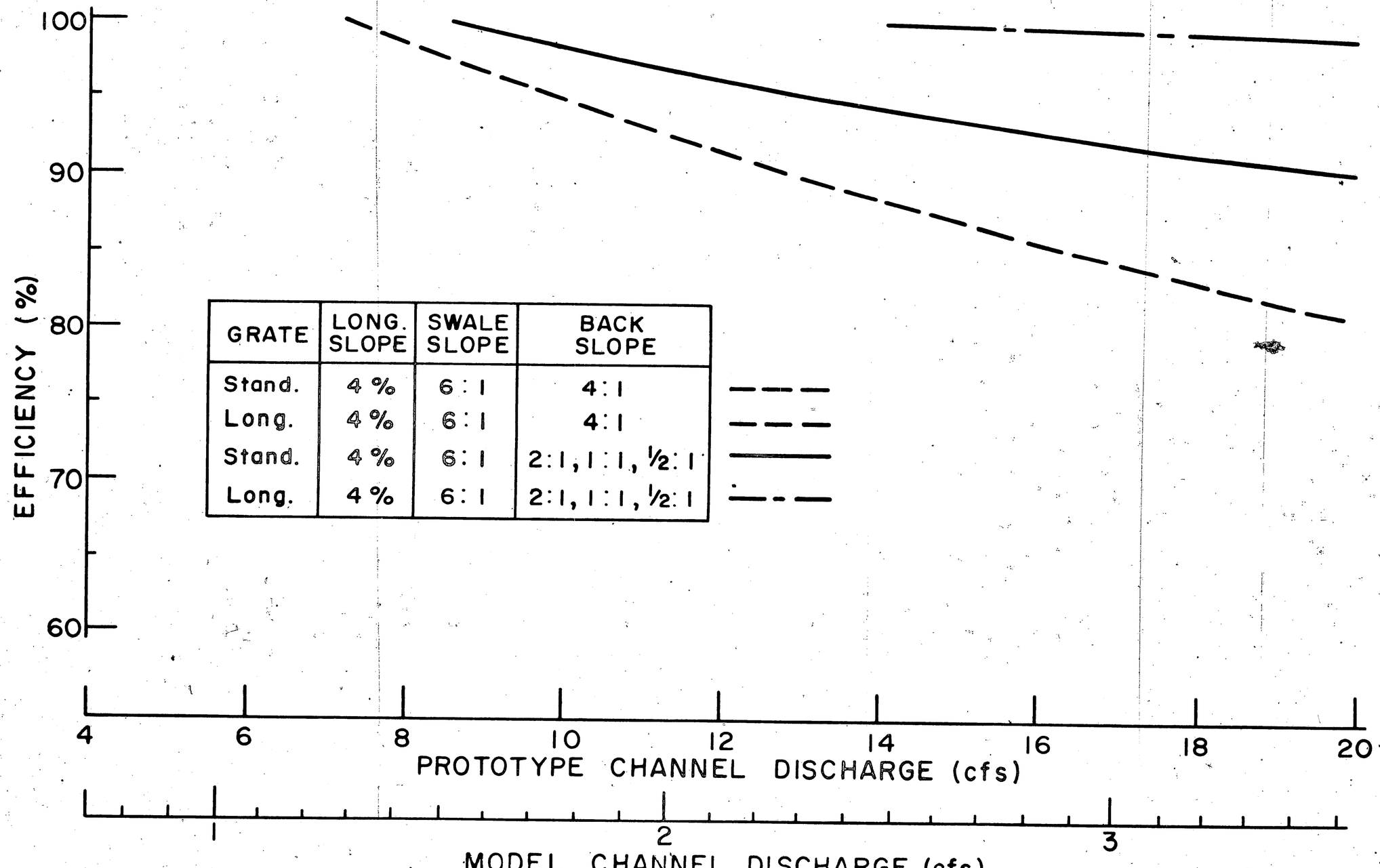

GRATE	LONG. SLOPE	SWALE SLOPE	BACK SLOPE
Stand.	4 %	6 : 1	4 : 1
Long.	4 %	6 : 1	4 : 1
Stand.	4 %	6 : 1	2:1, 1:1, ½:1
Long.	4 %	6 : 1	2:1, 1:1, ½:1

Fig. 5.11: Efficiency Curves for Type H Inlet Gratings (Long. Slope 4%, Swale Slope 6:1)

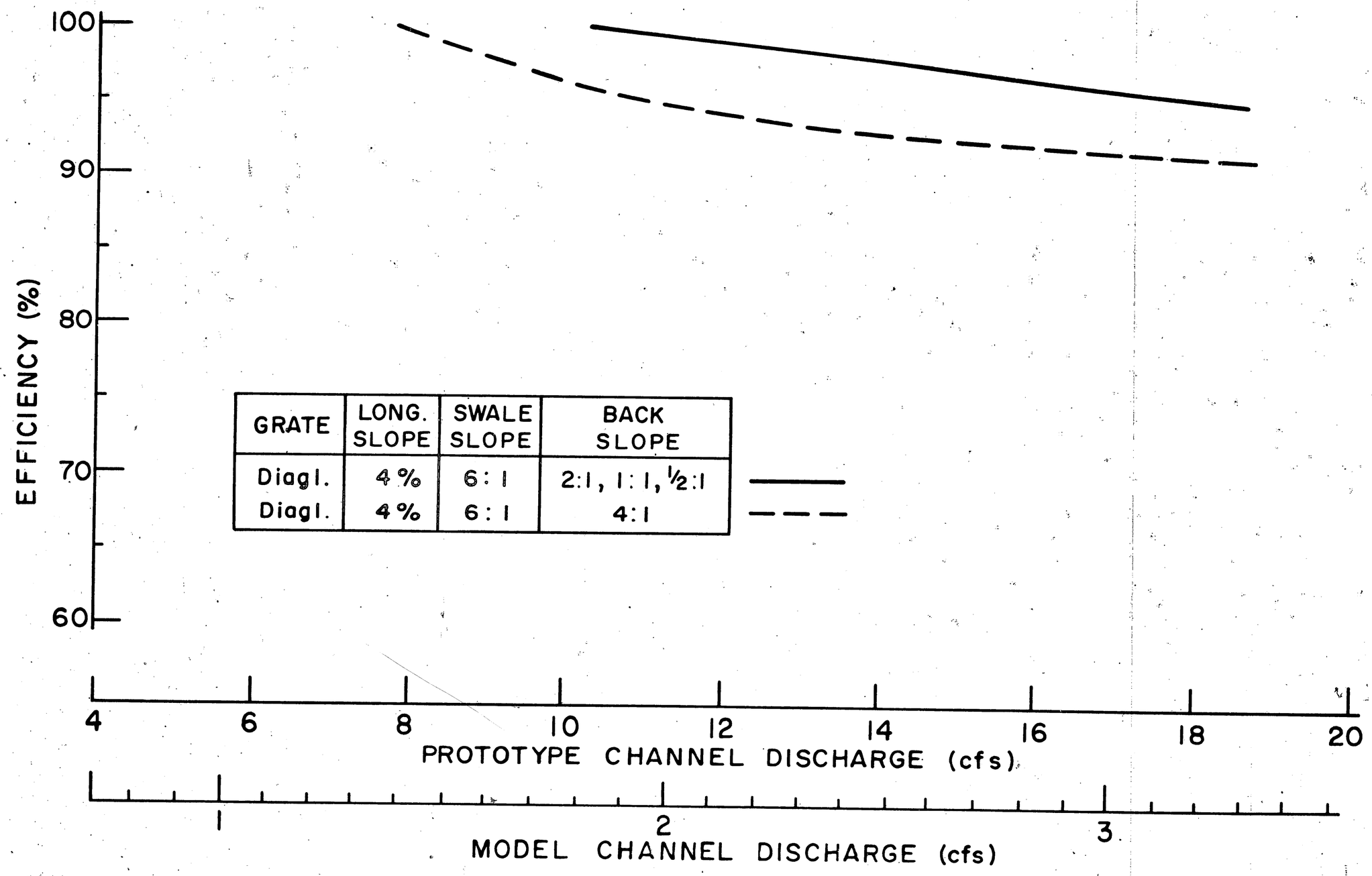

GRATE	LONG. SLOPE	SWALE SLOPE	BACK SLOPE
Diagl.	4%	6:1	2:1, 1:1, ½:1
Diagl.	4%	6:1	4:1

Fig. 5.12: Efficiency Curves for Type H Inlet Grating with Diagonal Bars (Long. Slope 4%, Swale Slope 6:1)

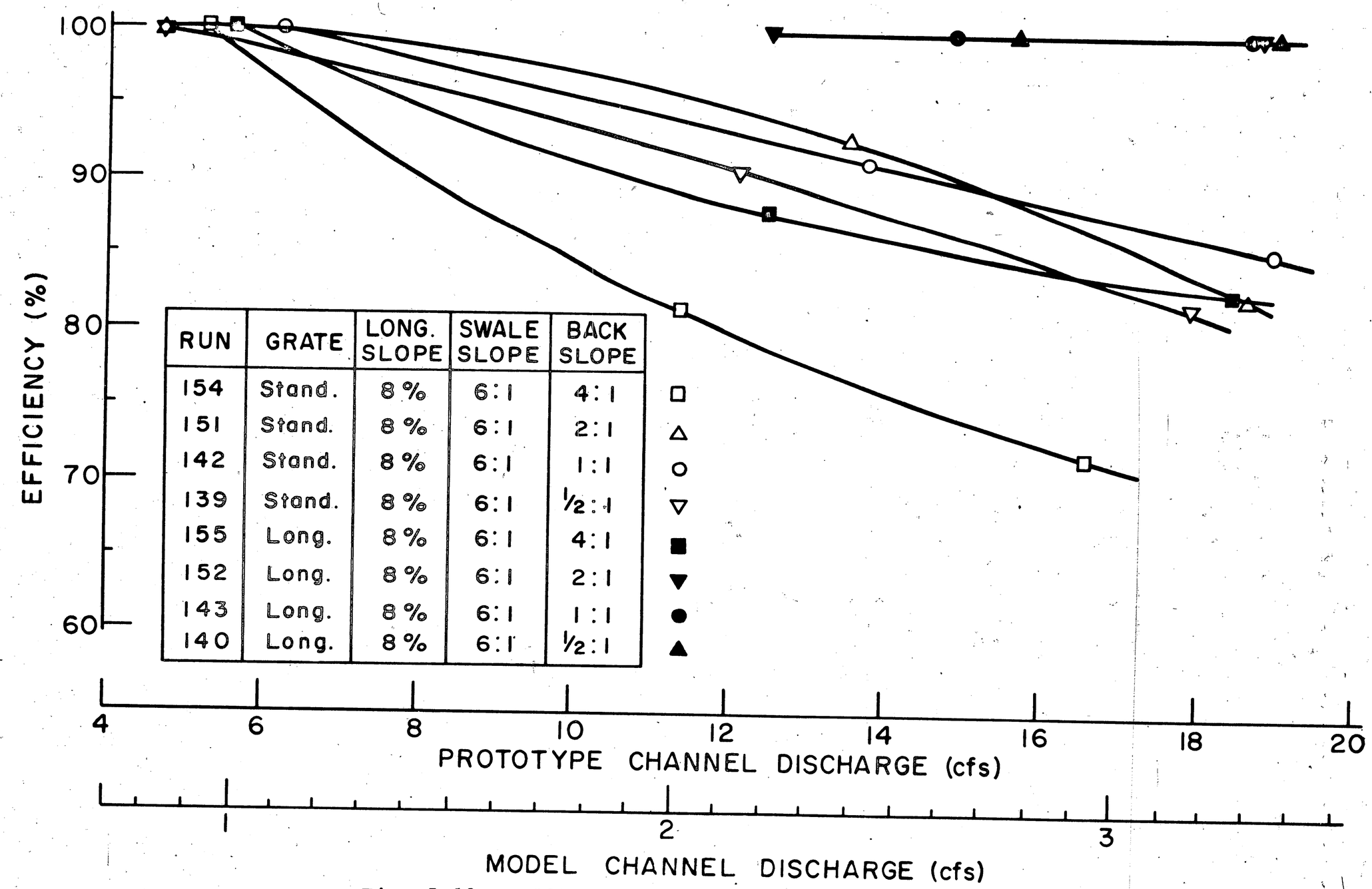

RUN	GRATE	LONG. SLOPE	SWALE SLOPE	BACK SLOPE	
154	Stand.	8 %	6:1	4:1	□
151	Stand.	8 %	6:1	2:1	△
142	Stand.	8 %	6:1	1:1	○
139	Stand.	8 %	6:1	½:1	▽
155	Long.	8 %	6:1	4:1	■
152	Long.	8 %	6:1	2:1	▼
143	Long.	8 %	6:1	1:1	●
140	Long.	8 %	6:1	½:1	▲

Fig. 5.13: Efficiency Curves for Type H Inlet Gratings (Long. Slope 8%, Swale Slope 6:1)

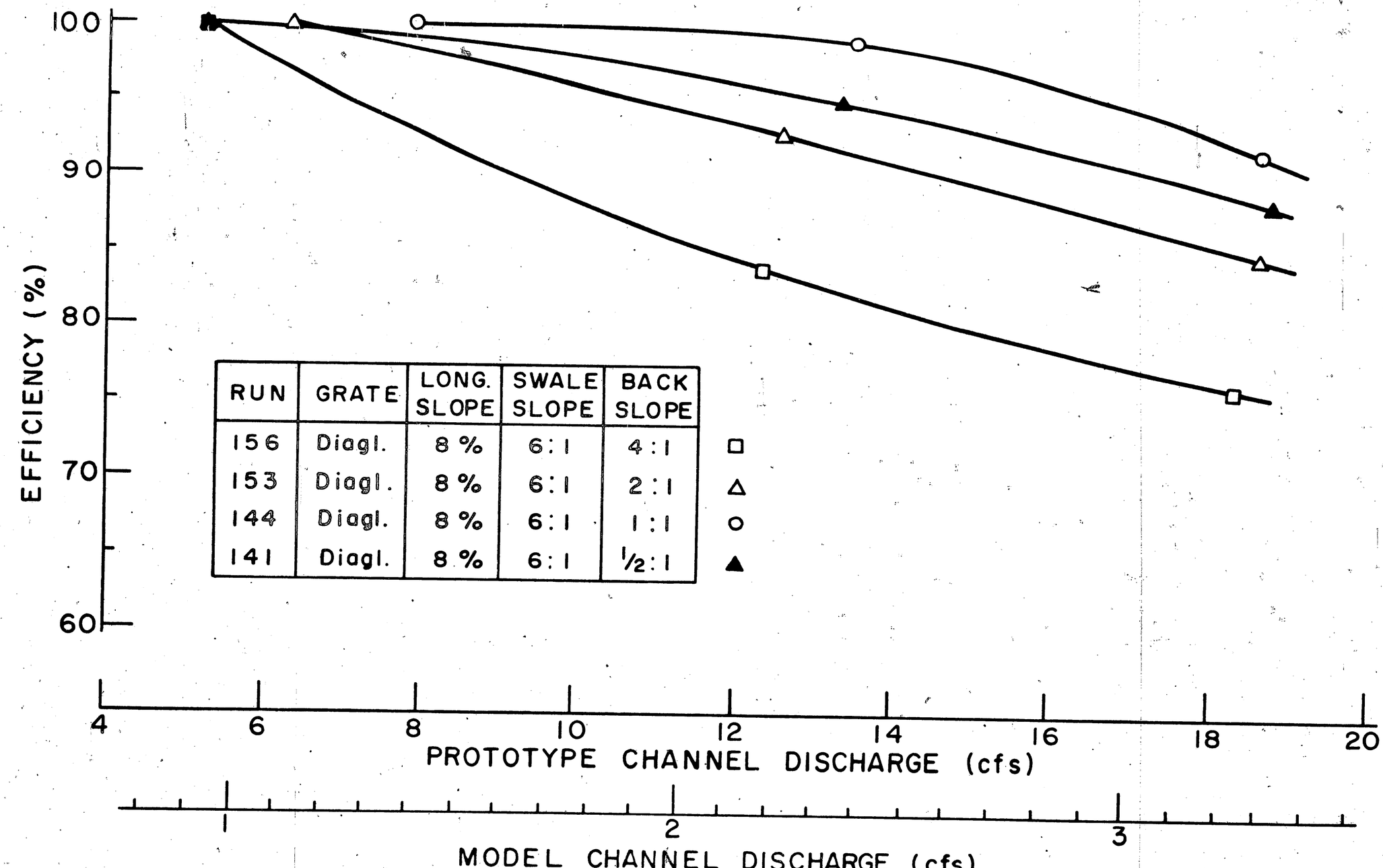

RUN	GRATE	LONG. SLOPE	SWALE SLOPE	BACK SLOPE	
156	Diagl.	8 %	6:1	4:1	□
153	Diagl.	8 %	6:1	2:1	△
144	Diagl.	8 %	6:1	1:1	○
141	Diagl.	8 %	6:1	½:1	▲

Fig. 5.14 Efficiency Curves for Type H Inlet Grating with Diagonal Bars (Long. Slope 8%, Swale Slope 6:1)

5.3.2 Efficiencies of Type 4-Ft Inlet and Type 6-Ft Inlet

5.3.2.1 General Remarks

Figures 5.15 through 5.24 show the efficiency curves for the gratings of the Type 4-Ft Inlet and the Type 6-Ft Inlet. Tables 5.2 through 5.5 summarize the testing program for the two gratings and the capacity of the gratings for an efficiency of 100%.

Figures 5.15 and 5.20 show for the Type 4-Ft Inlet and the Type 6-Ft Inlet, respectively, two curves for each longitudinal slope; one curve presents the highest efficiencies obtained and the other curve presents the lowest efficiencies obtained for a longitudinal slope. Thus, all the efficiency curves (48) that were obtained for that longitudinal slope lie between these two curves. The set of side slopes (swale and back) that gave the highest efficiency is 6:1 and 6:1, and the set giving the lowest efficiency was 12:1 and 4:1, as indicated on Figs. 5.15 and 5.20. The efficiencies of the inlet gratings were also determined for depressed gratings; they were tested for model depressions of ½-inch and 1-inch. For a given channel configuration, an inlet grating has lowest efficiency with no depression and highest efficiency for a 2-inch depression, as also indicated on Figs. 5.15 and 5.20. However, the difference between the efficiency of a zero-depressed grating and a 2-inch depressed grating was not more than 5% in most cases; only a few tests at a relatively steep (8%) longitudinal slope gave differences up to 10%.

The steepness of the back slope was found to be somewhat more significant for the efficiency of an inlet grating than the degree of

depression, whereas the swale slope was found to be a predominating factor for the efficiency of an inlet grating. For a fixed longitudinal slope and swale slope, it was possible to separate the efficiency curves for a grating into two groups, each with different back slopes, as illustrated in Fig. 5.16. A representative curve has been drawn for each group, depicting the efficiency curves with an accuracy of approximately 5%.

5.3.2.2 Efficiencies of Type 4-Ft Inlet

Figures 5.16 through 5.19 show the efficiencies of the Type 4-Ft Inlet grating for a longitudinal slope of ½%, 2%, 4%, and 8%, respectively. Four curves have been drawn to represent the efficiencies of the inlet grating installed for different channel configurations and grating depressions. The representative curves present the true efficiency with an accuracy of approximately 5%.

As can be observed from the graphs, back slopes of 12:1 and 4:1 are channel configurations that commonly result in low efficiencies. An example is the efficiency curve in Fig. 5.18 for a channel with a swale slope of 6:1 and a back slope of 12:1, which is from 6% to 14% below the efficiency curve for a channel with the same swale slope but steeper back slopes. This indicates that if one side slope is steep and the other side slope flat, then the efficiency of an inlet grating installed in such a channel will be relatively low.

5.3.2.3 Efficiencies of Type 6-Ft Inlet

Figures 5.21 through 5.24 show the efficiencies of the Type 6-Ft Inlet grating for a longitudinal slope of ½%, 2%, 4%, and 8%, respectively. The accuracy of the efficiencies is approximately 5%.

Table 5.2: Efficiencies of Type 4-Ft and Type 6-Ft Inlet Gratings at 0.5% Longitudinal Slope

Run No.	Grating	Swale Slope	Back Slope	Q_2^{100} (cfs)	Run No.	Grating	Swale Slope	Back Slope	Q_2^{100} (cfs)
184	4'-0"	12:1	4:1	3.56	209	4'-2"	6:1	12:1	5.21
185	6'-0"	"	"	4.07	210	6'-2"	"	"	5.94
186	6'-1"	"	"	4.81	211	6'-1"	"	"	5.66
187	4'-1"	"	"	4.64	212	4'-1"	"	"	4.93
188	4'-2"	"	"	4.46	213	4'-0"	"	"	4.30
189	6'-2"	"	"	4.59	214	6'-0"	"	"	6.06
190	4'-0"	12:1	6:1	4.02	215	6'-0"	6:1	8:1	10.20
191	6'-0"	"	"	4.86	216	4'-0"	"	"	7.70
192	6'-1"	"	"	5.49	217	4'-1"	"	"	7.36
193	4'-1"	"	"	5.43	218	6'-1"	"	"	10.71
194	4'-2"	"	"	5.83	219	6'-2"	"	"	9.75
195	6'-2"	"	"	5.72	220	4'-2"	"	"	8.73
196	6'-0"	12:1	8:1	5.71	221	4'-2"	6:1	6:1	10.99
197	4'-0"	"	"	4.41	222	6'-2"	"	"	13.70
198	4'-1"	"	"	5.89	223	6'-1"	"	"	13.60
199	6'-1"	"	"	6.40	224	4'-1"	"	"	9.79
200	6'-2"	"	"	6.69	225	4'-0"	"	"	8.95
201	4'-2"	"	"	6.06	226	6'-0"	"	"	12.90
202	4'-0"	12:1	12:1	4.64	227	6'-0"	6:1	4:1	12.45
203	6'-0"	"	"	6.29	228	4'-0"	"	"	8.37
204	6'-1"	"	"	6.91	229	4'-1"	"	"	8.61
205	4'-1"	"	"	6.35	230	6'-1"	"	"	11.79
206	4'-2"	"	"	6.69	231	6'-2"	"	"	11.90
207	6'-2"	"	"	7.36	232	4'-2"	"	"	10.20

Note: (1) 4' and 6': Type 4-Ft and Type 6-Ft, respectively
(2) 0", 1", and 2": Grating depressed 0-inch, 1-inch, and 2 inches, respectively
(3) Q_2^{100} : Capacity of prototype grating for an efficiency of 100%

Table 5.3: Efficiencies of Type 4-Ft and Type 6-Ft Inlet Gratings at 2.0% Longitudinal Slope

Run No.	Grating	Swale Slope	Back Slope	Q_2^{100} (cfs)	Run No.	Grating	Swale Slope	Back Slope	Q_2^{100} (cfs)
233	4'-0"	12:1	4:1	3.45	257	4'-0"	12:1	8:1	3.62
234	6'-0"	"	"	4.19	258	6'-0"	"	"	4.42
235	6'-1"	"	"	4.58	259	6'-1"	"	"	4.75
236	4'-1"	"	"	3.24	260	4'-1"	"	"	4.30
237	4'-2"	"	"	4.07	261	4'-2"	"	"	4.58
238	6'-2"	"	"	4.76	262	6'-2"	"	"	5.26
239	6'-0"D	"	"	15.30[a]	263	6'-0"D	"	"	18.30[a]
240	4'-0"D	"	"	13.09[a]	264	4'-0"D	"	"	15.30[a]
241	4'-1"D	"	"	15.40[a]	265	4'-1"D	"	"	15.85[a]
242	6'-1"D	"	"	15.61[a]	266	6'-1"D	"	"	19.15[a]
243	6'-2"D	"	"	16.20[a]	267	6'-2"D	"	"	19.25[b]
244	4'-2"D	"	"	16.15[a]	268	4'-2"D	"	"	16.42[a]
245	4'-0"	12:1	6:1	3.40	269	4'-0"	12:1	12:1	3.74
246	6'-0"	"	"	4.42	270	6'-0"	"	"	4.47
247	6'-1"	"	"	4.70	271	6'-1"	"	"	5.04
248	4'-1"	"	"	4.25	272	4'-1"	"	"	4.58
249	4'-2"	"	"	4.64	273	4'-2"	"	"	5.15
250	6'-2"	"	"	4.75	274	6'-2"	"	"	5.60
251	6'-0"D	"	"	16.70[a]	275	6'-0"D	"	"	18.80[a]
252	4'-0"D	"	"	15.12[a]	276	4'-0"D	"	"	17.58[b]
253	4'-1"D	"	"	15.23[a]	277	4'-1"D	"	"	17.61[a]
254	6'-1"D	"	"	16.99[a]	278	6'-1"D	"	"	18.71[b]
255	6'-2"D	"	"	17.00[a]	279	6'-2"D	"	"	18.60[b]
256	4'-2"D	"	"	15.61[a]	280	4'-2"D	"	"	18.40[a]

Note: (1) 4' and 6': Type 4-Ft and Type 6-Ft, respectively
(2) 0", 1", and 2": Grating depressed 0-inch, 1-inch, and 2 inches, respectively
(3) D: Dike installed downstream from inlet grating
(4) Q_2^{100} : Capacity of prototype grating for an efficiency of 100%
(5) [a]: Maximum capacity of prototype grating for 100% efficiency. Dike installed
(6) [b]: Maximum capacity of prototype grating for 100% efficiency not reached. Dike installed

Table 5.3: Contd.

Run No.	Grating	Swale Slope	Back Slope	Q_2^{100} (cfs)	Run No.	Grating	Swale Slope	Back Slope	Q_2^{100} (cfs)
281	4'-0"	6:1	4:1	7.70	305	4'-0"	6:1	8:1	7.25
282	6'-0"	"	"	11.30	306	6'-0"	"	"	9.06
283	6'-1"	"	"	11.28	307	6'-1"	"	"	9.35
284	4'-1"	"	"	8.39	308	4'-1"	"	"	7.47
285	4'-2"	"	"	9.24	309	4'-2"	"	"	7.93
286	6'-2"	"	"	11.32	310	6'-2"	"	"	9.56
287	6'-0"D	"	"	19.20[b]	311	6'-0"D	"	"	19.22[b]
288	4'-0"D	"	"	16.31[a]	312	4'-0"D	"	"	16.39[a]
289	4'-1"D	"	"	16.71[a]	313	4'-1"D	"	"	16.45[a]
290	6'-1"D	"	"	19.00[b]	314	6'-1"D	"	"	18.81[b]
291	6'-2"D	"	"	19.00[b]	315	6'-2"D	"	"	18.78[b]
292	4'-2"D	"	"	18.41[a]	316	4'-2"D	"	"	17.05[a]
293	4'-0"	6:1	6:1	9.01	317	4'-0"	6:1	12:1	4.70
294	6'-0"	"	"	11.00	318	6'-0"	"	"	5.44
295	6'-1"	"	"	12.30	319	6'-1"	"	"	5.78
296	4'-1"	"	"	9.29	320	4'-1"	"	"	4.87
297	4'-2"	"	"	9.91	321	4'-2"	"	"	4.87
298	6'-2"	"	"	12.49	322	6'-2"	"	"	6.00
299	6'-0"D	"	"	18.75[b]	323	6'-0"D	"	"	18.80[b]
300	4'-0"D	"	"	15.85[a]	324	4'-0"D	"	"	15.41[a]
301	4'-1"D	"	"	17.85[a]	325	4'-1"D	"	"	15.59[a]
302	6'-1"D	"	"	18.70[b]	326	6'-1"D	"	"	18.75[b]
303	6'-2"D	"	"	18.70[b]	327	6'-2"D	"	"	19.10[b]
304	4'-2"D	"	"	18.89[a]	328	4'-2"D	"	"	16.69[a]

Note: (1) 4' and 6': Type 4-Ft and Type 6-Ft, respectively
(2) 0", 1", and 2": Grating depressed 0-inch, 1-inch, and 2 inches, respectively
(3) D: Dike installed downstream from inlet grating
(4) Q_2^{100} : Capacity of prototype grating for an efficiency of 100%
(5) [a]: Maximum capacity of prototype grating for 100% efficiency. Dike installed
(6) [b]: Maximum capacity of prototype grating for 100% efficiency not reached. Dike installed

Table 5.4: Efficiencies of Type 4-Ft and Type 6-Ft Inlet Gratings at 4.0% Longitudinal Slope

Run No.	Grating	Swale Slope	Back Slope	Q_2^{100} (cfs)	Run No.	Grating	Swale Slope	Back Slope	Q_2^{100} (cfs)
329	4'-0"	12:1	4:1	1.98	353	4'-0"	12:1	8:1	3.18
330	6'-0"	"	"	3.18	354	6'-0"	"	"	3.74
331	6'-1"	"	"	3.29	355	6'-1"	"	"	3.91
332	4'-1"	"	"	2.84	356	4'-1"	"	"	3.28
333	4'-2"	"	"	3.23	357	4'-2"	"	"	3.57
334	6'-2"	"	"	3.40	358	6'-2"	"	"	4.02
335	6'-0"D	"	"	14.72[a]	359	6'-0"D	"	"	15.30[a]
336	4'-0"D	"	"	10.79[a]	360	4'-0"D	"	"	12.86[a]
337	4'-1"D	"	"	11.32[a]	361	4'-1"D	"	"	13.32[a]
338	6'-1"D	"	"	13.92[a]	362	6'-1"D	"	"	16.00[a]
339	6'-2"D	"	"	12.72[a]	363	6'-2"D	"	"	16.79[a]
340	4'-2"D	"	"	11.80[a]	364	4'-2"D	"	"	12.01[a]
341	4'-0"	12:1	4:1	3.06	365	4'-0"	12:1	12:1	3.23
342	6'-0"	"	"	3.12	366	6'-0"	"	"	3.85
343	6'-1"	"	"	3.28	367	6'-1"	"	"	4.02
344	4'-1"	"	"	3.23	368	4'-1"	"	"	3.46
345	4'-2"	"	"	3.40	369	4'-2"	"	"	4.08
346	6'-2"	"	"	3.74	370	6'-2"	"	"	4.31
347	6'-0"D	"	"	15.25[a]	371	6'-0"D	"	"	16.79[a]
348	4'-0"D	"	"	12.86[a]	372	4'-0"D	"	"	13.41[a]
349	4'-1"D	"	"	13.26[a]	373	4'-1"D	"	"	13.71[a]
350	6'-1"D	"	"	15.30[a]	374	6'-1"D	"	"	16.71[a]
351	6'-2"D	"	"	16.05[a]	375	6'-2"D	"	"	18.60[a]
352	4'-2"D	"	"	13.65[a]	376	4'-2"D	"	"	14.69[a]

Note: (1) 4' and 6': Type 4-Ft and Type 6-Ft, respectively
(2) 0", 1", and 2": Grating depressed 0-inch, 1-inch, and 2 inches, respectively
(3) D: Dike installed downstream from inlet grating
(4) Q_2^{100} : Capacity of prototype grating for an efficiency of 100%
(5) [a]: Maximum capacity of prototype grating for 100% efficiency. Dike installed

Table 5.4: Contd.

Run No.	Grating	Swale Slope	Back Slope	Q_2^{100} (cfs)	Run No.	Grating	Swale Slope	Back Slope	Q_2^{100} (cfs)
377	4'-0"	6:1	4:1	7.98	401	4'-0"	6:1	8:1	7.35
378	6'-0"	"	"	10.27	402	6'-0"	"	"	8.26
379	6'-1"	"	"	10.89	403	6'-1"	"	"	8.05
380	4'-1"	"	"	8.65	404	4'-1"	"	"	8.36
381	4'-2"	"	"	9.22	405	4'-2"	"	"	8.66
382	6'-2"	"	"	11.02	406	6'-2"	"	"	9.00
383	6'-0"D	"	"	18.71[a]	407	6'-0"D	"	"	18.63[a]
384	4'-0"D	"	"	13.70[a]	408	4'-0"D	"	"	14.72[a]
385	4'-1"D	"	"	15.19[a]	409	4'-1"D	"	"	14.72[a]
386	6'-1"D	"	"	17.45[b]	410	6'-1"D	"	"	18.00[b]
387	6'-2"D	"	"	18.59[b]	411	6'-2"D	"	"	18.10[b]
388	4'-2"D	"	"	16.49[a]	412	4'-2"D	"	"	15.13[b]
389	4'-0"	6:1	6:1	8.73	413	4'-0"	6:1	12:1	3.68
390	6'-0"	"	"	10.91	414	6'-0"	"	"	3.97
391	6'-1"	"	"	11.50	415	6'-1"	"	"	4.02
392	4'-1"	"	"	9.75	416	4'-1"	"	"	3.85
393	4'-2"	"	"	10.60	417	4'-2"	"	"	4.02
394	6'-2"	"	"	12.46	418	6'-2"	"	"	4.25
395	6'-0"D	"	"	17.95[b]	419	6'-0"D	"	"	16.71[a]
396	4'-0"D	"	"	14.72[a]	420	4'-0"D	"	"	13.30[a]
397	4'-1"D	"	"	15.75[a]	421	4'-1"D	"	"	14.71[a]
398	6'-1"D	"	"	18.15[b]	422	6'-1"D	"	"	18.12[a]
399	6'-2"D	"	"	18.70[b]	423	6'-2"D	"	"	18.12[a]
400	4'-2"D	"	"	16.81[a]	424	4'-2"D	"	"	15.81[a]

Note: (1) 4' and 6': Type 4-Ft and Type 6-Ft, respectively
(2) 0", 1", and 2": Grating depressed 0-inch, 1-inch, and 2 inches, respectively
(3) D: Dike installed downstream from inlet grating
(4) Q_2^{100} : Capacity of prototype grating for an efficiency of 100%
(5) [a]: Maximum capacity of prototype grating for 100% efficiency. Dike installed
(6) [b]: Maximum capacity of prototype grating for 100% efficiency not reached. Dike installed

Table 5.5: Efficiencies of Type 4-Ft and Type 6-Ft Inlet Gratings at 8.0% Longitudinal Slope

Run No.	Grating	Swale Slope	Back Slope	Q_2^{100} (cfs)	Run No.	Grating	Swale Slope	Back Slope	Q_2^{100} (cfs)
425	4'-0"	12:1	4:1	1.98	473	4'-0"	6:1	4:1	6.23
426	6'-0"	"	"	1.98	474	6'-0"	"	"	8.10
427	6'-1"	"	"	2.26	475	6'-1"	"	"	8.34
428	4'-1"	"	"	1.98	476	4'-1"	"	"	6.80
429	4'-2"	"	"	2.09	477	4'-2"	"	"	7.54
430	6'-2"	"	"	2.15	478	6'-2"	"	"	9.06
437	4'-0"	12:1	6:1	2.26	485	4'-0"	6:1	6:1	9.64
438	6'-0"	"	"	2.49	486	6'-0"	"	"	7.26
439	6'-1"	"	"	2.72	487	6'-1"	"	"	6.85
440	4'-1"	"	"	2.38	488	4'-1"	"	"	8.73
441	4'-2"	"	"	2.83	489	4'-2"	"	"	8.10
442	6'-2"	"	"	2.87	490	6'-2"	"	"	9.80
449	4'-0"	12:1	8:1	2.66	497	4'-0"	6:1	8:1	6.23
450	6'-0"	"	"	2.94	498	6'-0"	"	"	7.70
451	6'-1"	"	"	3.00	499	6'-1"	"	"	8.26
452	4'-1"	"	"	2.83	500	4'-1"	"	"	6.63
453	4'-2"	"	"	2.94	501	4'-2"	"	"	7.48
454	6'-2"	"	"	3.11	502	6'-2"	"	"	8.28
461	4'-0"	12:1	12:1	2.38	509	4'-0"	6:1	12:1	3.23
462	6'-0"	"	"	2.49	510	6'-0"	"	"	3.40
463	6'-1"	"	"	2.60	511	6'-1"	"	"	3.40
464	4'-1"	"	"	2.49	512	4'-1"	"	"	3.23
465	4'-2"	"	"	2.72	513	4'-2"	"	"	3.28
466	6'-2"	"	"	2.83	514	6'-2"	"	"	3.45

Note: (1) 4' and 6': Type 4-Ft and Type 6-Ft, respectively
(2) 0", 1", and 2": Grating depressed 0-inch, 1-inch, and 2 inches, respectively
(3) Q_2^{100} : Capacity of prototype grating for an efficiency of 100%

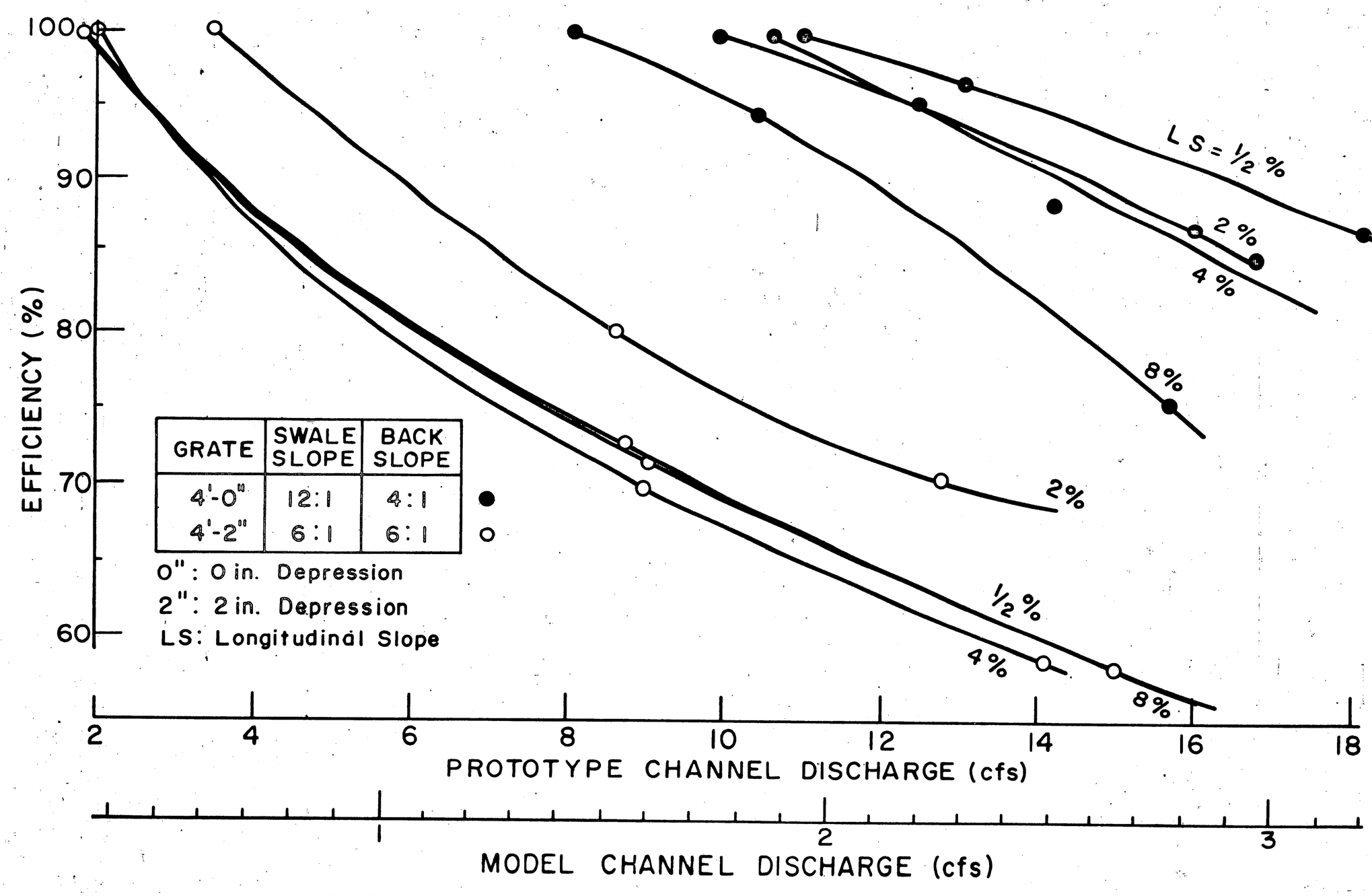

Fig. 5.15: Highest and Lowest Efficiencies for Type 4-Ft Inlet Grating (Long. Slope ½% to 8%)

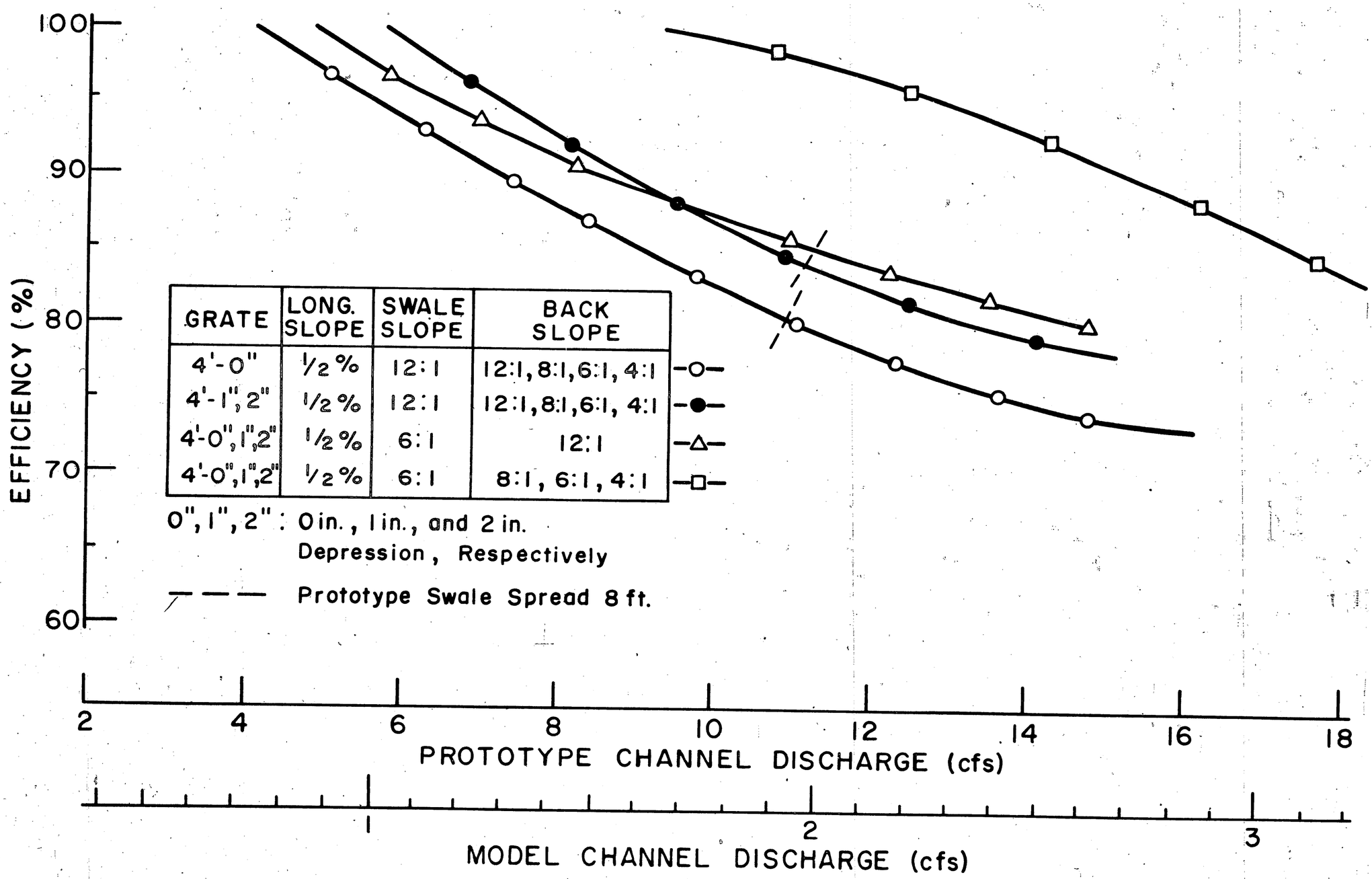

Fig. 5.16 Efficiency Curves for Type 4-Ft Inlet (Long Slope 1/2%)

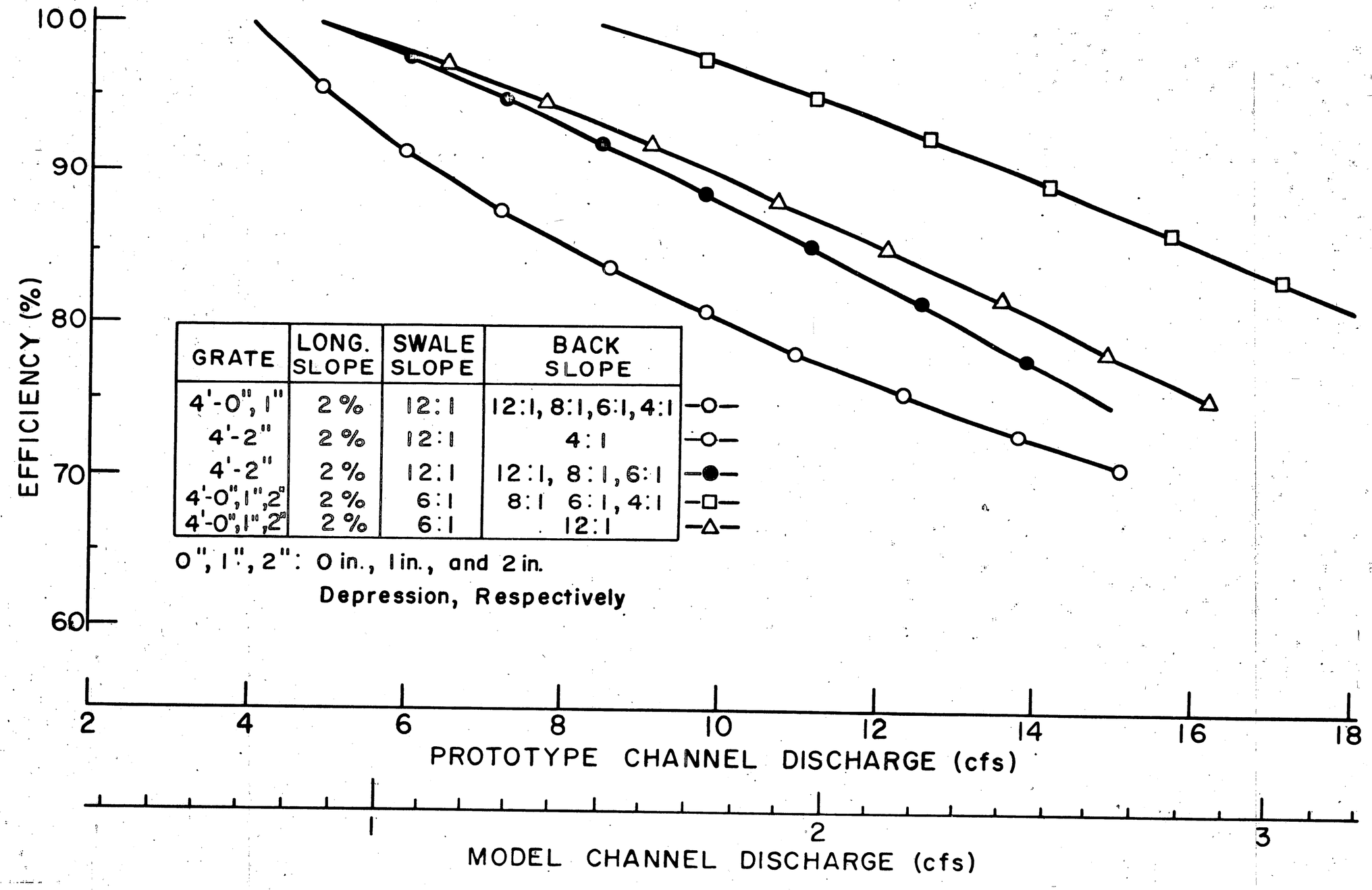

GRATE	LONG. SLOPE	SWALE SLOPE	BACK SLOPE	
4'-0", 1"	2%	12:1	12:1, 8:1, 6:1, 4:1	—○—
4'-2"	2%	12:1	4:1	—○—
4'-2"	2%	12:1	12:1, 8:1, 6:1	—●—
4'-0", 1", 2"	2%	6:1	8:1 6:1, 4:1	—□—
4'-0", 1", 2"	2%	6:1	12:1	—△—

0", 1", 2": 0 in., 1 in., and 2 in. Depression, Respectively

Fig. 5.17 Efficiency Curves for Type 4-Ft Inlet Grating (Long. Slope 2%)

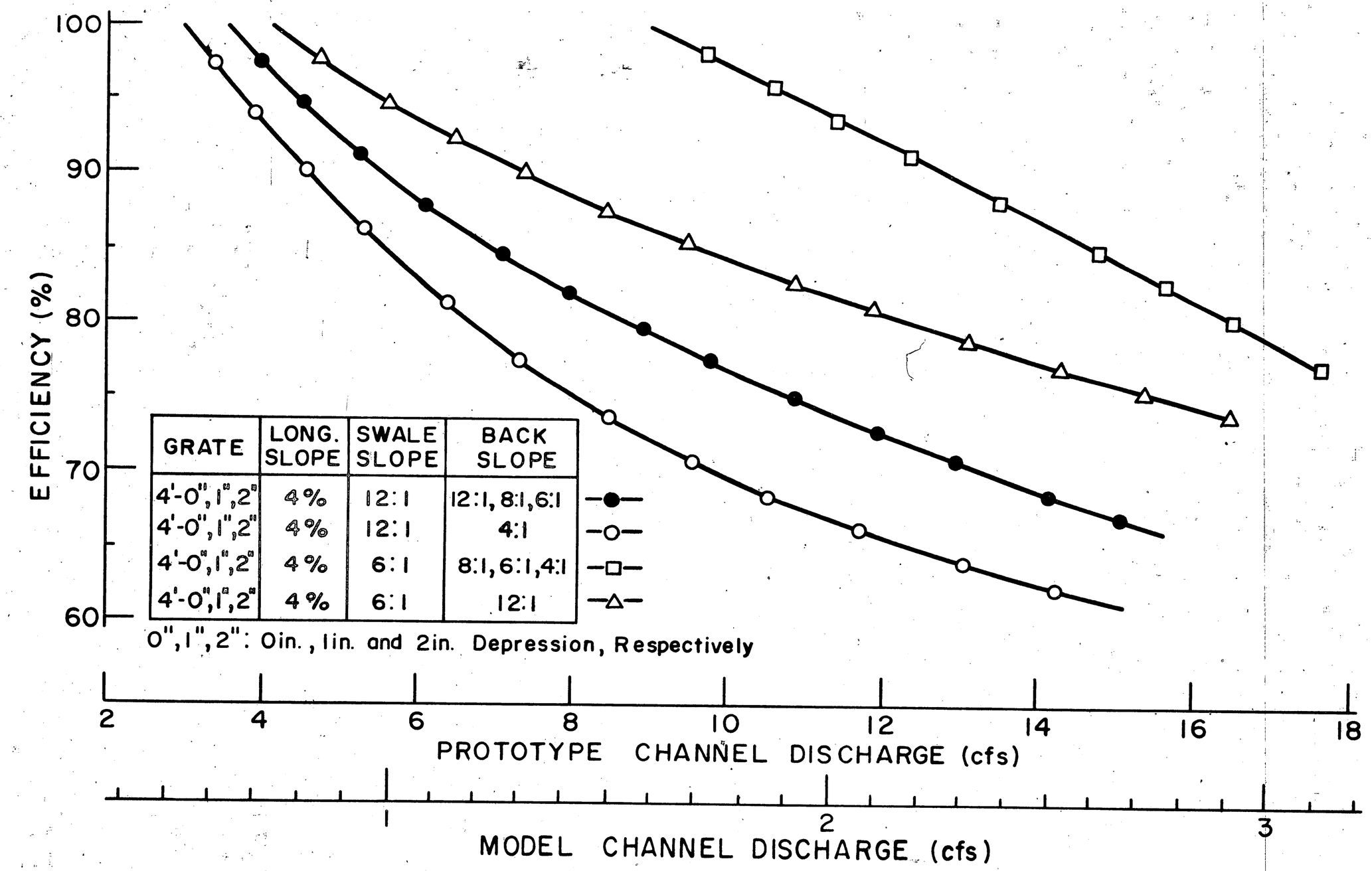

Fig. 5.18 Efficiency Curves for Type 4-Ft Inlet Grating (Long. Slope 4%)

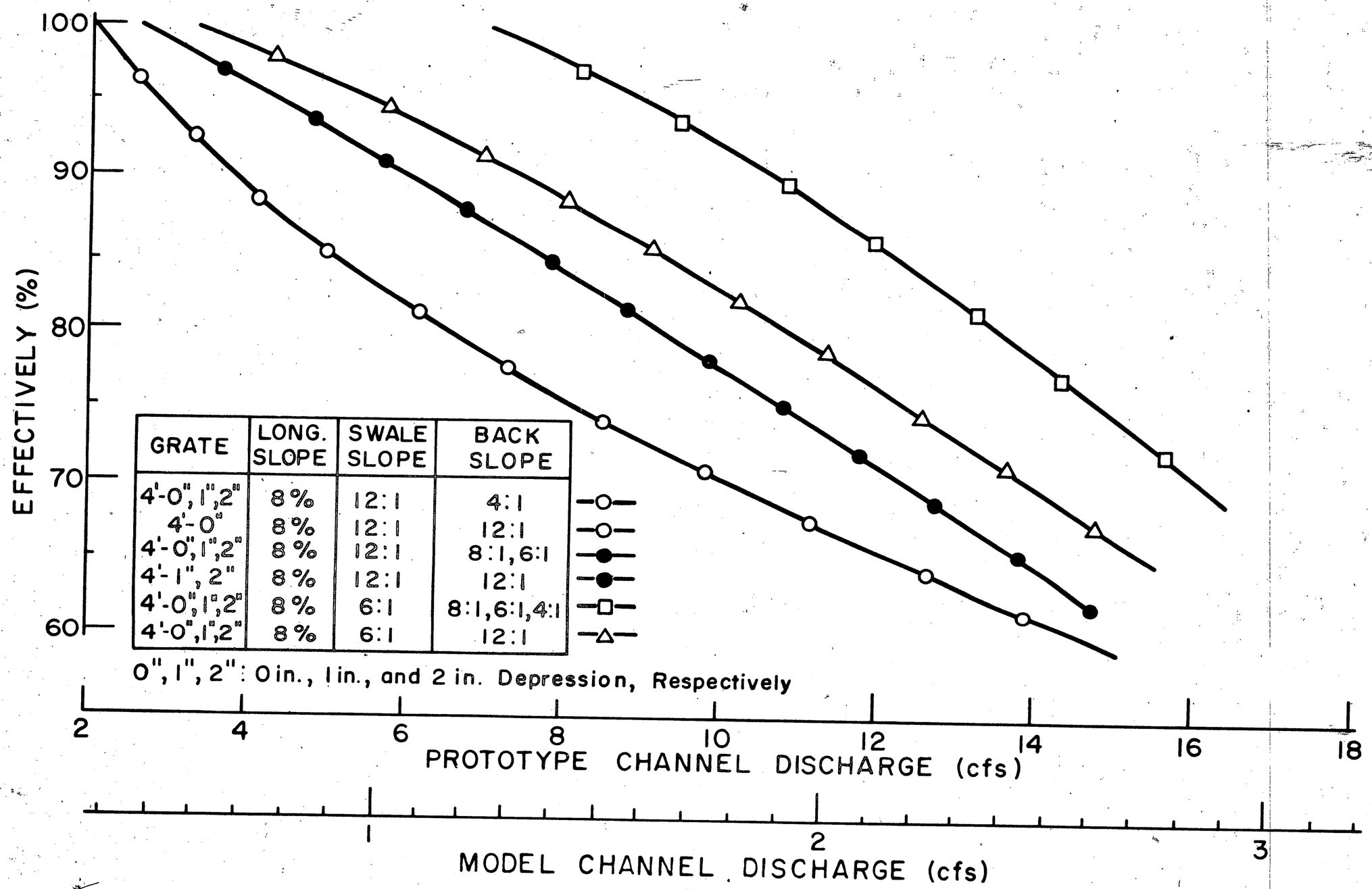

Fig. 5.19 Efficiency Curves at Type 4-Ft Inlet Grating (Long. Slope 8%)

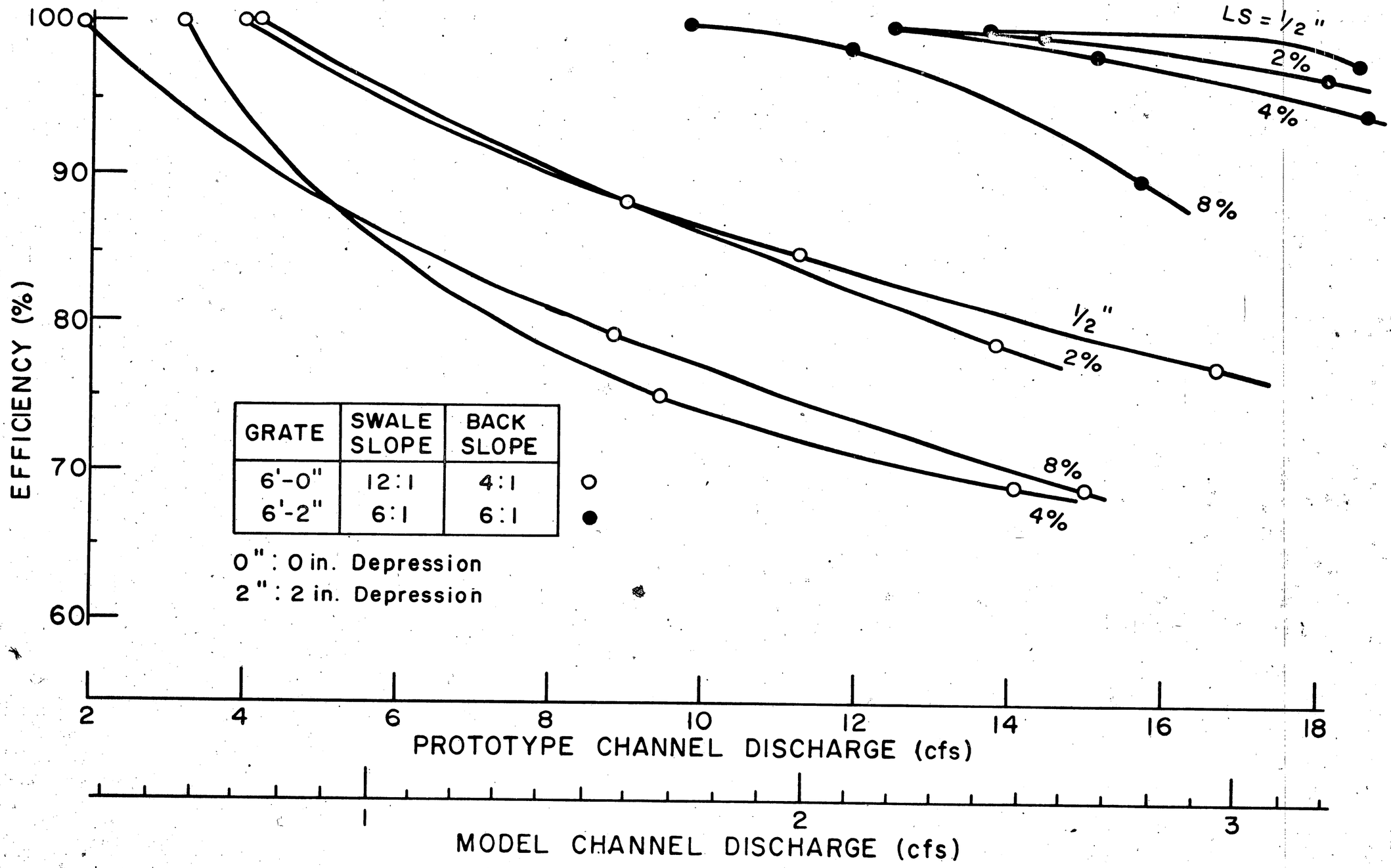

Fig. 5.20 Highest and Lowest Efficiencies for Type 6-Ft Inlet Grating (Long. Slope ½% to 8%)

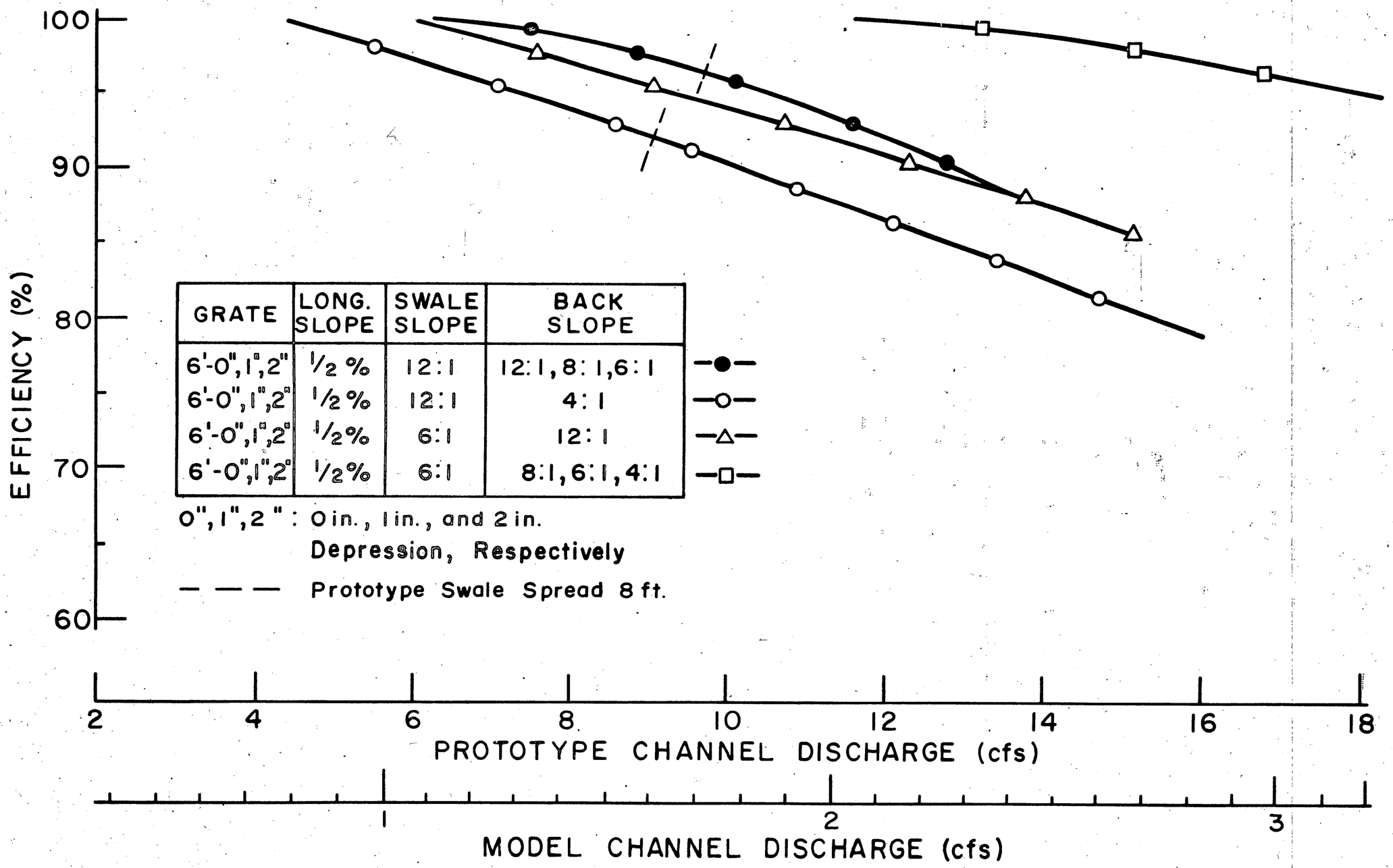

GRATE	LONG. SLOPE	SWALE SLOPE	BACK SLOPE
6'-0",1",2"	1/2 %	12:1	12:1, 8:1, 6:1
6'-0",1",2"	1/2 %	12:1	4:1
6'-0",1",2"	1/2 %	6:1	12:1
6'-0",1",2"	1/2 %	6:1	8:1, 6:1, 4:1

Fig. 5.21 Efficiency Curves for Type 6-Ft Inlet Grating (Long. Slope ½%)

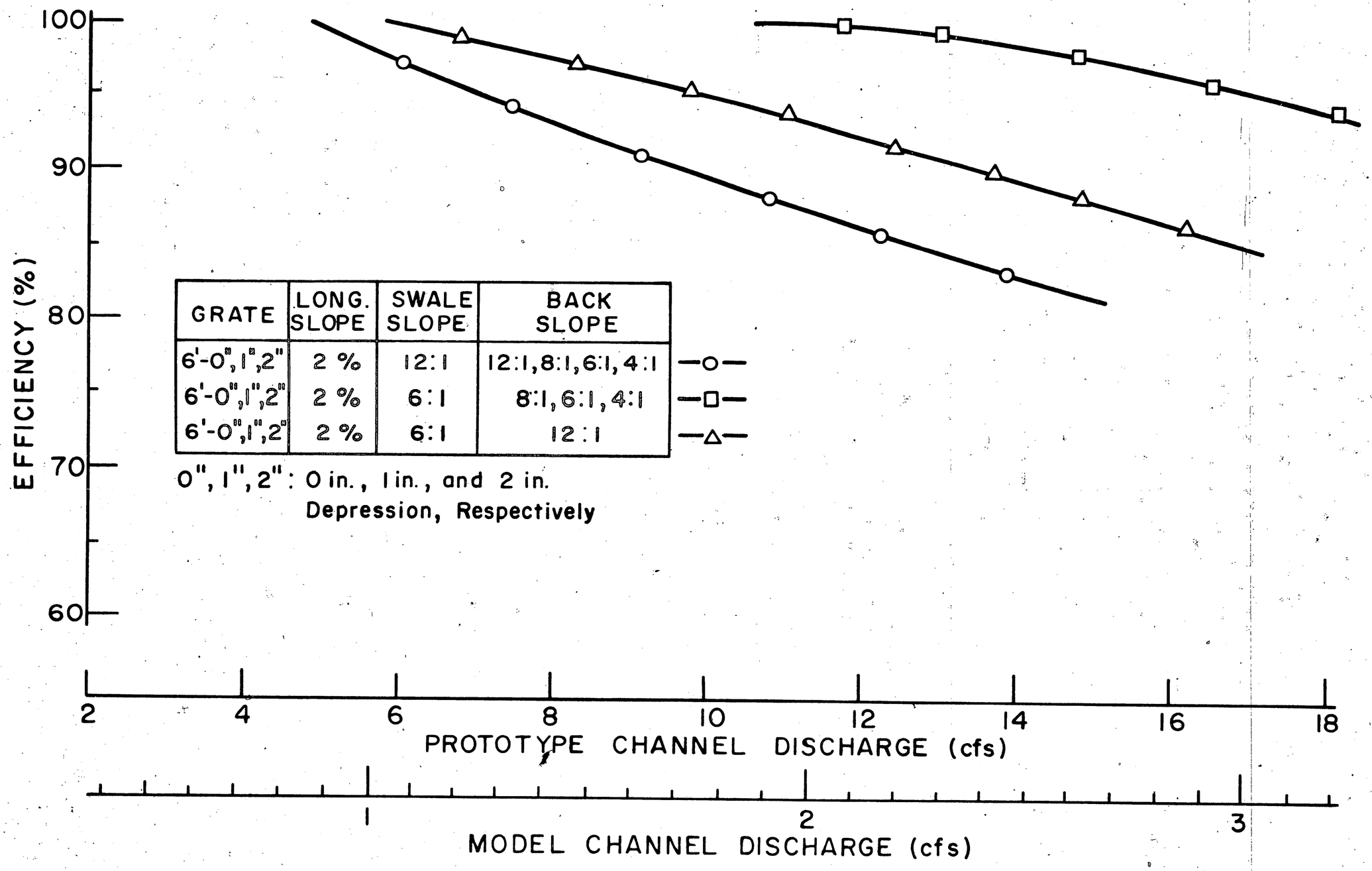

Fig. 5.22 Efficiency Curves of Type 6-Ft Inlet Grating (Long. Slope 2%)

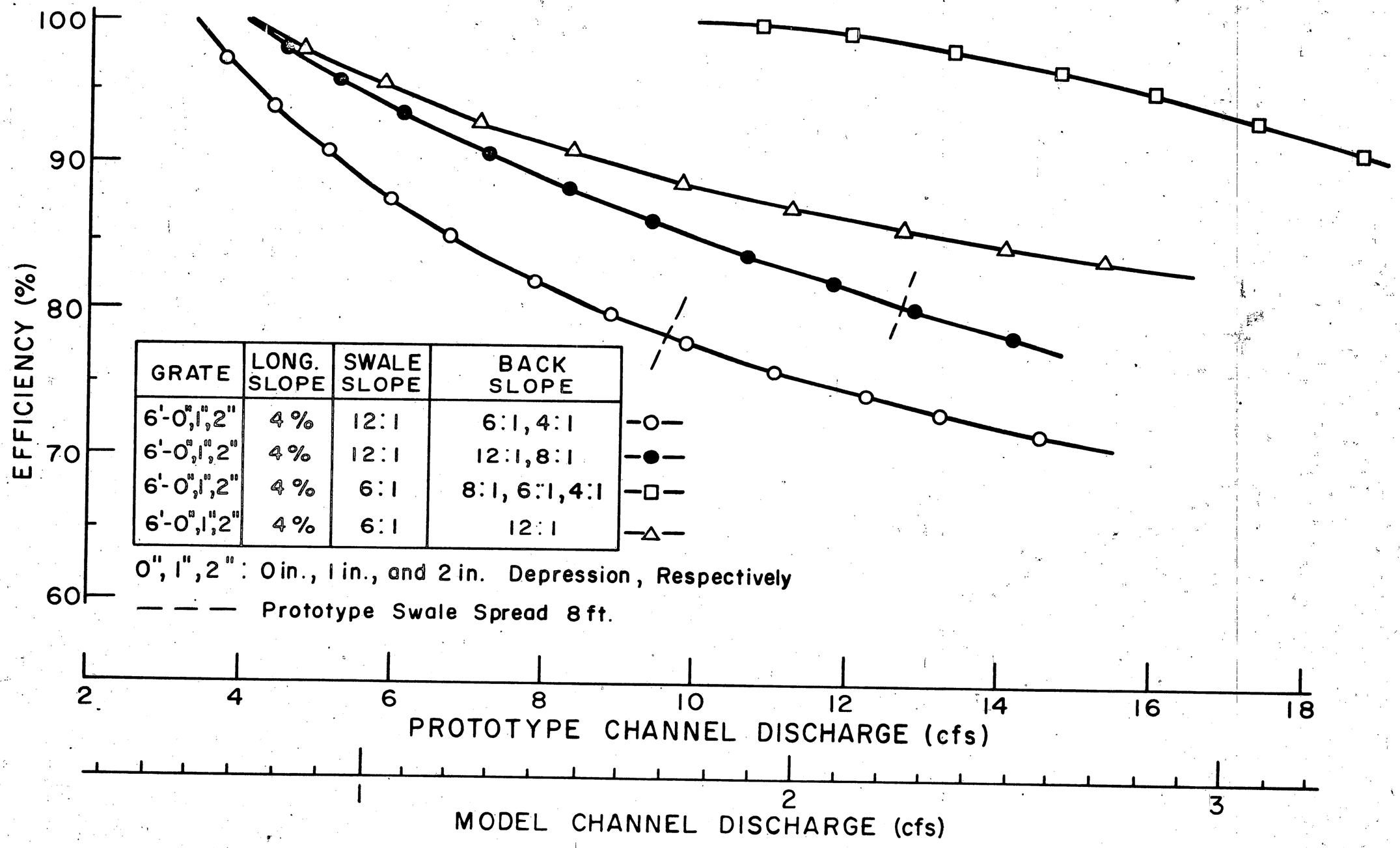

Fig. 5.23 Efficiency Curves for Type 6-Ft Inlet (Long. Slope 4%)

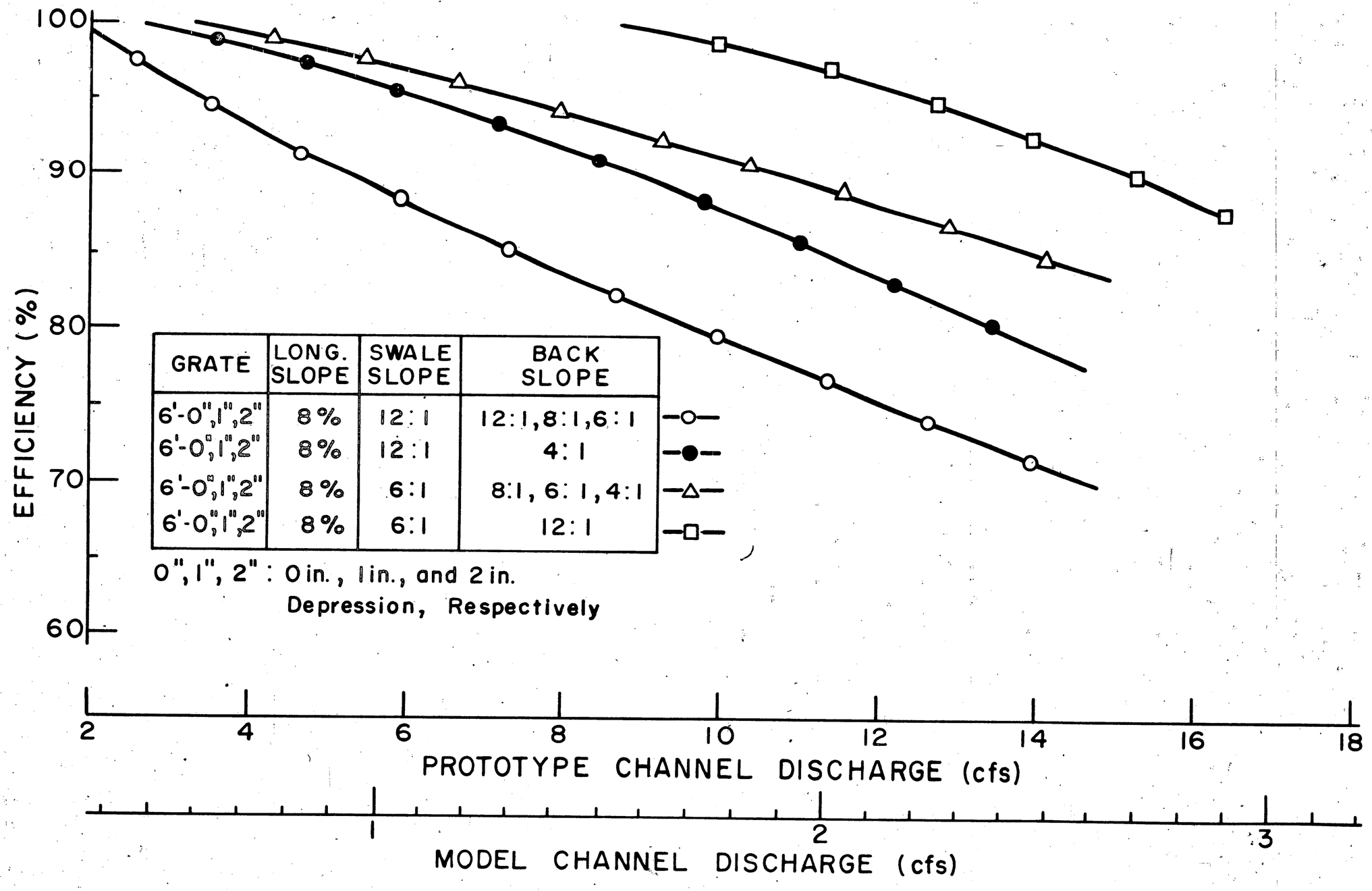

GRATE	LONG. SLOPE	SWALE SLOPE	BACK SLOPE	
6'-0",1",2"	8%	12:1	12:1, 8:1, 6:1	—○—
6'-0",1",2"	8%	12:1	4:1	—●—
6'-0",1",2"	8%	6:1	8:1, 6:1, 4:1	—△—
6'-0",1",2"	8%	6:1	12:1	—□—

0", 1", 2" : 0 in., 1 in., and 2 in. Depression, Respectively

Fig. 5.24 Efficiency Curves for Type 6-Ft Inlet Grating (Long. Slope 8%)

In general, the efficiencies of the Type 6-Ft Inlet grating for a particular channel configuration are 10-20% higher than the corresponding efficiencies of the Type 4-Ft Inlet grating. The slopes of the efficiency curves for the Type 6-Ft Inlet grating are slightly flatter than those of the Type 4-Ft Inlet grating, indicating the ability of the larger grating to intercept relatively more water.

For various channel configurations and depressions of the grating, the grating was completely removed from the channel, so that an empty hole was left, and the depth and spread measurements were repeated. No significant difference was observed in the measurements from the channel with and without the grating installed, indicating that for the 6-ft inlet grating the size and form of the frame of the grating are more important for the efficiency than the geometry of the grate.

5.4 Effect of Installation of a Dike

A dike was installed according to Fig. 4.10, and the Type 4-Ft and the Type 6-Ft Inlet gratings were tested for a longitudinal slope of 2% and 4% and a variety of side slopes as indicated in Tables 5.3 and 5.4. The tables also contain the maximal capacities of the Type 4-Ft and the Type 6-Ft Inlet gratings for an efficiency of 100%, which means that the carryover, Q_3, was zero for all these tests; in this condition the water was just about to flow over the dike.

The spread of water onto the swale slope for all but three tests did not exceed 4.0 feet in the model, which spread corresponds

to one of 8.0 feet in the prototype. For test numbers 239, 242, and 243 the spread of water reached 4.1 feet in the model.

The installation of a dike improved the capacities of the gratings significantly, that is, by a factor of 3 to 5, as can be seen in Tables 5.3 and 5.4. However, for channel configurations where the side slopes differed from each other, a very strong vortex with high velocities developed on top of the downstream end of the inlet gratings (see Fig. 5.25) indicating that substantial scour could occur at a field installation. This suggests that the surface adjacent to the grating be covered by a resistant material, such as macadam, asphalt, or concrete.

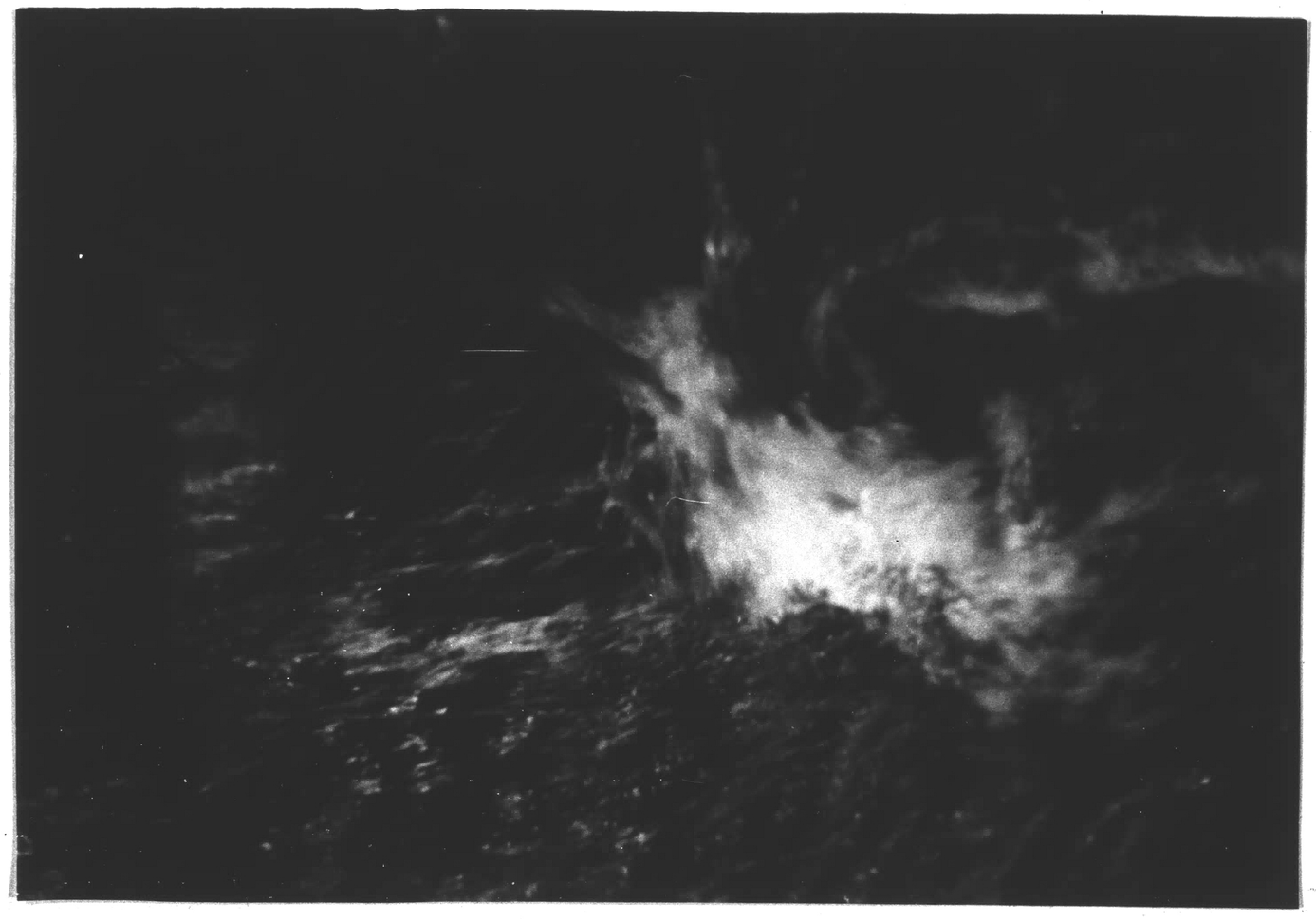

Fig. 5.25: Vortex Developed in Test No. 268

5.5 Sump Effect for Type H Inlet

5.5.1 General Remarks

A drainage inlet is usually installed at the lowest point of a vertical curve along a highway. Such inlets have to drain away the water that flows toward the inlets from opposite directions along the channel; thus a sump effect occurs.

The sump effect was produced in the present experiment by installing a vertical barrier, 8 inches in height and 12 feet in width, at the center of the inlet, the barrier being at right angles to the channel. Water was then introduced from the upstream end of the channel, and only the upstream half of the grate opening was effective in draining the water while the other half was inoperative (see Fig. 4.9).

The longitudinal slope of the channel was set at 0.2%. The data obtained from the tests are plotted in the form of curves, see Fig. 5.26 through 5.31, which relate the depth of the water along the invert of the channel one-foot upstream from the inlet grating to the rate of flow for different side slopes.

5.5.2 Results of Sump Effect

The data about the Type H Inlet gratings for the sump effect are shown in Figs. 5.26 to 5.31 and summarized in Table 5.6. The model discharges were doubled and converted into prototype flow rates using Eq. (10b) in order to take into account the fact that the water in the prototype approaches the inlet from both directions.

Table 5.6: Discharge and Spread for Different Back and Swale Slopes for Type H Inlet Gratings Installed for Sump Condition

Run No.	Type of Grating	Swale Slope	Back Slope	Discharge (cfs)	Spread of Water on Swale Slope (ft)
160	Standard	12:1	½:1	33.0	23.2
161	Longitudinal	"	"	32.8	23.2
162	Diagonal	"	"	32.8	22.8
163	Standard	6:1	½:1	33.0	14.0
164	Longitudinal	"	"	32.8	14.0
165	Diagonal	"	"	32.0	14.4
166	Standard	6:1	1:1	33.0	14.0
167	Longitudinal	"	"	33.6	14.0
168	Diagonal	"	"	33.0	14.0
169	Standard	12:1	1:1	33.0	23.2
170	Longitudinal	"	"	33.0	23.6
171	Diagonal	"	"	33.2	23.6
172	Standard	12:1	2:1	32.8	22.8
173	Longitudinal	"	"	32.8	22.8
174	Diagonal	"	"	33.2	21.6
175	Standard	6:1	2:1	32.8	12.8
176	Longitudinal	"	"	32.8	12.8
177	Diagonal	"	"	33.2	13.2
178	Standard	6:1	4:1	33.4	12.0
179	Longitudinal	"	"	33.4	12.0
180	Diagonal	"	"	33.4	12.0
181	Standard	12:1	4:1	32.8	19.2
182	Longitudinal	"	"	33.2	20.8
183	Diagonal	"	"	31.6	20.4

Note: (1) The discharge was the maximum for each test.
(2) Longitudinal slope was 0.2%.

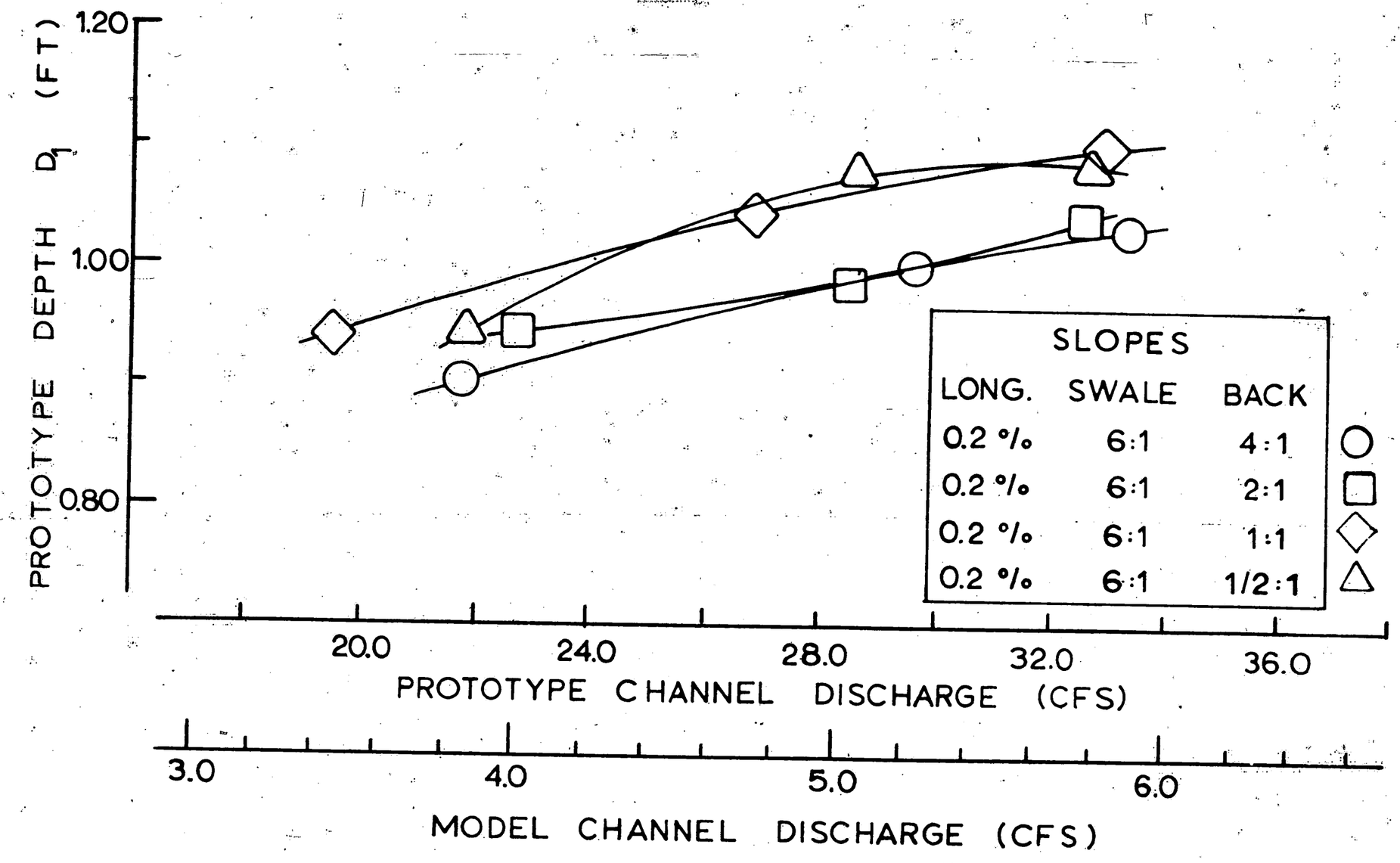

Fig. 5.26: Sump Effect for Type H Inlet - Standard Grating

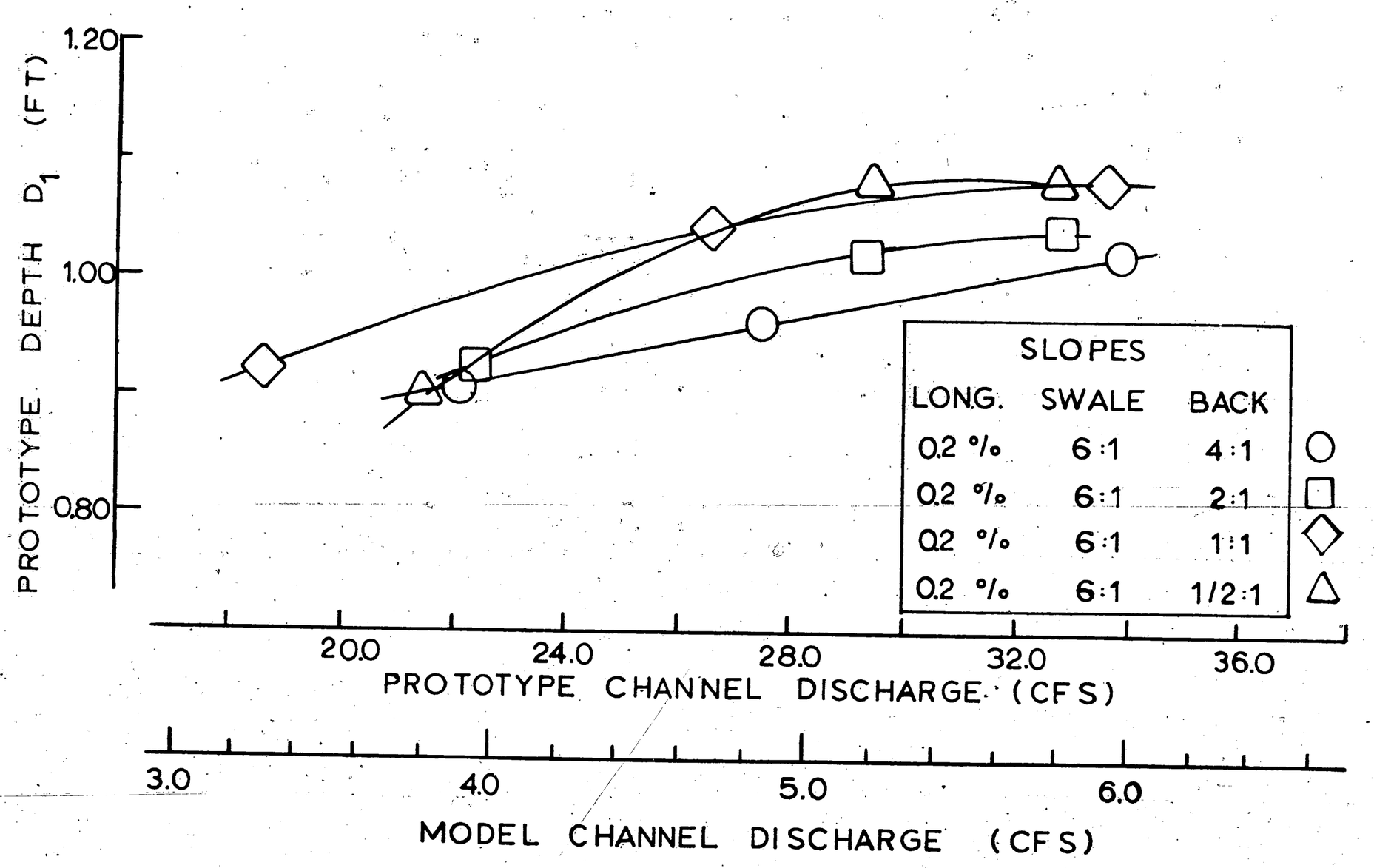

Fig. 5.27: Sump Effect for Type H Inlet - Longitudinal Bars

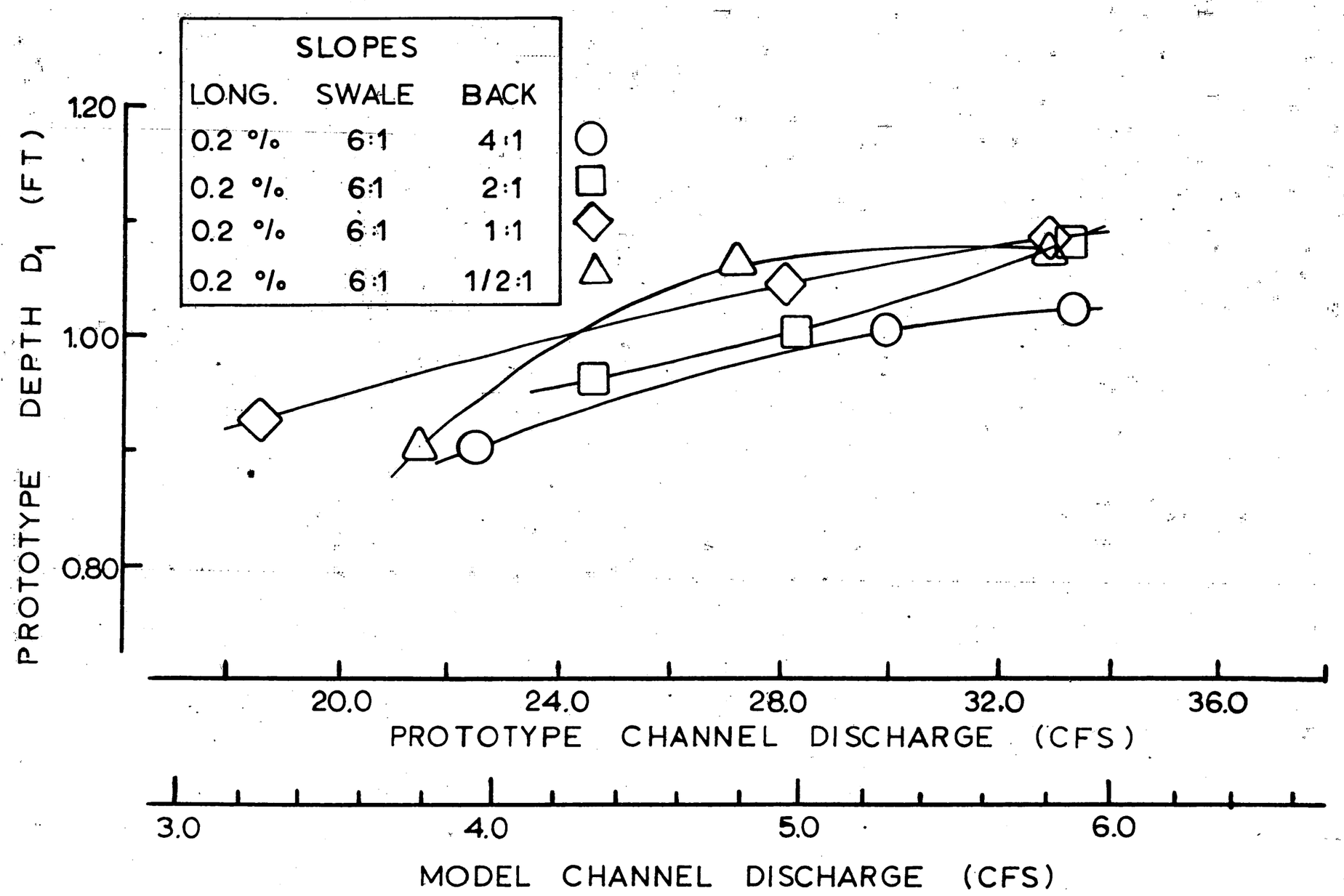

Fig. 5.28: Sump Effect for Type H Inlet - Diagonal Bars

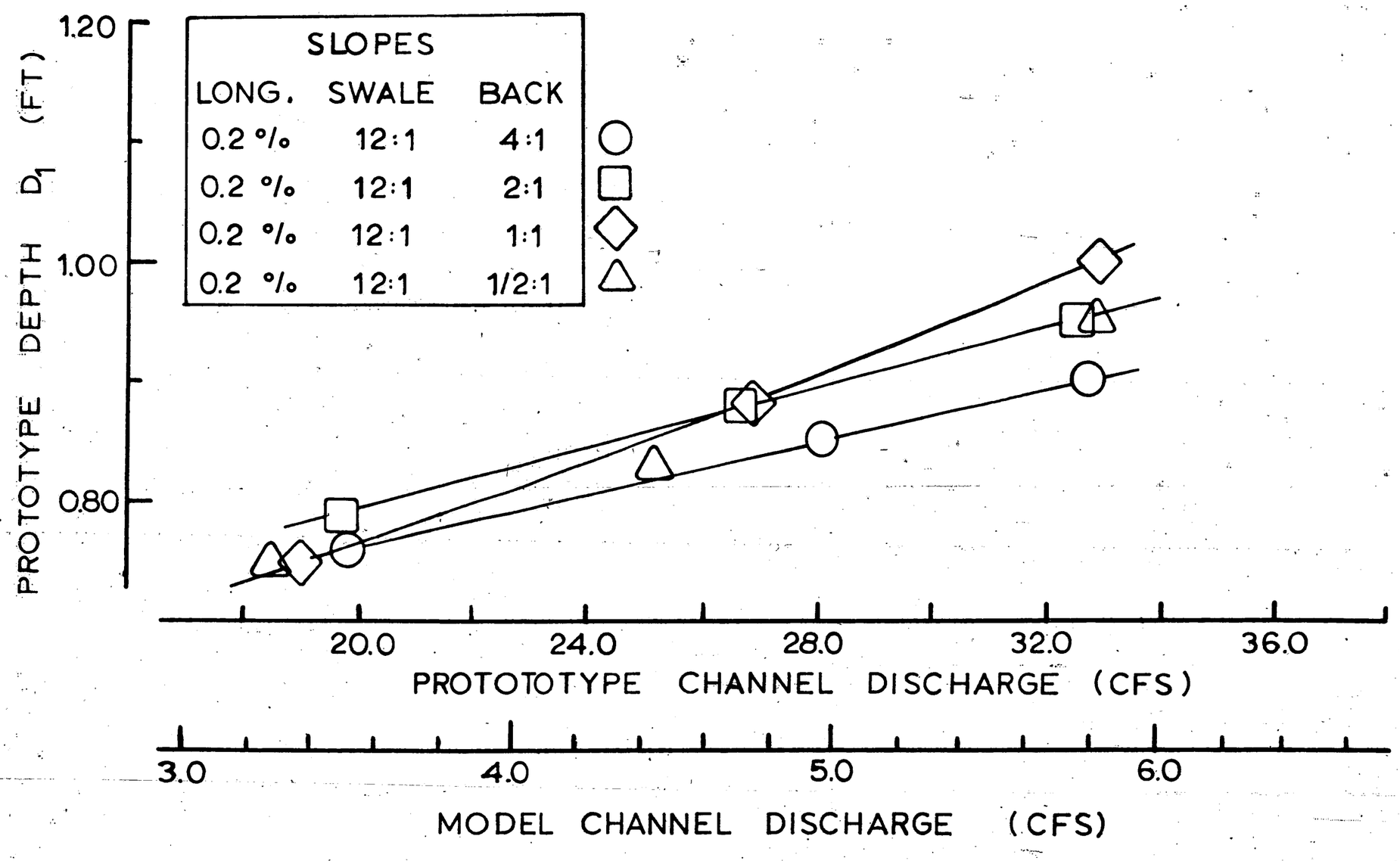

Fig. 5.29: Sump Effect for Type H Inlet - Standard Grating

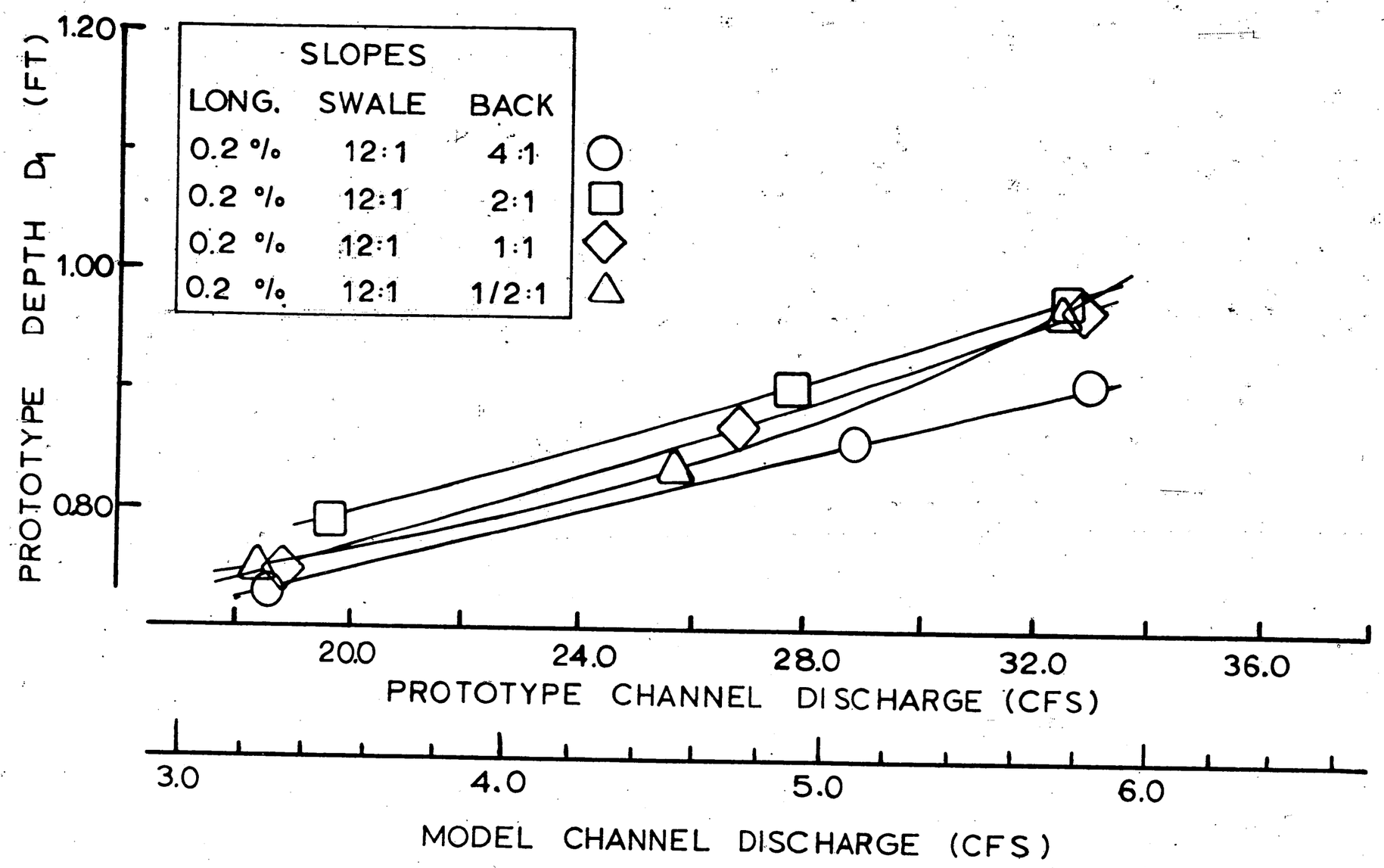

Fig. 5.30: Sump Effect for Type H Inlet - Longitudinal Bars

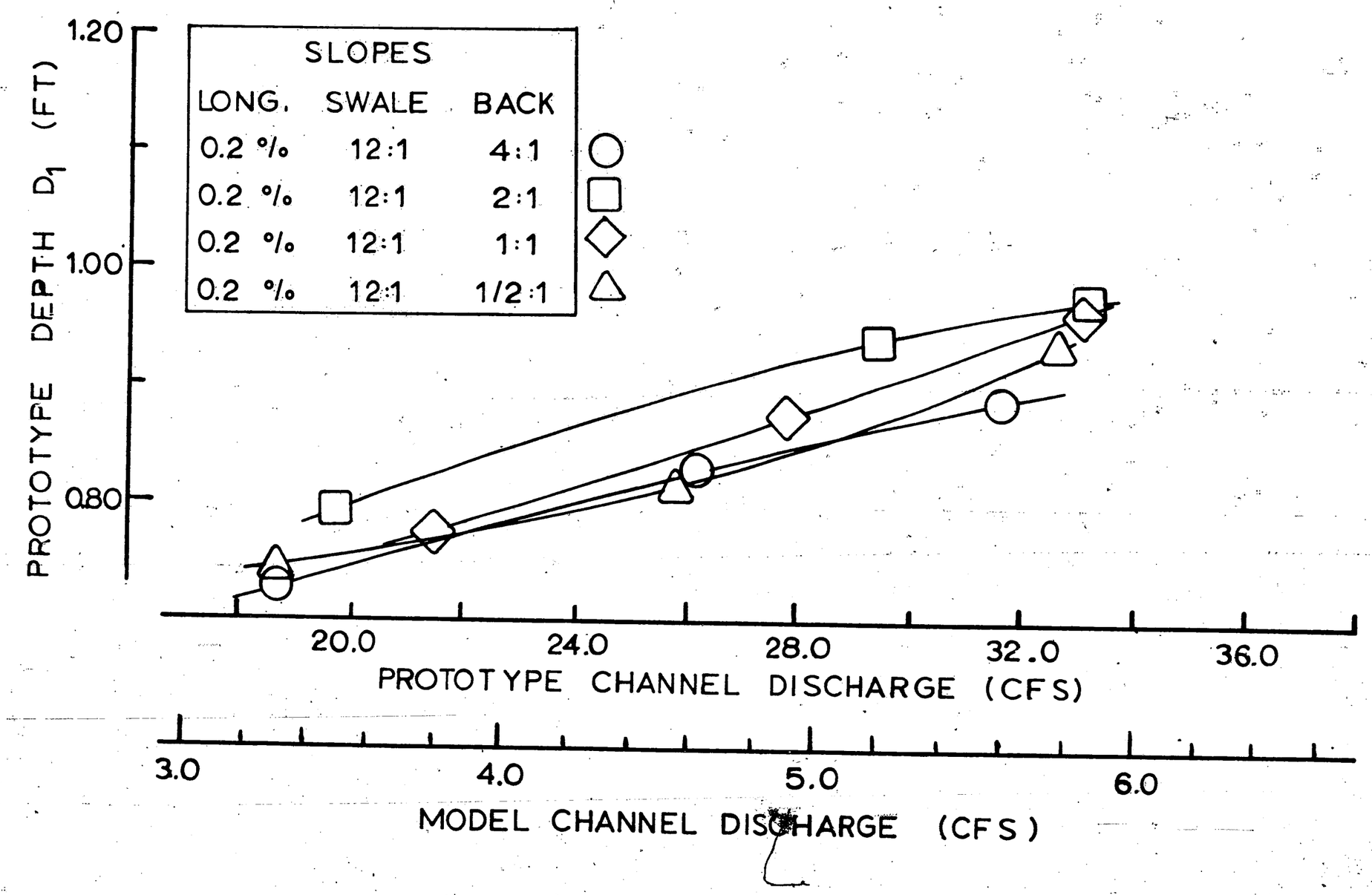

Fig. 5.31: Sump Effect for Type H Inlet - Diagonal Bars

The inlet gratings, except for the standard grating, were not completely covered by water, indicating that the shape of these gratings was not significant for the sump effect. The standard inlet grating was completely covered for only the highest flow rates, which were above 25 cfs, and the depth of water over the grate surface did not exceed 1-inch in the model. The depth of water in the channel, D_1, did not differ significantly for the three different inlet gratings for the same rate of flow.

6. CONCLUSION

Experiments on the hydraulic performance of three different types of drainage inlet gratings installed in grassed channels were conducted in a model. The effect of different side and longitudinal slopes of the channel have been investigated.

6.1 General Conclusions

The following conclusions can be drawn from the present study.

The efficiency of an inlet grating placed in a chamel with fixed side slopes decreases with increasing longitudinal slope.

The efficiency of a particular grating increases significantly with increasing swale slope and is maximal if the back slope is equal to the swale slope.

The geometry of the inlet grating becomes significant as the longitudinal slope increases. Thus, the grating with longitudinal bars has a higher efficiency than the grating with diagonal bars at a steep longitudinal slope (8%), whereas this difference in efficiency is negligible for a flat longitudinal slope (½%).

6.2 Type H Inlet Gratings

The efficiencies of the three gratings of this type do not range farther than 5% from each other, if installed in a channel with a 12:1 swale slope, a back slope ranging from 4:1 to ½:1, and the longitudinal slope being fixed. For a steep longitudinal slope of 8% and

for the same range of side slopes, the differences in efficiencies between the three gratings increases to approximately 10%.

The efficiencies of the gratings placed in a channel with the same range of side slopes, as in the preceding paragraph, decrease only a few percent for a longitudinal slope that changes from ½% to 4%. An increase in longitudinal slope from 4% to 8% results in a decrease in efficiency of the gratings of less than 10%.

An increase in the swale slope from 12:1 to 6:1 increases the efficiencies of the gratings about 12%. The particular type of grating, back slope, and longitudinal slope become significant for the efficiency of a grating installed at a swale slope of 6:1. The grating with longitudinal bars is generally the most efficient.

6.3 Type 4-Ft and Type 6-Ft Inlet Gratings

These inlets were installed at different depressions. The efficient of an inlet grating increases with increasing depression. However, the improvement in efficiency of a grating installed at zero depression and at 2-inch depression for a particular channel configuration is no more than 10%.

The grade of the swale slope is of significance for the efficiency of the grating. An increase in swale slope from 12:1 to 6:1 results in an increase in efficiency of the grating of 5% to 20%, depending only slightly on the grade of the back slope.

The efficiency of the Type 6-Ft Inlet grating for a particular channel configuration is due to its larger size, generally 10% to 20% higher than the efficiency of the Type 4-Ft Inlet grating.

Experiments that have been carried out indicate that the geometry of this particular grating is insignificant for the efficiency of the grating. Thus, the efficiency is governed by the size and form of the grating opening and not by the geometry of the grate.

Significance of Dike

A dike 6 inches high installed downstream of both the Type 4-Ft and the Type 6-Ft Inlet gratings was found to increase the capacity of each grating by 3 to 5 times, depending on the channel configuration.

As a result of the installation of the dike, a strong vortex is developed over the downstream end of the grating, indicating that substantial scour could occur at a field installation.

Sump Effect

A sump condition was established for the Type H Inlet gratings. The effects of the sump condition do not depend significantly on the type of grating.

The maximal prototype channel flow rate for which a sump condition was tested was 32 cfs corresponding to a depth measured one-foot upstream from the grating of approximately one-foot and a spread of less than 8 feet.

7. LIST OF RECURRING SYMBOLS

A	area, ft^2
D	depth of channel, ft
Eu	Euler number
F	force, lbs
Fr	Froude number
g	gravitational acceleration, ft/sec^2
ΔH	pressure-head drop across orifice, ft
L	length, ft
ℓ	characteristic length, ft
n	Manning's roughness coefficient, $ft^{1/6}$
Q	flow rate (discharge) ft^3/sec
Q_1	channel flow rate, ft^3/sec
Q_2	intercepted flow rate, ft^3/sec
Q_3	carryover flow rate, ft^3/sec
Re	Reynolds number
R_h	hydraulic radius, ft
S	slope of energy line
T	time, sec
$\forall$	volume, ft^3
η	efficiency, percent
ρ	density, $slug/ft^3$
μ	dynamic viscosity, slug/(ft-sec)

Subscripts

m	model
p	prototype
R	ratio

8. BIBLIOGRAPHY

1. Chow, V. T.
OPEN-CHANNEL HYDRAULICS, McGraw-Hill Book Company, New York, New York (1959).

2. Einstein, H. A. and E. S. El-Samni
HYDRODYNAMIC FORCES ON A ROUGH WALL, p. 521, Review of Modern Physics, Vol. 21 (1949).

3. Engelund, F.
TEXTBOOK IN HYDRAULICS, pp. 38-52, Statens Trykningskontor, Un 04-258, Copenhagen, Denmark (1965). (In Danish)

4. Graf, W. H.
HYDRAULICS OF SEDIMENT TRANSPORT, pp. 385-398, McGraw-Hill Book Company, New York, New York (1971).

5. Hansen, A. G.
FLUID MECHANICS, pp. 395-413, Wiley, New York, New York (1967).

6. Johns Hopkins University
THE DESIGN OF STORM-WATER INLETS, Department of Sanitary Engineering and Water Resources, Report of the Storm Drainage Research Committee, Baltimore, Maryland (June 1956).

7. Larson, C. L. and L. G. Straub
GRATE INLETS FOR SURFACE DRAINAGE OF STREETS AND HIGHWAYS, University of Minnesota, St. Anthony Falls Hydraulic Laboratory, Bulletin 2 (June 1949).

8. Morris, H. M.
APPLIED HYDRAULICS IN ENGINEERING, The Ronald Press Company, New York, New York (1963).

9. Stevens, J. C. et al.
HYDRAULIC MODELS, The Committee of the Hydraulic Division on Hydraulic Research, ASCE, Manual of Engineering Practice 25 (1942).

10. U. S. Army Corps of Engineers
SURFACE DRAINAGE FACILITIES FOR AIRFIELDS, EM 1110-345-281 (1964).

11. Yee, P. P.
HYDRAULIC PERFORMANCE OF HIGHWAY DRAINAGE INLETS INSTALLED IN PAVED CHANNELS, Master's Thesis, Lehigh University, Bethlehem, Pennsylvania (1972).

12. Yucel, O. et al.
DEVELOPMENT OF IMPROVED DRAINAGE INLETS, PHASE 1: LITERATURE SURVEY, Lehigh University, Fritz Engineering Laboratory Report No. 364.2 (1969).

9. APPENDIX-DETERMINATION OF MANNING'S ROUGHNESS COEFFICIENT OF LANDSCAPE SURFACE "ASTROTURF"

1. Introduction

This study is concerned with the suitability of using Landscape Surface "Astroturf", a product of Monsanto Chemical Company, to simulate grass in a model drainage channel.

The roughness of the "Astroturf" was investigated in a flume using several different rates of discharge.

2. Testing Equipment

The tests were conducted in a glass-walled flume in the Hydraulics Laboratory of Lehigh University. The flume is an open, rectangular channel, 24 feet long and 18 inches wide, see Fig. A1.

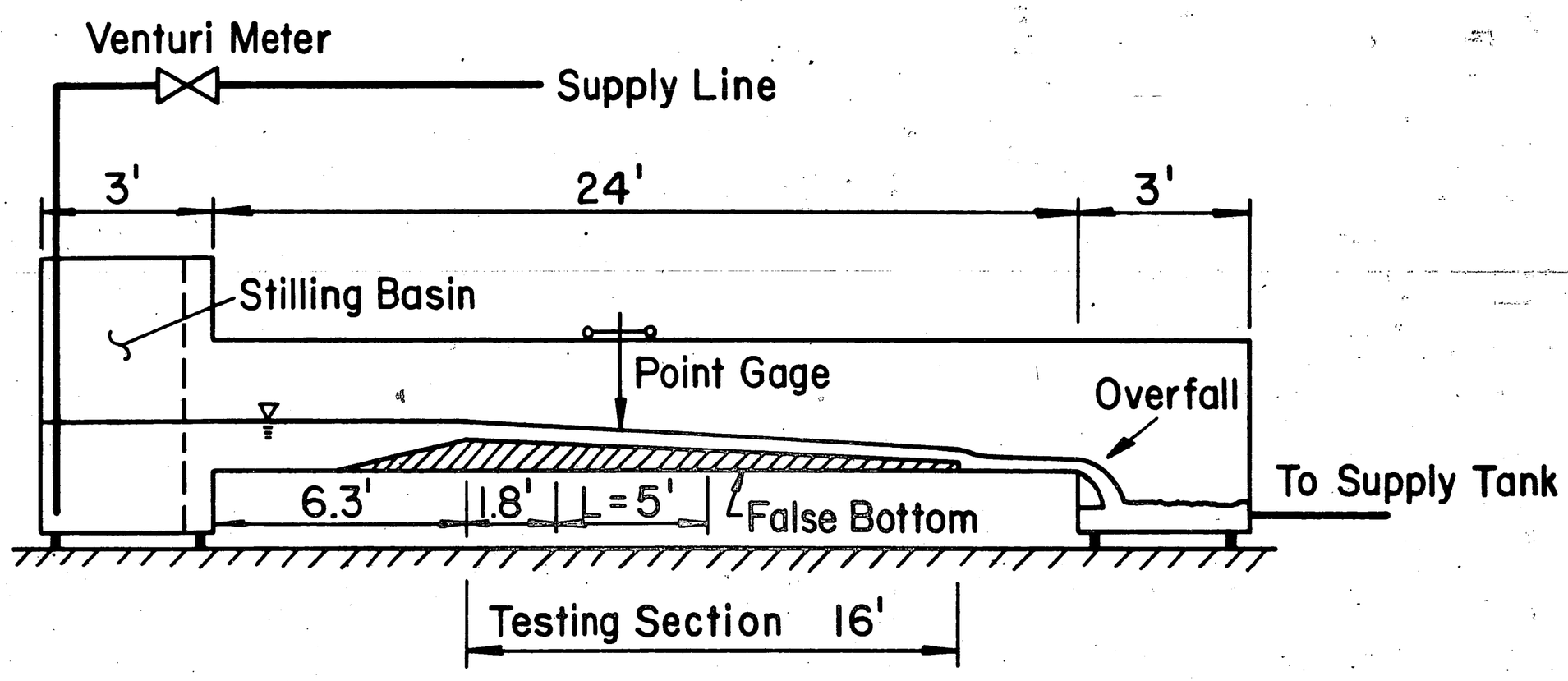

Fig. A1: Scheme of Experimental Arrangement, Not to Scale

The water for the flume was circulated by a centrifugal pump; the volumetric flow rate was determined by means of a Venturi

meter. The bottom of the channel is fixed in a horizontal position. A false bottom, 16 feet long, was installed in order to provide a constant slope of two percent downward in the direction of flow. The false bottom constituted the slope over which the tests were run. In order to establish a smooth transition onto the slope, a short approach was built, and to avoid disturbances, the false bottom was placed as far downstream from the channel entrance as possible and as far upstream from the channel exit as possible. The water depth in the test section was measured with a point gage, equipped with vernier scale which enabled measurements to be made with an accuracy of 0.001 ft. The point gage was mounted on a carriage; thus readings at any place along the section were possible.

3. Description of Artificial Roughness

"Astroturf" consists of groups of strips, each strip simulating a blade of grass, see Fig. A2. Each group is 1/4-inch in diameter at the

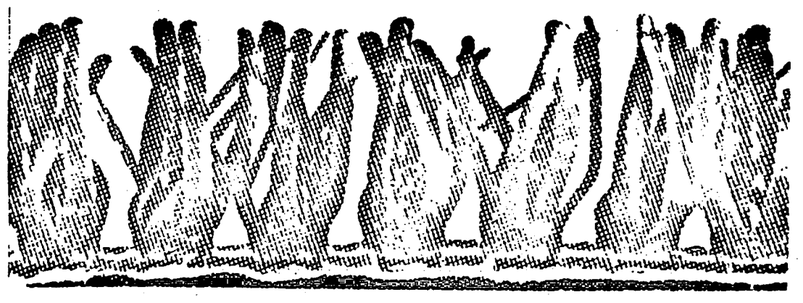

Fig. A2: "Astroturf", Scale 1:1

base and contains eight strips that rise upward and radiate outward, somewhat similar to the shape of a bush. The groups are mounted equidistant in rows on a mattress that is 1/16-inch thick. The distance between each group in any one row is 2/5-inch, and the distance between adjacent rows is also 2/5-inch. The height of the "Astroturf" is

15/16-inch, H in Fig. A3. The strips are well tangled, giving an appearance similar to that of natural grass having equal height. The mattress was stapled to the wooden slope at a density of one staple per 30 square inches.

4. Testing Procedure

All depth measurements were taken with the point gage and were computed as the difference in elevation between the false bottom and the water surface, $D_1 - D_2$ in Fig. A3.

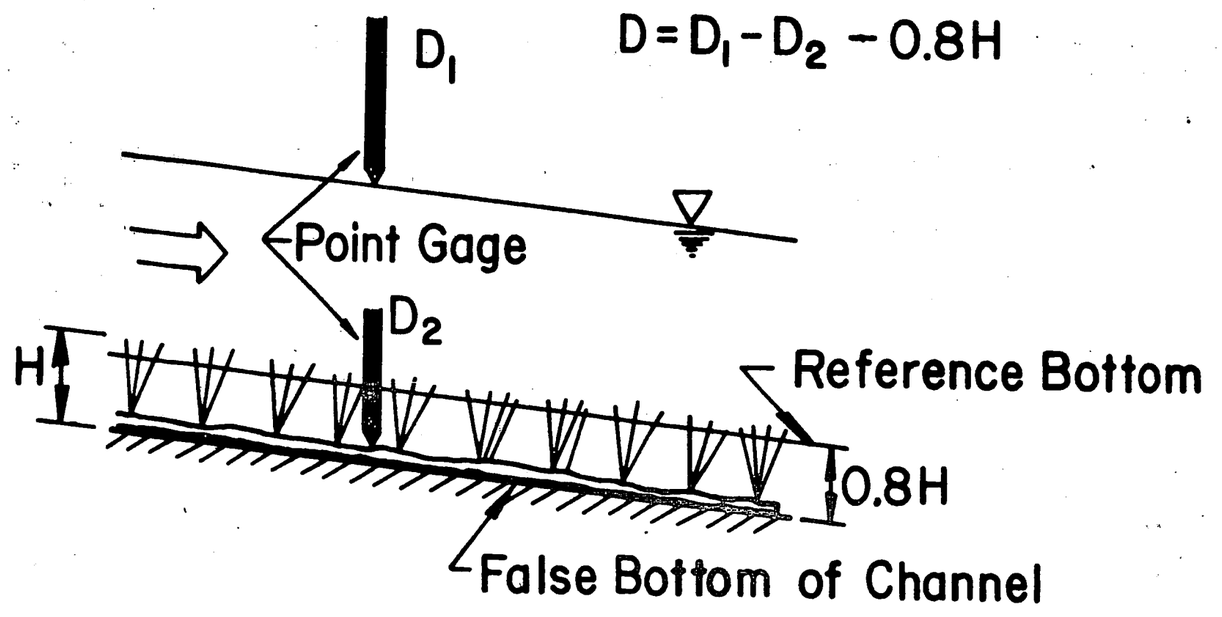

Fig. A3: Depth Measurement

For a given discharge the elevation was taken at every foot along the centerline of the test section, and the depth was computed. All these depth measurements were not exactly the same; however, the magnitude of discrepancy was not considered unacceptable, as it was commonly possible during each discharge to select a two-foot length within the test section wherein the deviation of the actual depths were less than one percent; in only one case was the deviation as much as five percent.

The two-foot length of section thus found was considered to have uniform flow; the depth as used in subsequent computations was then calculated as an average of three depths measured at the quarter points of a cross section within the selected length section. The two-foot lengths, wherein all measurements were made, were within a five-foot distance that was on the upper half of the slope; this is shown as L in Fig. A1. The range of discharge and corresponding depths are shown in Table A1.

Table A1: Experimental Data and Results

Discharge (cfs)	Depth (ft)	Manning's Roughness Coefficient
0.35	0.13	0.031
0.52	0.17	0.031
0.74	0.20	0.029
0.98	0.25	0.030
1.21	0.27	0.028
1.45	0.30	0.028
1.69	0.33	0.028
1.87	0.35	0.028
2.07	0.36	0.026

5. Results and Analysis

The channel is considered to have a composite roughness, one roughness being due to the "Astroturf" and the other being due to the glass walls; the latter was known from previous investigations. Manning's equation for composite roughness (CHOW) was used to calculate the unknown roughness coefficient. To ensure the proper application of Manning's equation, the Reynolds numbers were caused to lie between 84,000 and 470,000; thus the experiments are well within the range of turbulent flow.

To define a reference bottom, for an arrangement such as this, is a major problem. Apparently, the reference bottom is neither at the very bottom of the strip, as measured with the point gage, nor at the very top of the strips. Einstein et al. suggested, while testing spheres as artificial roughnesses, that the reference level is one-fifth of the roughness height below the top of the roughness elements. This suggestion was found to be a reasonable one in this investigation also, and the reference depth, D, was then computed as shown in Fig. A3.

Figure A4 shows the relationship between the roughness coefficient, n, and the discharge, Q, where n is calculated with respect to a reference depth previously defined. The relationship is tabulated in Table A1. The roughness coefficient was determined from Fig. A4 as 0.028.

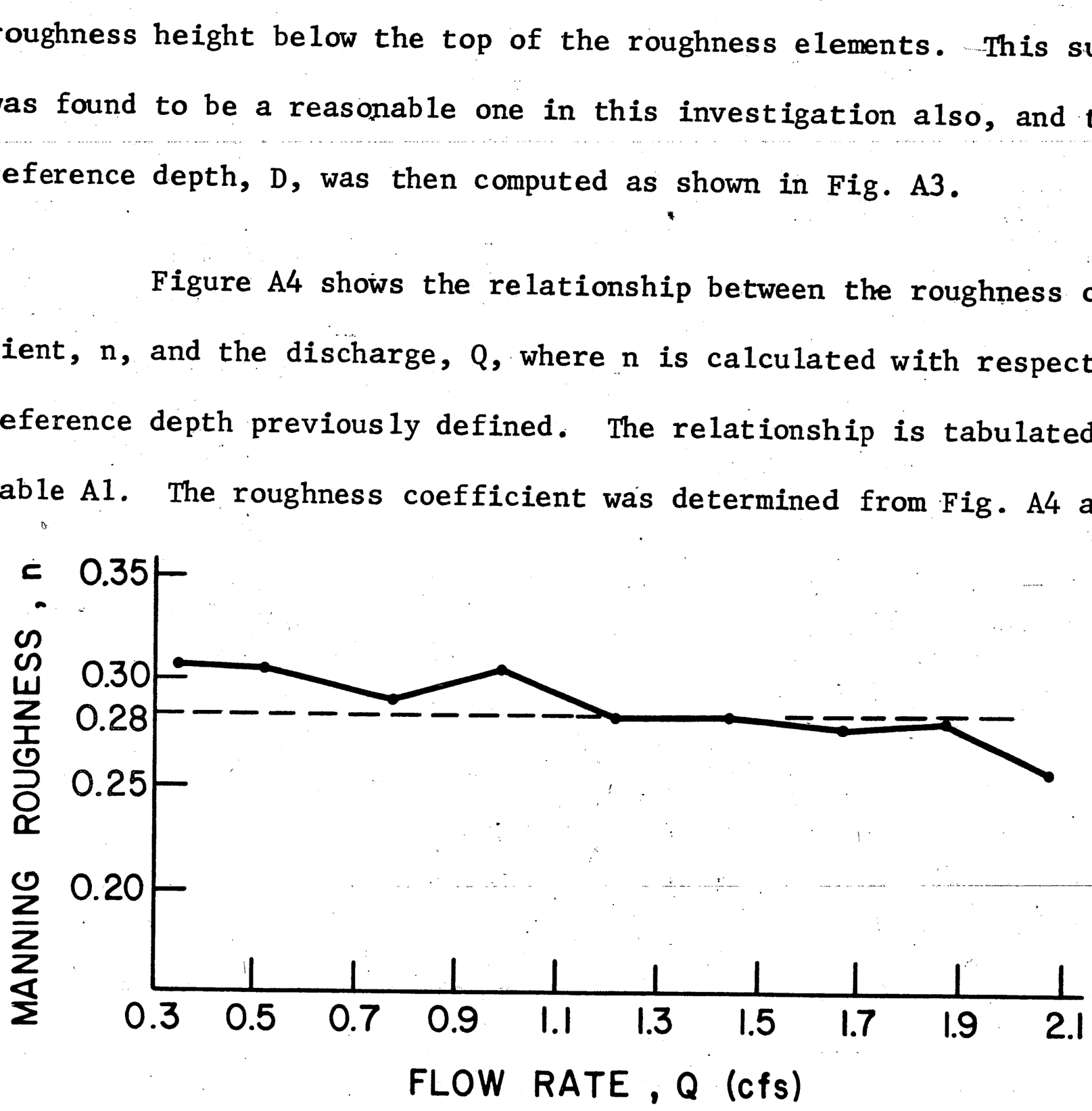

Fig. A4: Determination of Manning's Roughness Coefficient

6. Conclusion

Apparently, the Manning's roughness coefficient of "Astroturf" has not been determined previously; therefore, a comparison with results

of other investigators is not possible. However, there exist data for natural grasses, which can be compared to the results obtained for artificial grass used in this study. The roughness coefficient for natural grass, (CHOW), ranges from 0.010 to 0.050. The roughness coefficient, 0.028, obtained in this study is thus found to be within this range.

10. VITA

The author was born in Denmark, in Toksvaerd, a village located 50 miles south of Copenhagen, on August 2, 1946. He is the son of Mr. and Mrs. Henry Appel of Aakirkeby, Bornholm, Denmark.

After examination for the school-leaving certificate, the author studied Civil Engineering at the Engineering Academy of Denmark in Copenhagen. He received his engineering diploma in 1969. He was thereupon employed by the Danish Isotope Centre in 1969 and had a teaching engagement in 1970-71 at the Engineering Academy of Denmark in Copenhagen.

He was awarded a Research Assistantship to Lehigh University in September 1971, from which he was graduated in December 1972 receiving the degree of Master of Science in Civil Engineering.